Water jet steering concept

- evaluation of an environmental design, Part 1

Koncept för vattenjet styrning

- utvärdering av en miljövänlig konstruktion, Del 1

Viola Örtegren

Faculty of health, science and technology

Degree project for master of science in engineering, mechanical engineering

30 credit points

Supervisor: Anders Gåård

Examiner: Jens Bergström

Date: Autumn semester 2013, 2014-03-25

Abstract

The current hydraulic system that function as the power source for operating the water jet steering device, need to be located inside of the hull to avoid possible environmental damage. This will cause a height difference from where the power supply will be located and where the output is needed. The research of literature and the limitations given by Rolls-Royce laid the basis for the simulation work. The lever concept is a development of the original layout from Rolls-Royce. The current lever concept was formed by simulation of the individual parts it consists of. The modeling work is a starting point for further design changes and improved solutions depending on what results are achieved when simulation is performed on the parts. The modeling work is not part of this report but can be seen in the other master thesis *"Water jet steering concept - evaluation of an environmental design, Part 2"* which is not yet done but it will be soon. All simulations made are simplified and they are a solid starting point for further work with dimensioning, material selection and calculations. The results of the simulation show that further development is required before a theoretically functioning concept is achieved.

Sammanfattning

Det nuvarande hydraulsystemet som verkar som kraftkälla för att manövrera vattenjetens styrsystem, måste flyttas till insidan skrovet för att undvika eventuell miljöskada. Detta kommer bidra till en höjdskillnad mellan vart kraften verkar och vart den behöver verka. Litteraturundersökningen och begränsningar som erhållits från Rolls-Royce låg till grund för simuleringsdelen. Hävarmskonceptet är en version utav original idén från Rolls-Royce. Det framtagna hävarmskonceptet konstruerades med hjälp av simuleringar utav de individuella delarna som ingår i konceptet. Modelleringen är en startpunkt för vidare utveckling av design och förbättrade lösningar baserat på resultaten som erhållits från simuleringen på de olika delarna. Modelleringen är inte en del utav denna rapport men kan ses i examensarbetet ”Koncept för vattenjet styrning - utvärdering av en miljövänlig konstruktion, Del 2” som ännu inte är färdigt men kommer bli det vid senare tillfälle. Alla simuleringar är förenklade och de är en bra startpunkt för vidare bearbetning med dimensionering, materialval och beräkningar. Resultaten från simuleringarna visar att vidare utveckling behövs innan ett teoretisk funktionellt koncept kan uppnås.

Table of Contents

1. Introduction

For marine vessels there are two main approaches for achieving propulsion. The first method is conventional propeller propulsion and the second way of achieving thrust is by jet drive. This project treats the latter of the two and is based on a development task issued by Rolls-Royce. [1] The main principle of a jet engine is to take advantage of Newton's third law of motion, to every action there is always an equal and opposite reaction. By creating a jet stream of a fluid or gas, the jet stream will produce a forward motion in the opposite direction of the jet stream. In short the function of the water jet can be described as a pump unit squirting water out a nozzle in the opposite direction of the desired motion. By redirecting the jet stream maneuverability of the vessel is achieved.

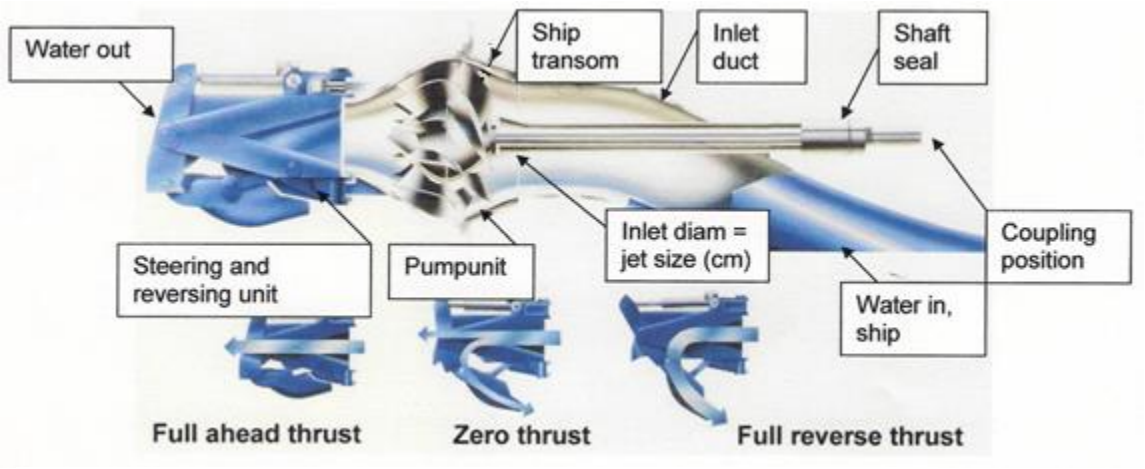

Figure 1a: Overview of the Kamewa water jet and the main parts it consists of. [1]

1.1 Aims

The present water jet design have all hydraulic driven actuators, cylinders, positioned outboard which presents a risk of oil spill due to the connections of flexible hoses. Figure 1.1a show the Kamewa water jet system with an illustrative environmental design, but development of an actual concept is required. The basis is to get the hydraulic cylinders, now placed inside of the hull, to maneuver the same system as they did before and the concept should also be compatible with the current jet system.

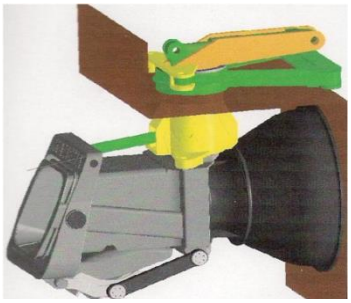

Figure 1.1a: Conceptual design provided by Rolls-Royce [1]

The main obstacle is that the relocated hydraulic cylinders should be able to generate the same force as before. Another factor which must be taken into consideration is the selection process concerning material properties like strength, environmental resistance, weight and cost. Main focus of the material properties lies within strength and environmental resistance.

1.2 Delimitation

The scope of this master thesis contains areas which need to be explored to be able to make a full analysis of which solution is the most suitable for this type of force transfer system. From the beginning this report was made up of two master theses which covered most of the critical aspects to investigate. Now fatigue, steel grade, seals, parameter variation, calculations and stress and strain evaluation remain. The focus is put on the stress and strain evaluation and therefor is the deepest analysis made regarding the fatigue and calculations. Stress and strain simulations are the result produced to be able to present a functional force transfer system to Rolls-Royce.

1.3 Function

There are several makes and models of different water jets but they all share the same basic function: accelerating water through a nozzle creating a jet stream of water propelling the vessel. The water jet system can roughly be divided into three areas: the inlet, the pump unit and the outlet area.

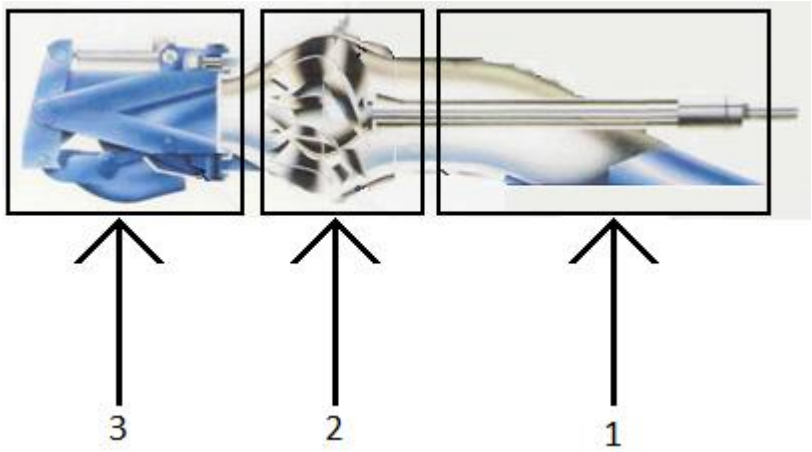

Figure 1.3a: The three areas: 1. Inlet, 2. Pump unit and 3. Outlet. [1]

The jet draws water from the inlet that is located beneath the water surface. The pump unit is the mechanism that draws water via the inlet, consisting of an impeller located inside the impeller housing. The impeller is the rotating element of the jet and is the part that connects and is powered by the engine. The water drawn from the inlet reaches the pump and is accelerated when it passes the impeller and forced backwards entering the outlet area. A nozzle and steering unit make out the outlet area. The accelerated water will reach the nozzle right after it exits the pump unit. The nozzle diameter at the outlet is reduced compared to the inlet and the accelerated water is forced through creating a focused jet stream. The last part of the outlet area is the steering unit. This part is what makes the vessel maneuverable. On models where reversing is an option this is also where the reversal mechanism is located. The design of the steering unit differs between different makes of water jets. The specific water jet that is reviewed in this report is the Kamewa water jet, and the steering function described apply only to this specific make. [1]

1.3.1 Steering unit

The steering unit provides maneuverability of the vessel by redirecting the jet stream. This is achieved by adding a box outside the nozzle that the jet stream can pass through. The box rotates around its point of attachment and redirects the jet stream in the desired direction. By doing this the thrust will push the boat and steering is achieved. [2]

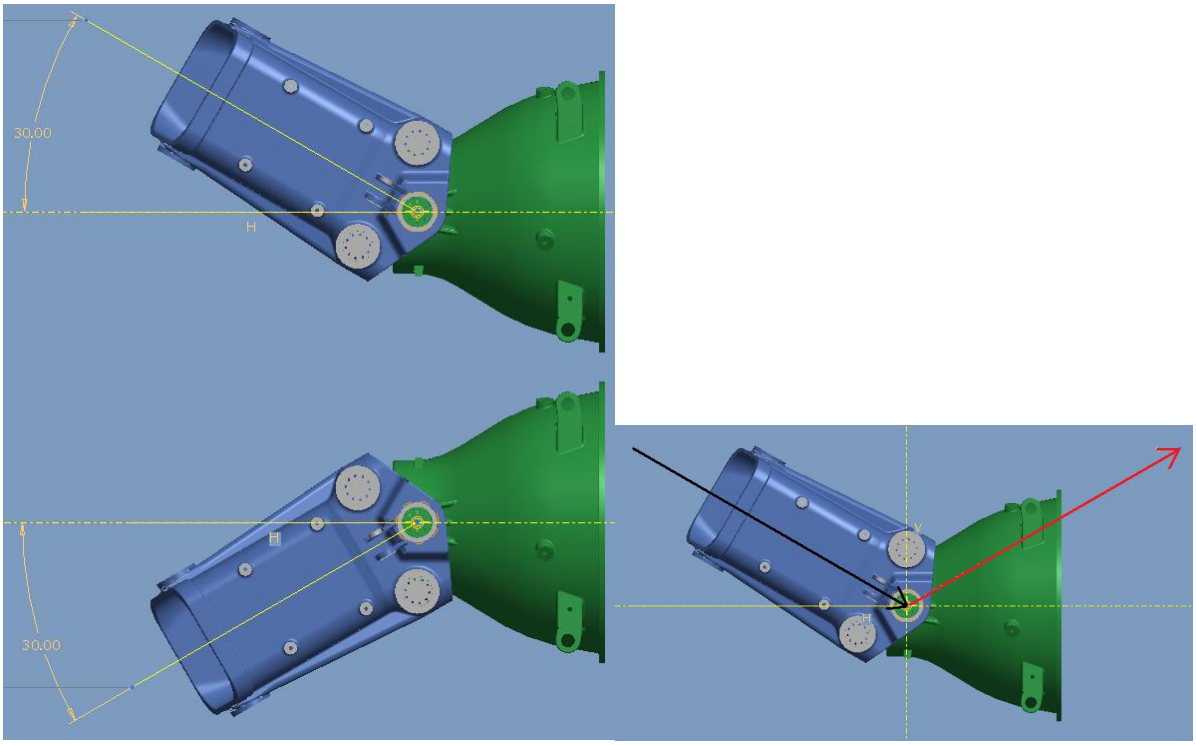

Figure 1.3b: Left; showing the point of attachment where the steering unit will rotate around. The steering unit is allowed to rotate 30˚ in each direction. Right; black arrow represents the thrust when the steering unit is rotated 30˚ clockwise, the red arrow is the direction the vessel will turn towards as a result of the thrust.

The Kamewa water jet is equipped with an integrated reversing mechanism attached to the steering unit. Achieving a reversing thrust is done the same way as for achieving steering, namely by manipulating the direction of the jet stream. As established earlier the direction of thrust is always in the opposite direction of the flow of the jet stream. Achieving thrust in the reversing direction is done by redirecting the jet stream so it points towards the front of the vessel. [1]

Neutral thrust is achieved by splitting the jet stream in two parts. One part still pointing in the backwards direction and the other part pointing to the front, the result is equal thrust in opposite directions and they cancel each other out. [1]

Fig 1.3c: Illustration of how the reversal mechanism redirects the jet stream from full ahead thrust, zero thrust to full reverse thrust. [1]

1.4 Mechanics

The function of this mechanism is controlled with hydraulics described under “1.3 function” and in figure 1a these hydraulics are shown on top of the steering housing. This specific make let the hydraulics work in the same plan as the force is needed. In this report investigation regarding what happens if the same hydraulics are moved to an elevated plane compared to the plane the forced are needed in will be made and is the main condition described by Rolls-Royce in the development task.

One of the main influences of how well the mechanism works is the possibility to withstand fatigue which is the most significant failure modes regarding these types of structures. [3] The largest part of the literature study in this report handles this topic to get a good knowledge of this phenomenon.

1.5 Fatigue

When a component is subjected to cyclic stress or strain which causes permanent deformation fatigue failure may occur. When examining a fracture surface, the type of fracture mechanism can be determined. In case of a fatigue failure, which often arises during long time periods, a distinct pattern is often present. This pattern is called clam shell markings, arrest lines or beach markings and can look like figure 1.5a. The surface is rather flat which indicates that there has not been much severe plastic deformation. The beach markings indicate that the crack growth has increased little by little, that is one marking per cycle. This pattern is believed to be generated from the corrosion and/or oxidation on the surface at the different crack growth. Fatigue failure is not the only thing this pattern implies, it can also indicate the crack growth origin which is found at the curvature center of the curved beach markings. [4]

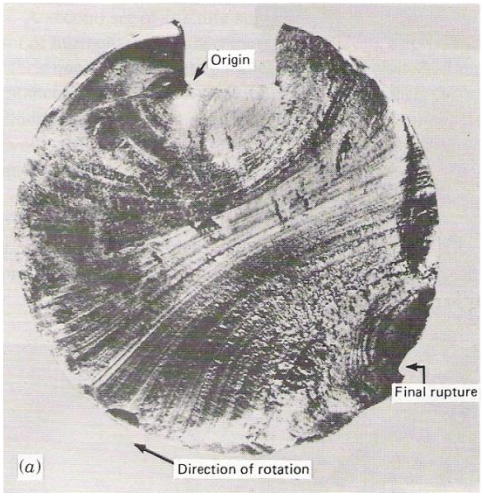

Figure 1.5a: Image of a fracture surface showing beach markings. [4]

The fatigue process consist of three main stages; initiation, propagation and final failure. This kind of failure is common for engineering applications and it is important to understand the mechanism. The existence of design defects or other flaws will contribute to a shorter or nonexistent initiation stage, that will lead to a much shorter potential cyclic life. This is illustrated in figure 1.5b. [4]

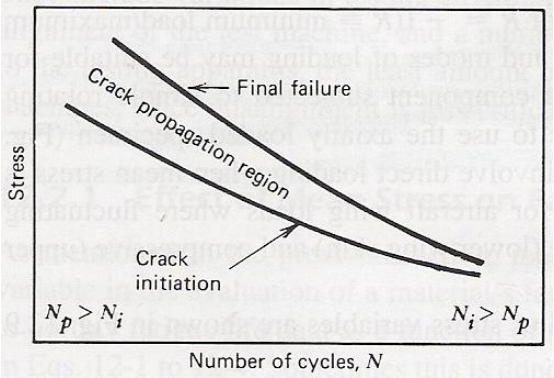

Figure 1.5b: Fatigue life dependence on crack initiation and propagation. [4]

There are different tests to get fatigue data from different materials and there are two main categories; cyclic stress fatigue or cyclic strain fatigue. For cyclic stress the different tests concern conditions with constant load or constant torque, which can be from rotating with bending or axial loading for example. The result are often plotted in so called S-N diagrams, stress versus cycles to failure which can be seen in figure 1.5c. [4]

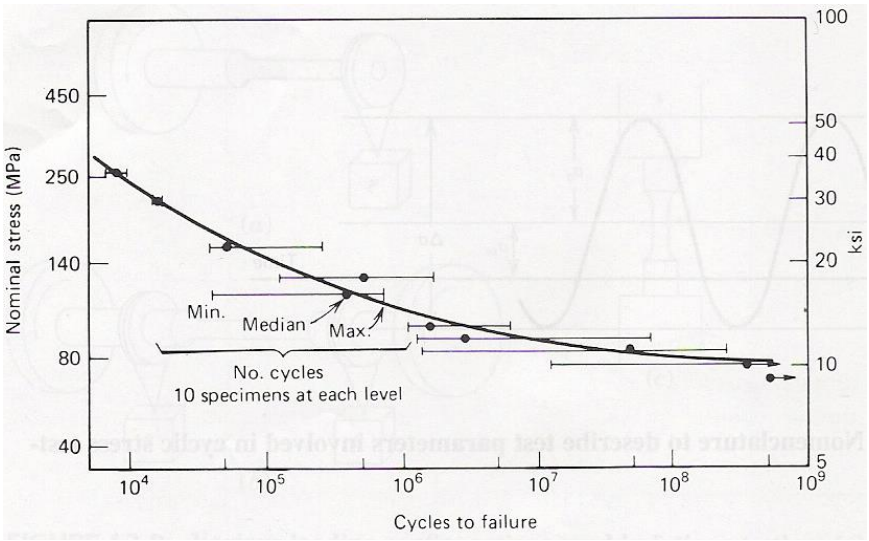

Figure 1.5c: S-N diagram for Al alloy 7075-T6. [4]

This result in particular concerns notched specimens of 7075-T6 aluminum alloy, tested under constant load amplitude fatigue at different stress levels with ten specimens at each level. Notice the amount of scatter at each level. This is common and believed to be because of differences like testing environment, specimen preparation, alignment in the test machine and also different metallurgical variables. In figure 1.5c it can also be seen that there is less scatter at higher stress levels and this is believed to be because of a shorter initiation stage of the crack. As mentioned, the results in figure 1.5c are generated from constant load amplitude and such a case is not realistic in reality even though it gives a good base. In

reality a structure often has to withstand different load fluctuations. The problem is then to predict the fatigue life of a component exposed to variable load fluctuations with constant load results. There are different theories concerning this issue and one of them used today is the often called Palmgren-Miner cumulative damage law due to its creators Palmgren and Miner. [4]

$$\sum_{i=1}^{k} \frac{n_i}{N_i} = 1 \qquad \text{Eq. (1.5a)}$$

Where k = number of stress levels in the block loading spectrum

σ_i = i^{th} stress level

n_i = number of cycles applied at σ_i

N_i = fatigue life at σ_i

This is a general form of an assumption that equal amount of damage is done at each stress level for a component. As a result of this law together with an S-N diagram, a prediction of the total or residual service lifetime of the component can be done. When calculating the safe-life it results in a certain number of cycles which will indicate a certain allowable stress level, σ_1. To be certain that the component will not fail during this life-time σ_1 is divided with a safety factor, F, which will give the design stress. The variables often involved in the safety factor are manufacturing, environmental, geometrical etc and the design stress is the maximum allowed stress level which the component must not exceed. [4]

The Palmgren-Miner law does not take accumulated damage dependence into consideration and is therefore unrealistic in reality. As an example, different sized magnitude of loads blocks acting on a component one by one. If the first block is a high load block the damage done to the component is expected to be higher than if it was a low load block due to that crack propagations starts earlier at higher loads. Although this is the case, this computation is commonly used for prediction of engineering components safe-life. [4]

Concerning cyclic strain-controlled fatigue, there are test methods evolved to evaluate the life of a component where notches are present. At the notch, localized plastic strains evolve, which is a strain-controlled condition due to the lager amount of surrounding mass of mostly elastic material. The tests insinuate that one can assume that the number of loading cycles needed for crack initiation at the notch root of a notched sample is the equal to the loading cycles of an unnotched sample. During experiments the stress and strain values are received and used to make a hysteresis loop which will help to determine the materials response. The area inside of the loop represents the amount of plastic deformation work which the material has experienced. Figure 1.5d shows the hysteresis loop for

materials experiencing elastic and homogenous plastic deformation. For the elastic case the strain is 100% reversed and for the plastic case the strain is permanent. [4]

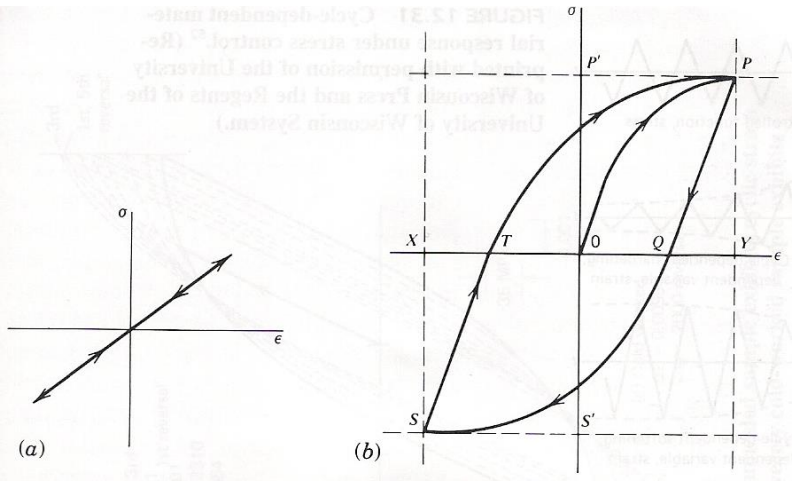

Figure 1.5d: Hysteresis loop for elastic (a) and elastic-plastic deformation (b). [4]

This means that fatigue damage is only achieved during plastic strain. This should not be interpreted as fatigue damage will only occur at stresses exceeding the yield strength, where plastic deformation of a material starts (see 1.5.1). This is because stresses below the yield strength can exceed local stresses and associated strains causing local plastic deformation. [4]

The hysteresis loop changes appearance when measuring cyclic-dependent material response as figure 1.5e illustrates. The change in the loop is continued until it reaches cyclic stability which means that the material exhibits behavior which implies that it can resist the applied stresses and strains either better or worse. These phenomena's are called strain hardening and strain softening. Figure 1.5e shows the change of the loop for both strain hardening (first loop) and softening (third loop). If cycling a material for less than 100 cycles the hysteresis loop achieves an equilibrium condition concerning the acting strains and it will stabilize. The stabilizing curve is important concerning the cyclic response of a material due to that appearance may differ a lot from the original curve. This must be taken into consideration. [4]

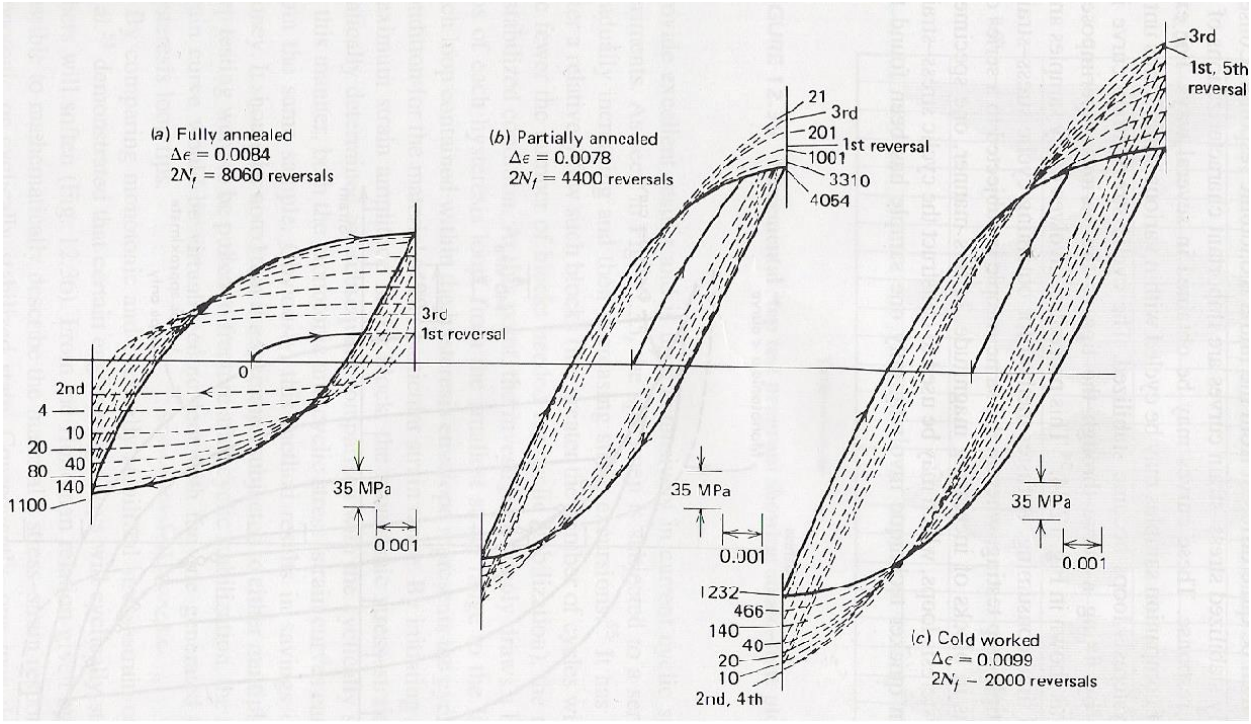

Figure 1.5e: Change in appearance of hysteresis loop due to multiple cycles.[4]

This hysteresis loop behavior of changing appearance exists for the case of stress control too. In that case the loop is seen to contract in width during cyclic softening and expand during cyclic hardening. In this case cyclic softening is the most undesirable due to that constant stress range will cause continuous strains, which contribute to early fracture. [4]

It has been observed that the ratio between monotonic ultimate strength and the 2% offset yield strength (see 1.5.1) could to some extent predict if a material where to strain harden or soften. If the ratio was above 1.4 it would harden and below 1.2 it would soften. In the interval between the outcomes were not as easy to determine, although the properties of the material is not expected to vary that much. This leads to the statement that initially hard and strong materials will generally experience strain softening while materials which are initially soft will experience strain hardening. Why materials strain hardens and softens is due to how stable the dislocation substructure in a material is. For an initially hard material which is exposed of strain cycling the dislocations in the material rearranges and lead to a structure which is less resistant to deformation, causing it to strain soften. While an initially to soft material exposed of strain cycling will rapidly increase its low dislocations density and cause significant strain hardening. [4]

Stacking fault energy (SFE) is the contributing factor to the ability to move for the dislocation causing dependence on the dislocations substructure stability. When the SFE is high the mobility of the dislocations is large due to the improved cross-slip which means that if the SFE is low the cross-slip and therefore the mobility is lower. This behavior contributes to differences in the amount and rate of strain harden or soften in a material. [4]

The cyclic softening process is called the Bauschinger effect and is often seen in cold-worked metals. This is taken as an advantage considering some of the metal-forming process of these metals. For example a type of rolling when a metal sheet is passing thru a number of roll pairs which are separated with a distance that is shorter than the sheets thickness. Instead of fracture the metals ductility is enhanced. [4]

1.5.1 Fatigue limit

There are different types of stress levels. In point A, C and E in figure 1.5f the three basic stress limits are, yield strength, (ultimate) tensile strength and fracture strength. The diagram shown in figure 1.5f is a typical engineering stress (σ) and strain (ε) diagram for metals.

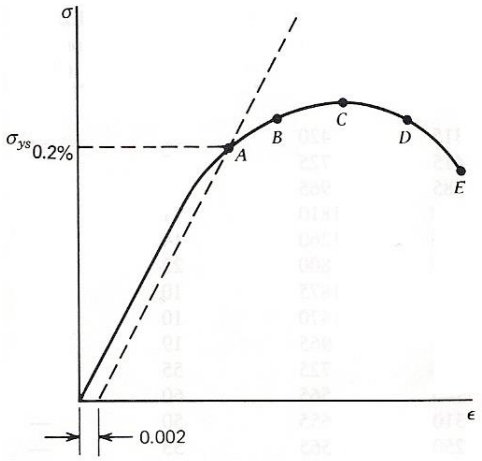

Figure 1.5f: A typical engineering stress-strain diagram. [4]

Up to the yield strength (A), the material experiences elastic behavior which means that when the material is unloaded the original geometry is recovered. After this point the material starts to plastically deform which mean that the material cannot recover its original geometry, because of the permanent deformation. It can be hard to determine exactly where the yield strength level is, but there are several ways to determine a good approximation. A common way is to determine $Rp_{0.2}$, which is done when the stress-strain diagram is known. The yield strength is then found by drawing a line parallel to the elastic part of the diagram as shown by the dashed line in figure 1.5f. The line should be drawn with a 0.2% strain offset from the origin. The yield strength, $Rp_{0.2}$, is defined as the intersection point of the two lines. [5], [4]

The tensile strength or the ultimate tensile strength (C) is the highest load achieved in a stress-strain diagram. At this point the phenomena necking occur for ductile materials. Necking is a local change in the cross-sectional area and due to this a smaller load is needed for continuation of deformation which is illustrated by the curve in the diagram. For a less ductile material the curvature is less bent and the extension of the curvature is shorter. [5]

Finally at point E is where the material breaks. It is called the fracture strength. As a summary it can be said that between zero stress and the yield strength level there is elastic behavior. Between the yield strength and tensile strength there is homogenous deformation and between the tensile strength and the fracture strength there is heterogeneous deformation. Figure 1.5g show this behavior as illustrative tensile test data.[5]

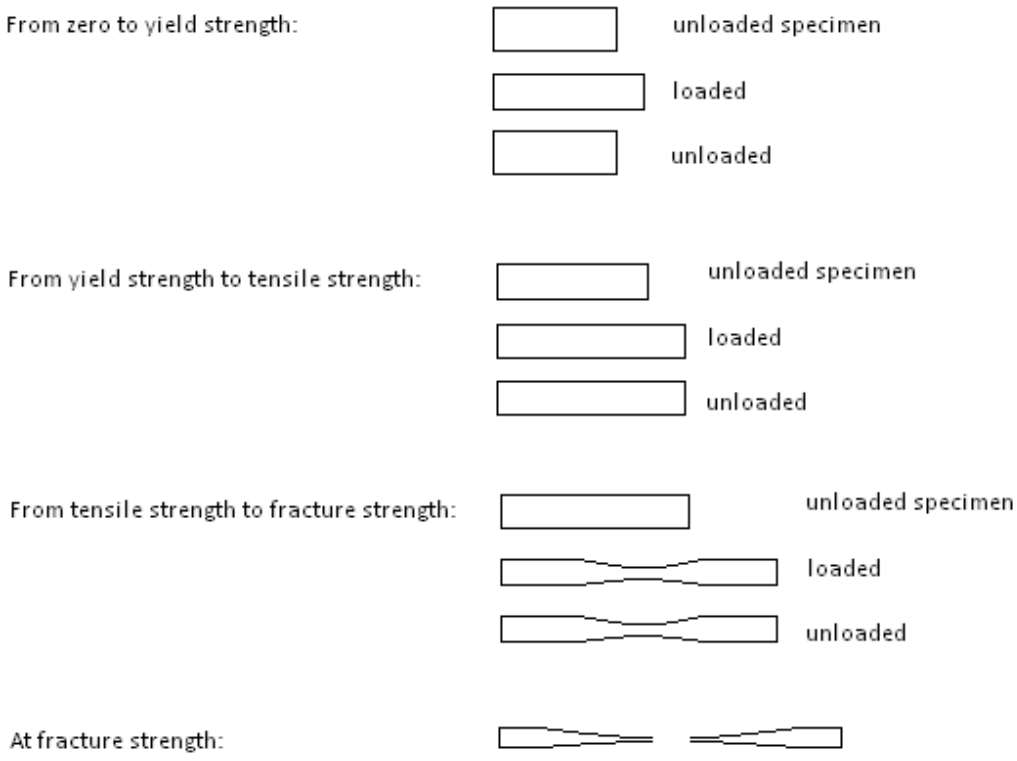

Figure 1.5g: Schematic illustration of what happens during a tensile test expressed as the different sections of a stress-strain diagram.

The fatigue limit is not shown in figure 1.5f but it is positioned in the part of the diagram from zero up to point A (in the elastic part). This implies that during elastic deformation the original shape is not completely recovered and that is due to that no material is a 100 percent perfect without defects. A 100 percent deformation recovery is not possible and after a certain number of loading cycles the material will break even if the yield strength was not ever exceeded. This applies for the region between the fatigue limit and the yield strength. Below the fatigue strength the material have close to infinite life or at least the number of cycles stated with the fatigue limit value. [4]

The S-N curve mentioned under 1.5 *Fatigue* is often illustrated by two different basic shapes. Either there is a curve which show a well-defined limit under which the material seems to possess infinite life,

or it consist of a curve which gradually decreases without any infinite life limit. The sooner is shown in figure 1.5h below and the latter is shown in figure 1.5c above. [4]

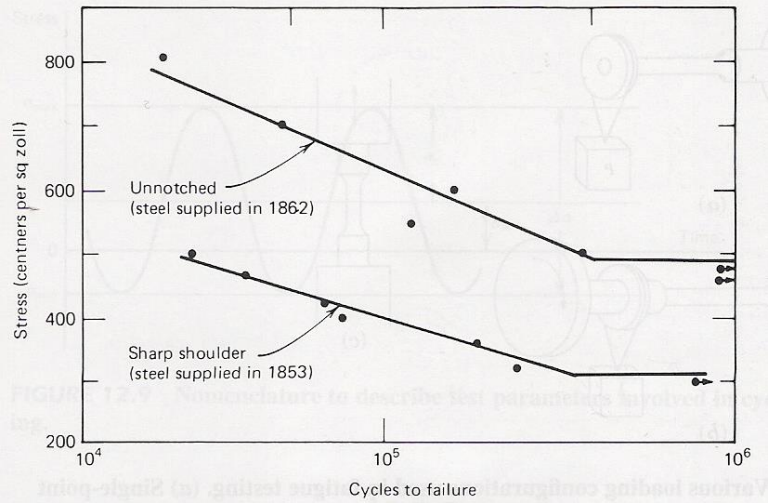

Figure 1.5h: S-N curve illustrating a well-define limit. [4]

The curve for multiple steel alloys often possess a knee. At the flat part of the knee the fatigue limit is determined. Another way to determine the fatigue limit for steel alloys is with help of the tensile strength value, because the fatigue limit is estimated to be half the tensile strength. The ratio between the tensile strength and the fatigue limit is not always 0.5, it varies between 0.35-0.60 as figure 1.5i shows. [4]

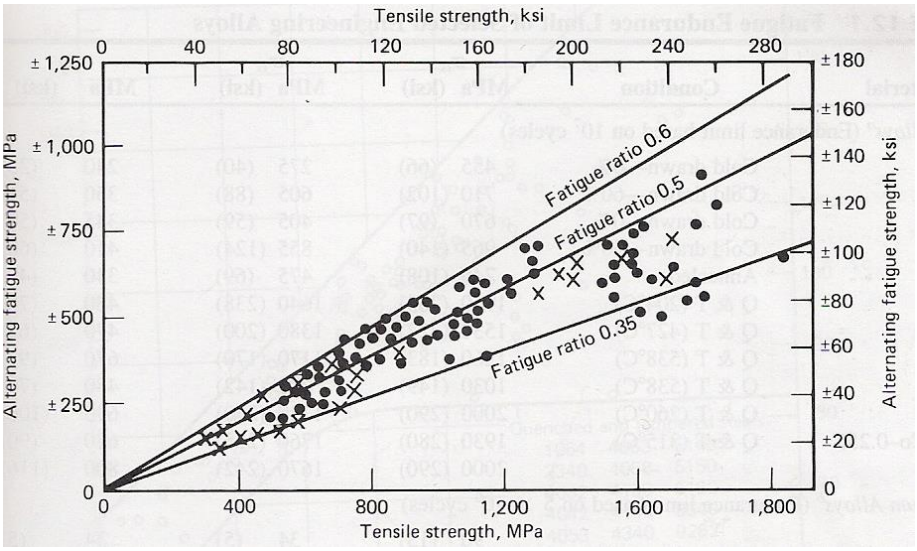

Figure 1.5i: Showing the ratio scatter, between the tensile strength and the fatigue limit. [4]

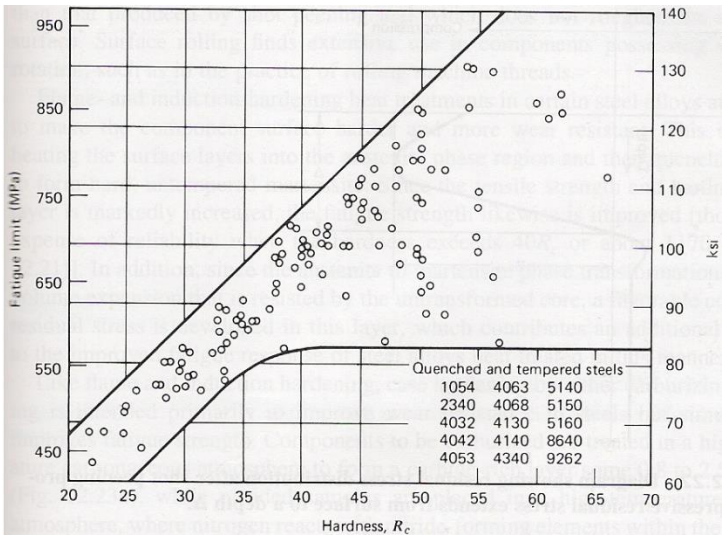

Figure 1.5j: The fatigue limit and hardness relation.[4]

As a conclusion with the previous statement in mind, the higher the tensile strength the higher fatigue limit. This is not always true, because with higher tensile strength the material will experience lower fracture toughness and be more environmental sensitive. There is another way to determine the fatigue limit of steel alloys with the help of tensile strength. Due to the hardness/tensile strength relation the fatigue limit can be estimated by measuring the hardness. This method works for harnesses up to 40RC. After that the result is too widely spread to give a good estimation, illustrated in figure 1.5j. [4]

For non-ferrous alloys, the fatigue curve is more in a gradually decreasing way which means that there is no clear fatigue limit. Instead it will be estimated at a certain amount of life cycles, often 10^7 cycles. There have been a lot of research concerning aluminum and copper alloys, which are included in the non-ferrous group of materials, Hertzberg, Richard W [4]. There are metals which are important to engineering components and the research concerns why they possess relatively poor fatigue resistance. It is believed to be due to precipitates which are especially fine and are atomically ordered within the Al-Cu alloys. They are affected of dislocations in such a way that it first contributes to strain hardening and then to localized softening. Localized softening leads to additional deformation at narrow segments which leads to crack initiation. This problem can be solved by adding larger plate like particles which affect the fatigue behavior in a positive way, but it must be done by careful melting methods and strict chemical alloying. If not, the plate like particles can serve as a nucleation sites for potential cracks and contribute to opposite behavior. [4]

Another way to enhance the fatigue behavior is to perform surface treatments because fatigue cracks often starts to grow on the surface. [4]

Fatigue crack growth rate is influenced by the surrounding environment. For austenitic stainless steel this phenomenon can be seen according to M.Jakubowski. The relative effect of environment is here defined as the ratio of the crack growth rate in a corrosive environment to its rate in air. The characteristics for fatigue crack growth rates can be described with; [6]

$$\frac{da}{dN} = f(\Delta K) \qquad \text{Eq. (1.5b)}$$

Where a = crack length

N = number of cycles

f = loading frequency

ΔK = stress intensity factor range

Above is true for stage II in the so called Paris region. The Paris region can be divided in two separate regions for different types of steels exposed to salt or sea water. For region I the main attribute it depends on is the net crack length (a_n). For region II the main attribute is the stress intensity factor range. These two regions corrosion fatigue crack growth rate equations are expressed below. [6]

For region I:

$$\frac{da}{dN} = \left(da/dN\right)_{air} \cdot A \cdot \log\left(C_I \cdot a_n\right) \qquad \text{Eq. (1.5c)}$$

where A, C_I are constants.

For region II:

$$\frac{da}{dN} = \left(da/dN\right)_{air} \cdot C_{II}\left(\Delta K\right)^{-n} \qquad \text{Eq. (1.5d)}$$

where C_{II}, n are constants.

At very low loading frequencies the fatigue strength, at $N=10^7$ cycles, is notably not as effected by the salt water. The fatigue crack growth rate in salt water environment is faster than in air at low loading frequency (≤ 1 Hz). Some of the results from the experiments in the article are seen in figures 1.5k, 1.5l, 1.5m. The steel tested was austenitic stainless steel 832 SKR-4 with properties showing in table 1.5a. [6]

Table 1.5a. Properties of the steel used in the experiment. [6]

Properties	
Yield strength	318MPa
Ultimate tensile strength	646 MPa
Elongation	50%
Chemical composition	Cr(17.4%), Ni(10.6%), Mo(3%), N(0.153%), Mn(1.63%), Si (0.5%), C(0.03%), P(0.027%), S(0.004%)

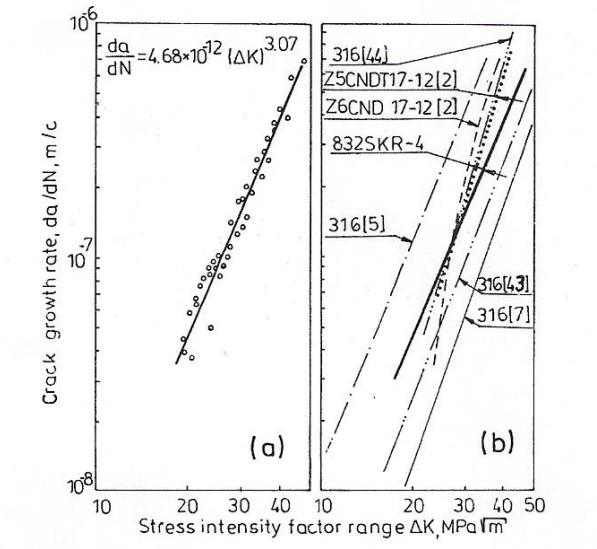

Figure 1.5k: (a) Fatigue Crack growth rate for 832 SKR-4 steel in air. (b) Comparison of 832 SKR-4 steel to other type of austenitic stainless steel, type 316. [6]

There is a great scatter of the fatigue crack growth rates of the different steels even though they are of the same type. In (b) the solid line represent them same line as in (a). [6]

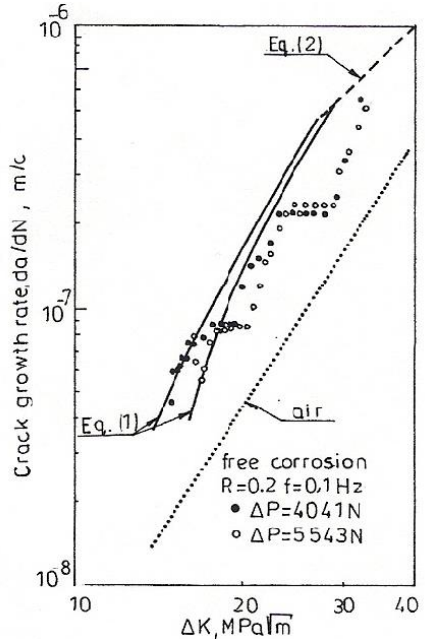

Figure 1.5l: Show Fatigue crack growth rate for 832 SKR-4 steel in salt water at free corrosion potential compared to calculated data from eq. (1.5c) and (1.5d).[6]

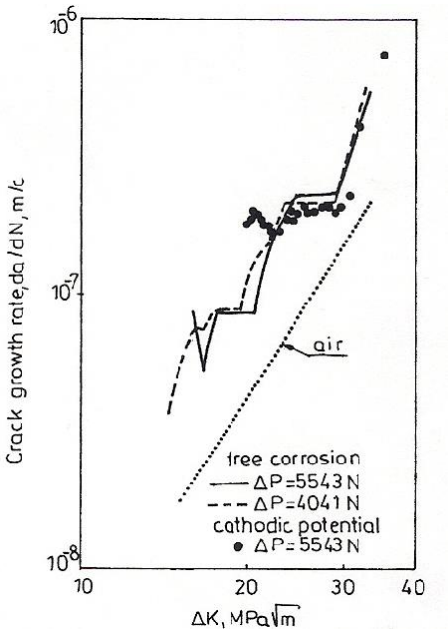

Figure 1.5m: Show fatigue crack growth rates for 832 SKR-4 steel at cathodic potential and the rates for the free corrosion potential for comparison. [6]

There are two different load levels for figure 1.5l and figure 1.5m. They are seen in the figures, ΔP=4041N or 5543N. In figure 1.5l, the corrosion fatigue crack growth rate decreases at the higher ΔP, which is when ΔK and the crack length increases (true for crack lengths a_n<4mm). This result agrees with the so called short crack effect. When a_n is larger or equal to 4mm, the fatigue crack growth rate will have a monotonically increase. When values for the constants are set for the corrosion-sensitive steels in equation (1.5c), the result describes the data for each curve along region I. By doing the same but instead with equation (1.5d) the results show a faster fatigue crack growth rate than for the present austenitic steel. The curve in figure 1.5m is only a plateau which implies that the fatigue crack growth rate is almost constant. At high ΔK values a rapid increase of the corrosion fatigue crack growth rate is seen and it has almost the same values as the rates for the free corrosion potential. [6]

When examine the samples of both potentials in a SEM (scanning electron microscope) and with XRD (x-ray diffraction) information about the fracture surface were obtained. The fracture surface consisted of mainly quasi-cleavage fractures combined with a small amount of intergranular fracture. This was when ΔK was low. When the fatigue crack growth rates were higher than $2.07\text{-}2.34\text{x}10^{-4}$ mm/c the pattern on the fracture surface were mostly plastic fatigue striations, which looks like beach markings but are on a microscopic level. It was also found that 8% α' martensite were present at the fracture surface, but the amount of α' martensite decreases slightly as the ΔK increases. The α' martensite can increase the hydrogen embrittling effect noteworthy. [6]

Conclusions drawn from this articles research and experiments are that the short crack effect arises due to the decreasing oxygen concentration inside of the crack. The relative effect of the environment depends only on the crack net length, a_n, due to the controlled transport of hydrogen and metal ions inside of the crack. The diffusion rate limits the crack propagation. There is domination of pure mechanical fatigue where the fatigue crack growth rate in figure 1.5m is almost constant and where the ΔK is high. [6]

1.6 Material properties

Since different parts of the concept are located at different places of the boat, different material types may be selected for the components. Figure 1.6a show a diagram over different metals Young's modulus and fatigue strength. The diagram is composed in CES EduPack 2009, a material database. The limiters chosen to achieve only these metals are that the base should be composed of carbon, iron, aluminum or titanium, and that Poisson's ratio lies between 0.25-0.35. That choice was made due to interest in the five groups; carbon steel, cast iron, stainless steel, aluminum alloys and titanium alloys. Also it was to have materials compatible with the properties first chosen in the simulation part which were those of general steel, a Young's modulus of 210GPa and a Poisson's ratio of 0.3. As seen in figure 1.6a aluminum and titanium does not reach the 210GPa modulus as mentioned above, but they are common structural steel and have other properties which are appealing and are stated in the text below. There are also a large amount of different types in the respectively metal group and they are given a denotation with different numbers and letters to separate them. This will not be discussed in this section, only mentioned if necessary. This can be further studied in handbooks.

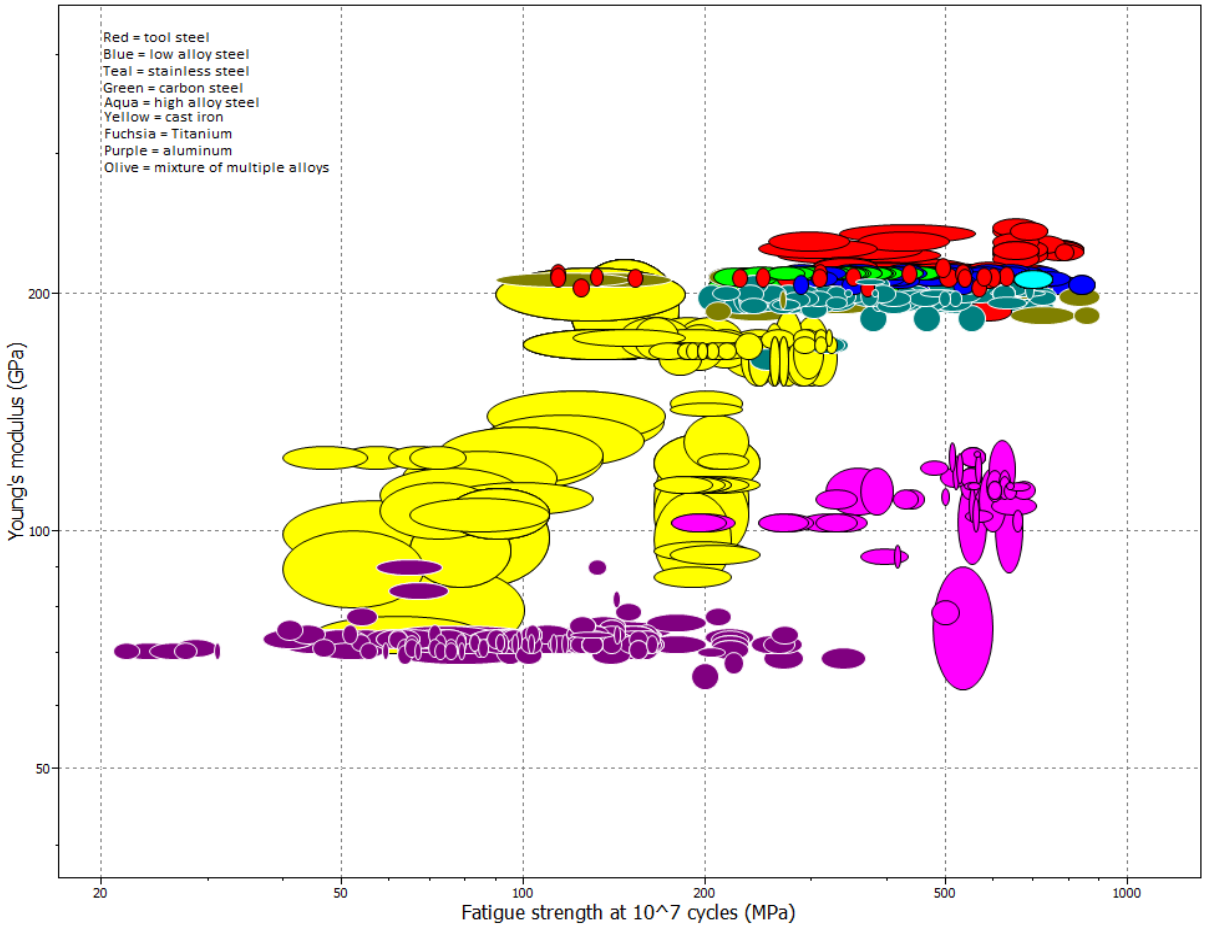

Figure 1.6a: Diagram from CES Edupack which compare Young's modulus to fatigue strength of different metals with limiters which state that the base material should consist of C, Fe, Al or Ti and the Poisson's ratio should be between 0.25 and 0.35.

A condition which some parts of the concepts need to accomplish is coping in fresh and/or salt water environment during a long time period. If that is added to the limiters the materials left to choose from is seen in figure 1.6b.

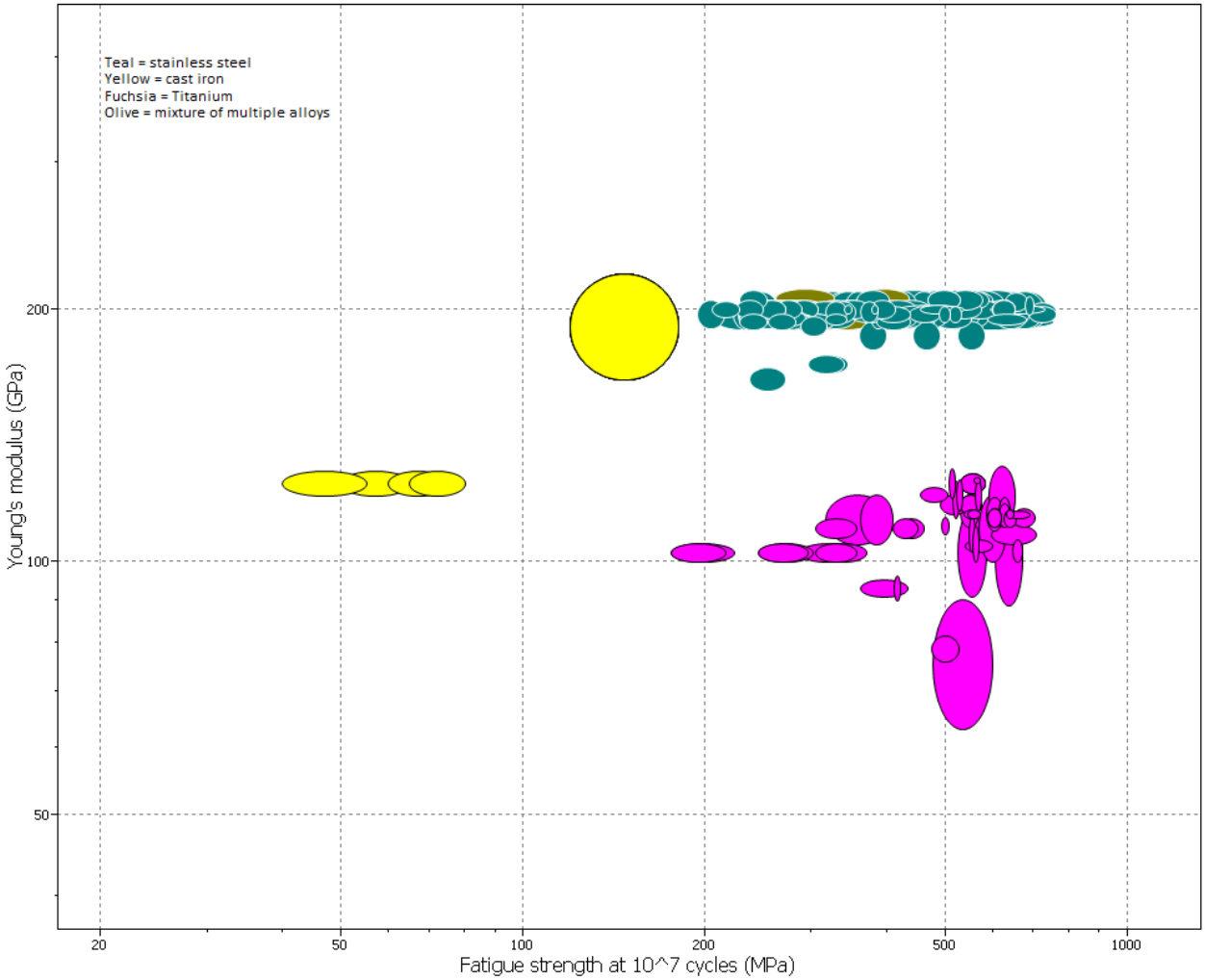

Figure 1.6b: Diagram from CES Edupack which compare Young's modulus to fatigue strength of different metals with limiters which state that the base material should consist of C, Fe, Al or Ti and the Poisson's ratio should be between 0.25 and 0.35. They also withstand fresh and salt water excellent.

1.6.1 Carbon, alloy and HSLA steel

The carbon steel has carbon as the major strengthening element and it is an alloy consisting of iron and carbon. These steels should according to the Iron and Steel Society contain up to 2% carbon with only a minority of other additives. Although there can be higher amounts of additions of deoxitation, like silicon (<0.6%), copper (<0.6%) or manganese (1.65%). The strengthening is done by solid solution, quench hardening or cold finishing. Three methods executed in different ways; In short solid solution strengthening is done by adding an element to a material where the element blends into the materials crystal lattice and hinder dislocation. Quench hardening can be performed if the carbon content is high

enough, it will then transform into a hard phase called martensite when rapidly cooled which contributes to the strengthening. Cold finishing contributes to increased strength by increased dislocation density and grain refinement. Usage of cold finished products should be when higher strength and tight dimension tolerance is wanted. This type of steel is also called amongst other things plain carbon steel or low-carbon steel and is used in products such as automobiles and in machine designs as structural members, housings, base plates etc. [7],[5]

Alloy steel is an accepted term for steels containing up to 1% carbon and a maximum alloying content below 5%. This means that alloy steels can have more than one major alloying element which contributes to complexity. Additives may be silicon, copper, manganese, aluminum, chromium, cobalt, molybdenum, nickel, titanium and others. See table 1.6a below for different elements and their contribution when used for alloying. Many elements are added to increase hardenability and some are added to increase corrosion resistance, improvement of machinability or physical properties. [7]

Table 1.6a. Alloying elements and their effects in carbon steel. [7]

	Typical Ranges in Alloy Steels (%)	Principal Effects
Aluminum	<2	Aids nitriding Restricts grain growth Removes oxygen in steel melting
Sulfur and phosphorus	<0.5	Adds machinability Reduces weldability, ductility, and toughness
Chromium	0.3–4	Increases resistance to corrosion and oxidation Increases hardenability (significant effect) Increases high-temperature strength Can combine with carbon to form hard, wear-resistant microconstituents
Nickel	0.3–5	Promotes an austenitic structure Increases hardenability (mild effect) Increases toughness
Copper	0.2–0.5	Promotes tenacious oxide film to aid atmospheric corrosion resistance
Manganese	0.3–2	Increases hardenability, lowers hardening temperature Promotes an austenitic structure Combines with sulfur to reduce its adverse effects
Silicon	0.2–2.5	Removes oxygen in steelmaking Improves toughness Increases hardenability
Molybdenum	0.1–0.5	Promotes grain refinement Increases hardenability Improves high-temperature strength
Vanadium	0.1–0.3	Promotes grain refinement Increases hardenability Will combine with carbon to form wear-resistant microconstituents
Boron	0.0005–0.003	Added in small amounts to increase hardenability
Lead	<0.3	Added only to aid machinability
Nitrogen	<0.1	Acts like carbon in strengthening

Elements that promote austenite formation: Mn, Ni, N, Co, Cu, C
Elements that promote ferrite formation: Cr, Mo, V, W, Ti, Zn, Cb, Ta, Si

These types of steel are produced to be heat treated structural components with properties like wear resistance, strength and toughness and they have application areas like shafts, gears and hand tools. [7]

HSLA is an abbreviation for high-strength low-alloy steel, a group which is also called micro alloyed steels due to that its chemical composition is "tailored" to have different mechanical properties. How this is done differs a lot just as the strengthening mechanisms used. General HSLA steels have low carbon content (0.2%) and their microstructure consists of the two phases ferrite and perlite. All HSLA steels also have a 1% manganese content to solid solution strengthen the ferrite. Additions of other elements to create other properties are also low, less than 0.5%. Copper for instance also solid solution strengthens the ferrite, but is added mostly due to that it improves the atmospheric corrosion resistance by forming a protective oxide film at the surface. Chromium, nickel and phosphorus can be added to assist the oxide film formation. The main attribute of this group is to keep the strength but to reduce the weight of structural applications like bridges. They are also intended where welding is a requirement due to its low carbon content, but as the strength of the HSLA steel gets higher the risk of welding problems increase.[7]

Table 1.6b. Data estimation intervals for different types of alloys in their respective group. Summarized from CES EduPack 2009, level 2.

Material group	Young's modulus [GPa]	Poisson's ratio	Fatigue strength at 10^7 cycles [MPa]	Tensile strength [MPa]	Yield strength [MPa]	Maximum service temp. [°C]	Minimum service temp. [°C]	Elongation [%]	Density [kg/m^3]	Price [SEK/kg]
High carbon steel	200 - 215	0.285 - 0.295	281 - 606	550 - 1640	400 - 1160	350 - 400	-73.2 - -33.2	7 - 30	7.8x10^3 - 7.9x10^3	5.86 - 6.44
Low carbon steel	200 - 215	0.285 - 0.295	203 - 293	345 - 580	250 - 395	350 - 400	-68.2 - -38.2	26 - 47	7.8x10^3 - 7.9x10^3	5.13 - 5.65
Low alloy steel	205 - 217	0.285 - 0.295	248 - 700	550 - 1760	400 - 1500	500 - 550	-73.2 - -33.2	3 - 38	7.8x10^3 - 7.9x10^3	6.53 - 7.18

1.6.2 Stainless steel

Stainless steel is a group of steels consisting of mainly iron and chromium, but also small additives of other elements to aid the purpose of the steel. To be labeled stainless the chromium content must be over 10% and in oxidizing environments the steel must experience passivity.

Their main purpose is to withstand different types of corrosion environments and that is enabled because of its high chromium content creates a protective oxide on the surface which works as a passive film. Measurements show that increased chromium content leads to decreased corrosion tendency. Stainless steels are grouped by the microstructure phase. They can be ferritic, martensitic, martensitic-austenitic, ferritic-austenitic (often called duplex stainless steels) and austenitic. [7]

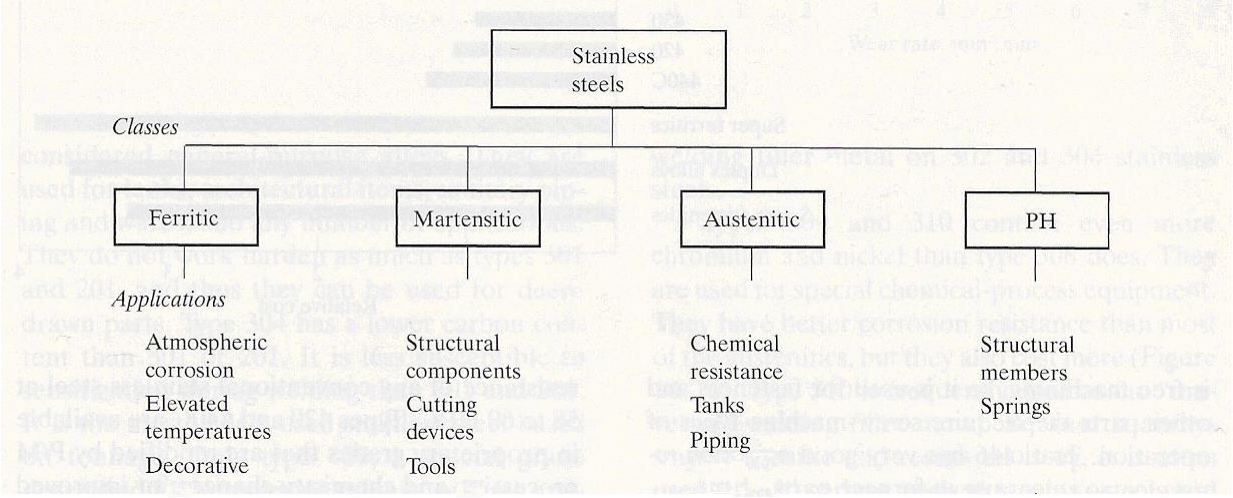

Figure 1.6c: Different classes of stainless steel and their application areas. [7]

The ferritic stainless steel structure consists of carbon content often less than 0.2% and chromium content between 16-20%. The microstructure is body-centered cubic (BCC) iron. Some stainless steels also have a small content of nitrogen and these stainless steels have ferritic structure at room temperature and all other temperatures up to the melting point. That is they do not undergo any crystal structure changes and they cannot be quenched hardened. There are some exceptions but otherwise this is the general behavior. Ferritic stainless steels experience notch sensitivity and due to embrittling phases and carbide precipitation formation during cooling from welding, ferritic stainless steels have poor weldability. The so called “475°C embrittlement phenomenon” decomposes ferritic steels into two different BCC structures which contributes to lower ductility and impact strength at temperatures between 343°C to 510°C. The carbide precipitation contributes to lowered corrosion resistance. On the other hand ferritic stainless steels manage stress corrosion cracking relatively good. Also ferritic structured stainless steels are a bit cheaper than the other structures. There are a group labeled special ferritics which have a low carbon and nitrogen content and consist mainly of a chromium content between 18-30% and a molybdenum content between 1-4%. They have properties like excellent corrosion resistance in sea water environments for example and they have relative immunity to stress corrosion tendencies. Also their weldability is improved compared to the other mentioned ferritic stainless steels. [7]

Martensitic stainless steels have carbon content up to 1.2% and the chromium content lies between 12-18%.

The higher carbon content contributes to martensite formation after first heating the steel and then quenching it. The high chromium content contributes to increased hardenability and enables martensitic structure at even lower carbon contents (0.07%). [7]

Austenitic stainless steels have the most complex nature compared to ferritic and martensitic. They consist of at least three different main alloying elements which are chromium, carbon and nickel. The content of the different elements are; chromium 16-26%, for nickel 8-24% and the carbon content is kept as low as possible but it should still have an influence. The nickel is added to stabilize the austenitic structure. Phase diagrams revel the austenite (and also ferrite) is the equilibrium structure for a nickel content of 8-10%. Austenitic stainless steels are often used in the annealing state which contributes to a metastable austenitic structure, but for normal condition temperatures the austenitic structure remains. By cold working or work hardening austenitic stainless steels, martensitic structure can be achieved due to the energy from the deformation encourage transformation of the metastable austenite. Austenitic stainless steels are the best to combine corrosion resistance and fabricabillity. For fatigue applications though, austenitic stainless steels are not recommended. [7]

Most duplex alloys compositions consist of 20-30% chromium, around 5% nickel and less than 0.003% carbon. The first two elements are of great importance for the structures in the stainless steel group, but for duplex stainless steels there are also other elements that contribute to a structure of up to 50% ferrite in austenitic structure. Elements added for ferrite formation are Cr, Si, Mo, V, Al, Ti, W and for austenite formation Ni, Co, Mg, Cu, C, N which are austenite stabilizers. Why a ferritic-austenitic alloys first where desirable was to decrease the amount of hot cracking. This combination can also contribute to increased yield strength, up to twice as much as for an all-austenitic structure. Other property improvements are increased resistance against stress corrosion and increased weldability. More modern duplex steels have a 0.12% nitrogen content to help balance the corrosion differences between the two phases and have the amount of ferrite and austenite in the interval 40%-60%. Their stress corrosion cracking resistance is not 100% and accelerated attacks can arise in certain environments due to the ferrite phase existence. [7]

Table 1.6c. Corrosion resistance for different alloys. [7]

AISI Type	UNS Number	Mild-Atmospheric and Fresh Water	Atmospheric			Chemical		
			Industrial	Marine	Salt water	Mild	Oxidizing	Reducing
201	S20100	×	×	×	—	×	×	—
202	S20200	×	×	×	—	×	×	—
205	S20500	×	×	×	—	×	×	—
301	S30100	×	×	×	—	×	×	—
302	S30200	×	×	×	—	×	×	—
302B	S30215	×	×	×	—	×	×	—
303	S30300	×	×	—	—	×	—	—
303 Se	S30323	×	×	—	—	×	—	—
304	S30400	×	×	×	—	×	×	—
304L	S30403	×	×	×	—	×	×	—
304Cu	S30430	×	×	×	—	×	×	—
304N	S30451	×	×	×	—	×	×	—
305	S30500	×	×	×	—	×	×	—
308	S30800	×	×	×	—	×	×	—
309	S30900	×	×	×	—	×	×	—
309S	S30908	×	×	×	—	×	×	—
310	S31000	×	×	×	—	×	×	—
310S	S31008	×	×	×	—	×	×	—
314	S31400	×	×	×	—	×	×	—
316	S31600	×	×	×	×	×	×	×
316F	S31620	×	×	×	×	×	×	×
316L	S31603	×	×	×	×	×	×	×
316N	S31651	×	×	×	×	×	×	×
317	S31700	×	×	×	×	×	×	×
317L	S31703	×	×	×	×	×	×	—
321	S32100	×	×	×	—	×	×	—
329	S32900	×	×	×	×	×	×	×
330	N08330	×	×	×	×	×	×	×
332	S33200	×	×	×	—	×	×	—
334	S33400	×	×	×	—	×	×	—
347	S34700	×	×	×	—	×	×	—
348	S34800	×	×	×	—	×	×	—
384	S38400	×	×	×	—	×	×	—
403	S40300	×	—	—	—	×	—	—
405	S40500	×	—	—	—	×	—	—
409	S40900	×	—	—	—	×	—	—
410	S41000	×	—	—	—	×	—	—
414	S41400	×	—	—	—	×	—	—
416	S41600	×	—	—	—	—	—	—
420	S42000	×	—	—	—	—	—	—
420F	S42020	×	—	—	—	—	—	—
422	S42200	×	—	—	—	—	—	—

Stainless steels conductivity of heat and electricity is not that good compared to carbon steels and stainless steels with austenitic structure are not ferromagnetic. The mechanical properties of stainless steel are their best properties and with them they can manage multiple structural applications. Some of them are piping, pumps, valves, and pressure vessels etc which require properties like good strength, toughness and formability. However there are limitations for stainless steels because in certain types of environments some types cannot withstand corrosions of type pitting, crevice or stress. Their performance is best in oxidizing environments. For high-strength applications precipitation hardening (PH) stainless steels are of the chosen. There are different types which have structures like martensitic, semiaustenitic or austenitic. They have low carbon content and varying chromium-nickel ratios with chromium having the largest share. Their tensile strength can be as high as 1880MPa, but still possess good toughness and resistance against crack propagation. Their corrosion resistance is general better than for ferritic and martensitic stainless steels and they can almost keep the level of austenitic stainless steels. The wear resistance off these stainless steels is not that good due to their low carbon content. [7]

Table 1.6d. Data estimation intervals over all groups of stainless steels. Summarized from CES EduPack 2009, level 2.

Material group	Young's modulus [GPa]	Poisson's ratio	Fatigue strength at 10^7 cycles [MPa]	Tensile strength [MPa]	Yield strength [MPa]	Maximum service temp. [°C]	Minimum service temp. [°C]	Elongation [%]	Density [kg/m^3]	Price [SEK/kg]
Stainless steels	189 - 210	0.265 - 0.275	175 - 753	480 - 2240	170 - 1000	750 - 820	-272 - -271	5 - 70	$7.6x10^3$ - $8.1x10^3$	52.8 - 58.1

The most important property of any steels is its high Young's modulus which makes it the stiffest and most useful metal in engineering. [7]

1.6.3 Cast iron

When different parts may need large amount of machining to get its right shape casting should be investigated due to economic reasons. This also applies if a large amount of the parts is needed. There are five different groups of cast iron; gray, malleable, ductile, white and alloy cast iron. The cast iron group consists of alloys containing iron, carbon and silicon as a base. The carbon content (which is often higher than 2%) is higher than what is possible to solid solute which leads to a presence of graphite or iron carbides in the alloys. [7]

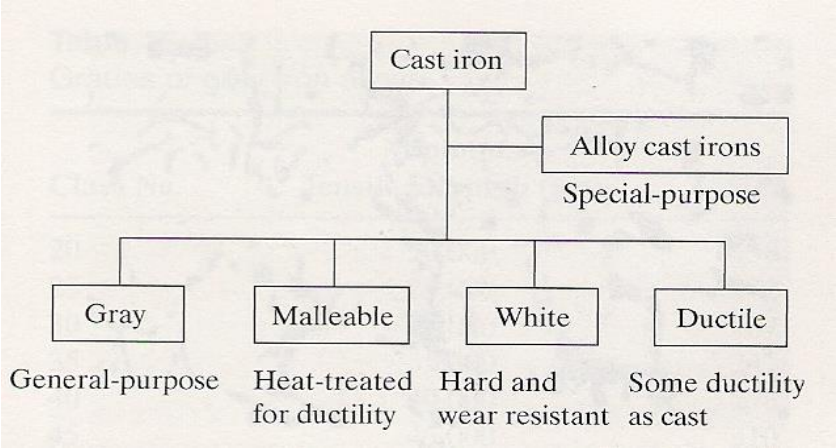

Figure 1.6d: Different types of cast iron their application areas. [7]

Gray cast irons have high carbon content between 2-4% and the silicon content is at least 1%. The silicon content aids the formation of graphite. The microstructure is often a matrix which has a ferritic, pearlitic or martensitic phase with 3D graphite roses in it (2D flakes when studying the surface).

The different matrix phases will contribute to different strength levels of the gray iron. Ferrite aids low strength, perlite aids higher strength and martensite aids high strength. The flakes will contribute to different properties in the iron depending on shape, size and distribution. The different grades of gray iron have an in common tensile strength interval spanning from 138MPa to 414MPa. Some of gray irons properties like thermal conductivity are similar to plain carbon steels due to gray iron is “simply” steel with graphite in it. The graphite affect other properties like damping capacity which is why gray iron is used as machine bases due to the elastic deflection and vibration resistance. Also the electrical resistivity is dependent on the graphite, coarser structure have higher resistivity. Gray cast iron has generally better corrosion resistance than carbon steels in most environments because the graphite emerges on the surface when the matrix dissolves in certain environments. This leads to a protective film on the surface reducing the rate of attack. Data for gray irons yield strength is hard to find because this group is brittle leading to that the yield strength is almost the same value as the tensile strength. This contributes to poor toughness. Loading cases which exert tensile loading on the parts should avoid usage of gray iron, this is also true for shock loading and stress concentration cases. If compressive strength is instead exerted on the parts then gray cast iron is a good alternative. Fatigue properties of gray cast iron are typically around 40% the tensile strength. One great quality of the gray cast iron is its wear resistance and is therefore often used in gear applications. It is the graphite which contributes to the good metal-to-metal wear resistance due to its lubrication quality. [7]

White irons are very hard and brittle and consist of perlite and free cementite, no graphite formation. The name white iron refers to its fracture surface appearance and the same is true for gray iron. Its chemical composition consists of carbon content between 2-4%, silicon between 0.5-2% and around 0.5% manganese. It structure is formed when gray iron is rapidly cooled (then called chilled-iron). This cast iron is used for rolls, wear plates and balls which have varied wear resistance and are important engineering designs. Then when alloying elements are added the same structure is generated but in heavy sections. Depending on the element addition these cast irons have grades of a wide range of properties. Some are good for corrosion resistance, some for oxidation resistance, some for creep strength etc. [7]

Malleable cast iron is made amongst others of white irons which have been transformed into a ferrite or perlite matrix. Malleable cast iron has a similar chemical content as the gray cast iron but there is a change in its structure to make it more ductile. This is done by time consuming thermal treatments. Depending on which strength level is desired the castings can be cooled in air or quenched in oil. The structure achieved is either perlite and temper carbon or ferrite and temper carbon. A majority of malleable iron properties are similar to gray iron properties. Tough the most important difference in properties is the ductility. It is possible to bend malleable iron without it breaking and impact loads is manageable. The tensile strength of the two structures mentioned above lies around 365MPa for the ferrite and up to 689MPa for the perlite. The Young’s modulus for malleable iron is almost as high as for steels. The wear resistance is good and the fatigue strength of malleable iron can be up to 60% of the tensile strength. [7]

Ductile irons have nodular or spheroidal graphite in its structure. They consist of temper carbon as for malleable iron. Ductile iron was created to avoid the brittleness of gray and white iron and to gain the ductility of malleable iron without the long processing. The chemical composition consist of a carbon content in an interval from 3-4%, silicon content between 2-3% and most of them also have a significant nickel content. The composition is close to gray iron and to avoid flake formation of the graphite and instead get nodular shape, magnesium or cerium is added. Other elements can also be added to control the size the nodule and achieve spherical shaped graphite in a matrix with ferritic, pearlitic or martensitic phase. The phase is controlled by melt chemistry and process controls. Ductile irons properties, except for ductility similar to malleable iron, are low electrical resistivity, wide range of tensile strengths in the different grades and a fatigue strength which is 40-50% of the tensile strength. The corrosion resistance is similar to grey cast irons resistance. [7]

Alloy irons are a variation of gray or white irons which have additions of different elements to increase hardness or corrosion resistance. [7]

Table1.6e. Properties of different groups of cast iron. [7]

Material	Tensile[a] Strength, ksi	Yield Strength, ksi	Compressive[a] Strength, ksi	Percent Elongation %	Modulus[b] of Elasticity, 10^6 psi	HB[c]	Minimum[d] Casting Section, in. (mm)	Characteristics
Gray iron—ASTM A 48								
Class 20	20	—	95	Nil	12	175	0.125 (3.1)	Good for thin sections and low-strength castings
Class 35	35	—	135	Nil	16	200	0.187 (4.7)	For structural parts, pumps, pipes, bases, etc.
Class 40	40	—	135	Nil	18	210	0.250 (6.3)	For medium-strength castings; can be hardened
Ductile iron—ASTM A 536								
Grade 5								
60-45-18	60	45	120	18	25	175	0.187 (4.7)	Excellent mechanical properties; can tolerate bending
Grade 3								
80-55-06	80	60	160	6	25	235	0.187 (4.7)	High strength, some ductility; hardenable
Malleable iron								
ASTM A 47-77 Grade 32510	50	32	208	10	26	125	0.125 (3.1)	Ferritic, free from casting strains
ASTM A 220-76 Grade 60004	80	60	240	3	26	225	0.125 (3.1)	Pearlitic, free from casting strains; hardenable
White iron								
ASTM A 532								
Grade A, Nitr–HiC	45	—	—	Nil	25	550	0.250 (6.3)	Extreme abrasion resistance; grinding balls, slurry pumps, etc.
Steel castings								
ASTM A 27								
Grade 60-30	60	30	50	24	30	156	0.250 (6.3)	For high stiffness, shock loading, and for welded fabrications

[a]1 ksi = 6.89 MPa. [b]1 psi = 6.89 kPa. [c]Brinell hardness. [d]Increases for large castings.

Cast irons properties differ significantly over a wide span, due to each grade is made to manage within a certain area better than the others. This is achieved with the different chemical contents contributing to different microstructures and the thermal treatments that follow. [7]

Table 1.6f. Data estimation intervals for the two most different groups in the cast iron family. Summarized from CES EduPack 2009, level 2.

Material group	Young's modulus [GPa]	Poisson's ratio	Fatigue strength at 10^7 cycles [MPa]	Tensile strength [MPa]	Yield strength [MPa]	Maximum service temp. [°C]	Minimum service temp. [°C]	Elongation [%]	Density [kg/m^3]	Price [SEK/kg]
Gray cast iron	80 - 138	0.26 - 0.28	40 - 170	140 - 448	140 - 420	350 - 450	-150 - -50	0.17 - 0.7	$7.05x10^3$ - $7.25x10^3$	4.61 - 5.07
Ductile cast iron	165 - 180	0.26 - 0.28	180 - 330	410 - 830	250 - 680	350 - 450	-98.2 - -38.2	3 - 18	$7.05x10^3$ - $7.25x10^3$	5.05 - 5.56

1.6.4 Aluminum alloys

Aluminum enables large structures due to its light weight, and is also used for architectural components because it does not rust in atmospheric environments. It is also used in machine design as a variety of structural components. Aluminum can therefore be a choice to steel when these properties are desired as well as a better conductor of heat and electricity. Aluminum has also a high ductility which makes it easy to shape and machine. The usage area for aluminum and its alloys is wide, from food packaging to airplanes. Grouping the alloys is done by how it is machined; wrought or casted. Then in its respective subgroup they wrought alloys are divided into smaller groups denoted with a four digit number code which indicates the major alloying element. There can also be a letter after the code indicating different types of tempers. The same principle is true for cast alloys although their number code gives a bit more information about the alloying elements and which product form it has. Alloying elements can be added to the aluminum in its liquid state but only a few percent of the alloying elements is solid soluted. Instead the formation of intermetallic compounds arises in the aluminum, creating an own phase. For the aluminum alloy to be useful the alloying content should not overcome 15%. These limitations enables precipitation hardening which can briefly be described as a process when an alloying element precipitates and form a compound together with the host material, this causes strains in the host materials lattice and that contributes to strengthening of the alloy. Depending on alloying element they can contribute to solid solution strengthening, improved machinability and corrosion resistance. Below in figure 1.6e different alloying elements can be seen and their effects. [7]

Alloying Element	Effects
Iron	Naturally occurs as an impurity in aluminum ores; small percentages increase the strength and hardness of some alloys and reduce hot-cracking tendencies in castings; reduces pickup in die-casting cavities.
Manganese	Used in combination with iron to improve castability; alters the nature of the intermetallic compounds and reduces shrinkage; the effect on mechanical properties is improved ductility and impact strength.
Silicon	Increases fluidity in casting and welding alloys and reduces solidification and hot-cracking tendencies; additions in excess of 13% make the alloy extremely difficult to machine; improves corrosion resistance.
Copper	Increases strength up to about 12%, higher concentrations cause brittleness; improves elevated temperature properties and machinability; concentrations over 5% reduce ability to hard coat.
Magnesium	Improves strength by solid solution strengthening, and alloys with over about 3% (0.5% when 0.5 % silicon is added) will precipitation harden; aluminum–magnesium alloys are difficult to cast because the molten alloy tends to "skin-over" (dross) in contact with air.
Zinc	Lowers castability; high-zinc alloys are prone to hot cracking and high shrinkage; percentages over 10% produce tendencies for stress corrosion cracking; in combination with other elements, zinc promotes very high strength; low concentrations in binary alloys (<3%) produce no useful effects.
Chromium	Improves conductivity in some alloys, and in small concentrations (<0.35%) it acts as a grain refiner.
Titanium	Naturally occurs as an impurity in aluminum ores, but it is intentionally added to some alloys as a grain refiner.
Lead/Bismuth	Added to some alloys to improve machinability; 2011 and 6062 are screw machine alloys containing Pb and Bi.
Zirconium	Used as a grain refiner in some aerospace alloys.
Lithium	Added to some aerospace alloys (Space Shuttle fuel tanks) to reduce weight. These alloys need a protective atmosphere when being cast.

Figure 1.6e: Elements and their effect in aluminum.[7]

Aluminum alloys should withstand atmospheric corrosion for indefinite time periods as mentioned above. Their corrosion resistance against outdoor environments depends on the chemicals in the air. Immersion in saltwater or salty sprays all aluminum alloys are attacked by corrosion, the corrosion rate in salty air is on the other hand extremely low. Seawater contributes to stress corrosion cracking but also pitting. About aluminum and water in general it can be said that it is water resistant in an interval of pH from 4.5 to 8.5. The purer the aluminum the better the corrosion resistance it will possess, valid for almost all corrosion environments. If the alloying additions consist of a significant amount of copper, silicon, zinc or magnesium the aluminum alloys are susceptible to stress corrosion cracking. [7]

The Young's modulus of aluminum is lower than for steels which are seen figure 1.6a. This must be taken into consideration when substituting steel in structural components as mentioned above. Small amount of lithium can be added to increase the Young's modulus, but it can have a negative effect of the toughness and ductility. Another option may be a composite with an aluminum matrix. The aluminum composite will increase the stiffness, and the tensile strength up to three times as much as regular aluminum, although this is not a cheap alternative. The tensile strength for different aluminum alloys varies between 90MPa to 676MPa. [7]

Table 1.6g. Data estimation intervals of different types in the aluminum alloy groups. Summarized from CES EduPack 2009, level 2.

Material group	Young's modulus [GPa]	Poisson's ratio	Fatigue strength at 10^7 cycles [MPa]	Tensile strength [MPa]	Yield strength [MPa]	Maximum service temp. [°C]	Minimum service temp. [°C]	Elongation [%]	Density [kg/m^3]	Price [SEK/kg]
Cast aluminum alloys	72 - 89	0.32 - 0.36	32 - 157	65 - 386	50 - 330	130 - 220	-273 -	0.4 - 10	$2.5x10^3$ - $2.9x10^3$	13.8 - 15.1
Wrought aluminum alloys	68 - 72	0.32 - 0.36	42 - 160	70 - 360	30 - 286	130 - 220	-273 -	2 - 41	$2.5x10^3$ - $2.9x10^3$	13.0 - 14.3
Wrought aluminum alloys (age - hardened)	68 - 80	0.32 - 0.36	57 - 210	180 - 620	95 - 610	120 - 200	-273 -	1 - 20	$2.5x10^3$ - $2.9x10^3$	12.4 - 13.7

1.6.5 Titanium alloys

Titanium is a light weight metal, but the major difference between titanium and other light weight metals (ex. aluminum, magnesium) is that it is much stiffer. This is seen in figure 1.6a. Titanium alloys are divided in different phases; alpha, alpha-beta, beta and closed to alpha and beta. [7]

Commercially pure titanium is strengthened by interstitial solid solution for example with carbon, oxygen and nitrogen, due to that quenching has no effect on titanium. The different types of titanium alloys have increasing amount of additives which leads to difference in strength levels. Titanium does not solid solute well in other metals but have a tendency of instead forming brittle intermetallic compounds. That is why titanium is not a choice for fusion welding because it forms intermetallic compounds in the fused zone which are brittle as glass. On the other hand these compounds can be used in P/M techniques. Pure titanium and titanium alloys also tend to form these compounds when welded in air or to another metal, so welding must take place in vacuum or in an inert gas. [7]

Alpha-phase titanium has a hexagonal closed-packed crystal structure which corresponds to the crystal structure form pure titanium at room temperature. These are often solid solution strengthened with aluminum, tin, nickel and copper as additives. This group cannot either be quench hardened, but its strength level is higher than commercially pure titanium. [7]

At about 882°C the pure titanium structure changes into a body-centered cubic structure. This is the beta-phase titanium. The alloys are made by adding beta stabilizing elements like molybdenum and vanadium which stabilize the beta structure even at room temperature. These alloys have, when not heat treated, good ductility and formability. If age hardening the beta alloys, very high strengths can be achieved but the ductility and the toughness is reduced. [7]

Alpha-beta alloys consist of one part alpha phase and one part beta phase. They are made by adding molybdenum, vanadium, columbium and tantalum to promote and stabilize the beta phase at room temperature. To strengthen this alloy, solution treating can be performed. First the alloy is heated turning everything into beta phase. Then it is rapidly cooled to room temperature causing some of the beta phase to be metastable. That is, it wants to convert to alpha phase but the water quench prevents it which contributes to strengthening. Increased strength and hardness can be obtained with aging when alpha phase precipitates from the metastable beta phase. The alpha-beta alloys have varying strength. [7]

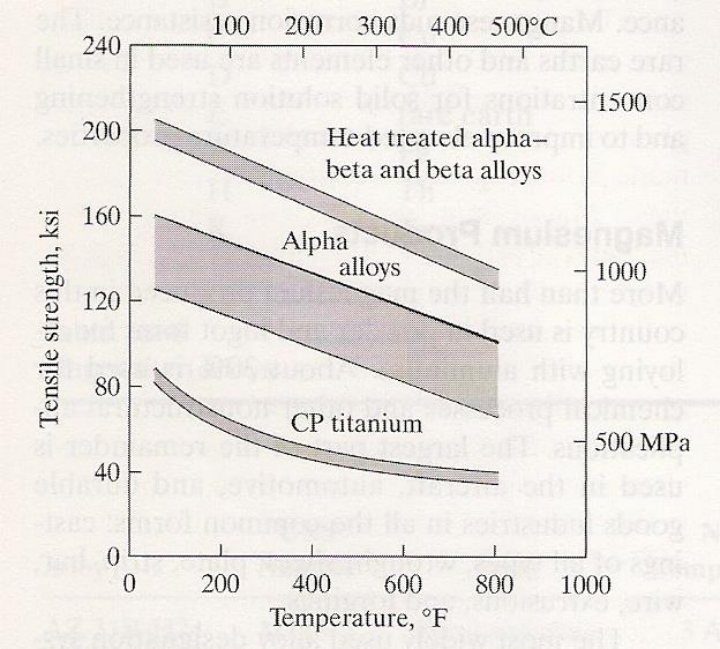

Figure 1.6f: tensile strength vs. temperature of titanium alloys. [7]

The corrosion resistance of titanium and titanium alloys is excellent against seawater and aqueous chloride solutions over a broad interval of temperature and concentrations. For best corrosion resistance pure grade should be chosen and this can also be combined with higher strength. [7]

Machinability of pure titanium is manageable but the hardness, often around 30 HCR, of the titanium alloys makes it difficult to machine. Also all alloys have low wear resistance, including abrasion, metal-to-metal wear and sold particle erosion. On the other hand the resistance against liquid erosion and cavitation is very good. [7]

One of many applications of titanium is aircrafts due to their strength and fatigue resistance. They are also used in tanks, piping systems, duct work etc due to their corrosion resistance. [7]

Table 1.6h. Data estimations intervals pure commercially pure titanium and all alloys combined. Summarized from CES EduPack 2009, level 2.

Material group	Young's modulus [GPa]	Poisson's ratio	Fatigue strength at 10^7 cycles [MPa]	Tensile strength [MPa]	Yield strength [MPa]	Maximum service temp. [°C]	Minimum service temp. [°C]	Elongation [%]	Density [kg/m^3]	Price [SEK/kg]
Commercially pure titanium	100 - 105	0.35 - 0.37	200 - 300	450 - 650	270 - 600	400 - 450	-273 -	5 - 25	$4.50x10^3$ - $4.52x10^3$	468 - 515
Titanium alloys	110 - 120	0.35 - 0.37	589 - 617	800 - 1450	750 - 1200	450 - 500	-273 -	5 - 10	$4.40x10^3$ - $4.80x10^3$	544 - 598

1.7 Seals

The main function of seals of any kind is to prevent leakage of a certain medium from one side of the seal to the other. The medium is either gas, liquid or semisolid. There are different types of seals and they are divided thereafter. They can be in contact with the parts to be sealed or in no contact at all. They can be static or dynamic and they can be radial or axial seals. A radial seal is a small column placed between the shaft and its corresponding hole. An axial seal is circular.

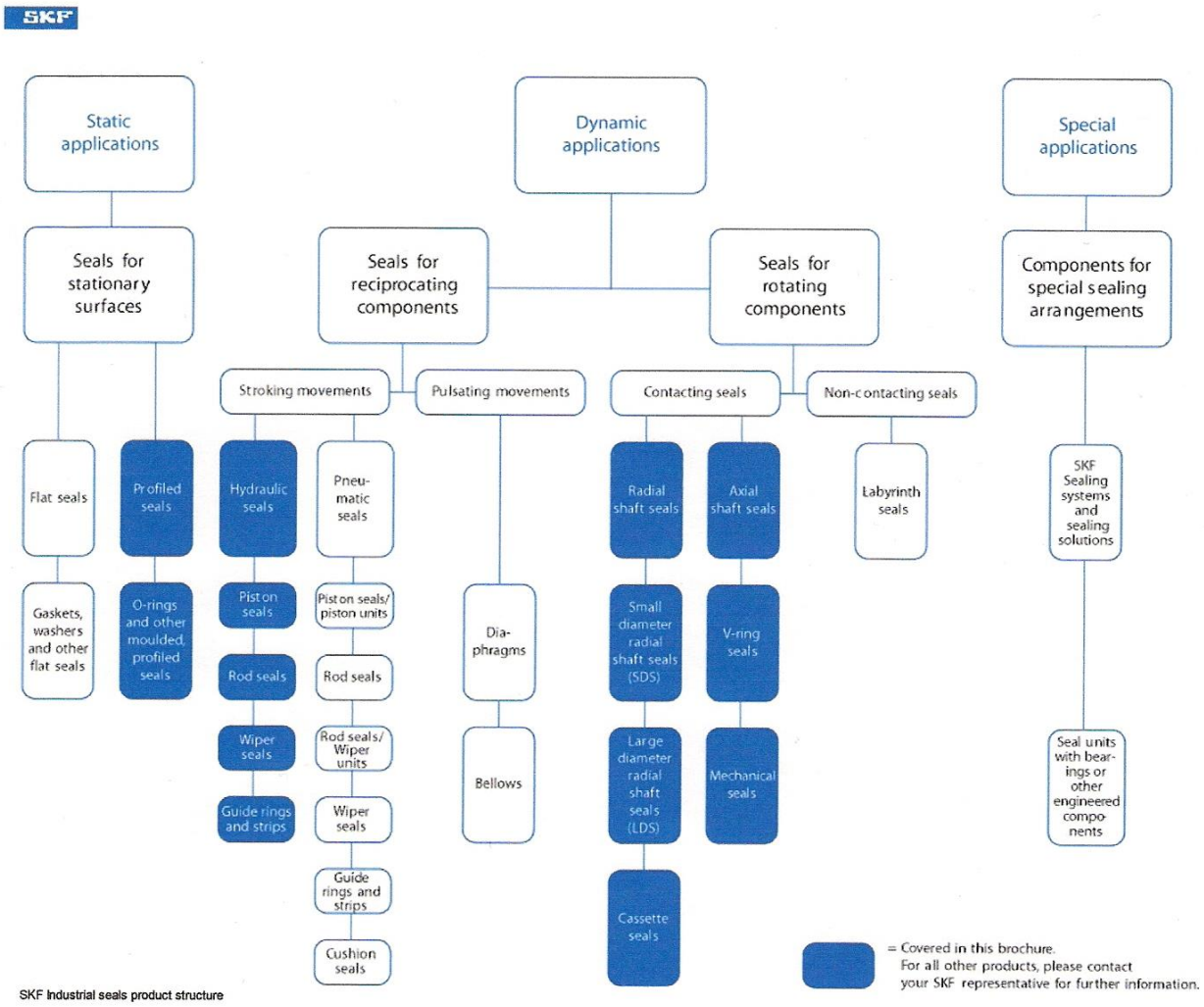

Figure 1.7a: Different types of seals [8]

Another way of dividing the different seals can be seen in figure 1.7a. It gives an impression concerning the enormous amount of different kinds of seals there are to be able to satisfy all different cases which need sealing.

The demand of sealing ability asked of the seals varies from situation to situation. Some allow minor controlled leakage and some need complete sealing. The higher demands the seal need to achieve almost always leads to increased friction which contributes to energy losses and wear. [9]

Some seals for usage concerning water proofing are mentioned in the following text. Elastomeric seals consist of at least one soft part made from rubber or plastic which will deform under pressure and seal the space between the shaft and the surrounding. This group has a lot of different types and application areas. They are often combined with some type of lubricant which implies as well as ability of complete sealing that one important property of these seals is their surface structure. It cannot be too rough or have too much pattern, if it does not contribute to providing lubricant, due to risk of leakage. The o-ring is one of the most common used seals today. It is simply a ring in the shape of the letter o. They are often made from rubber but there are some made from metal. The o-ring is positioned around the shaft and inside a slit of the surrounding housing. The o-ring deforms when placed in its position and causes sealing in the slit. [9]

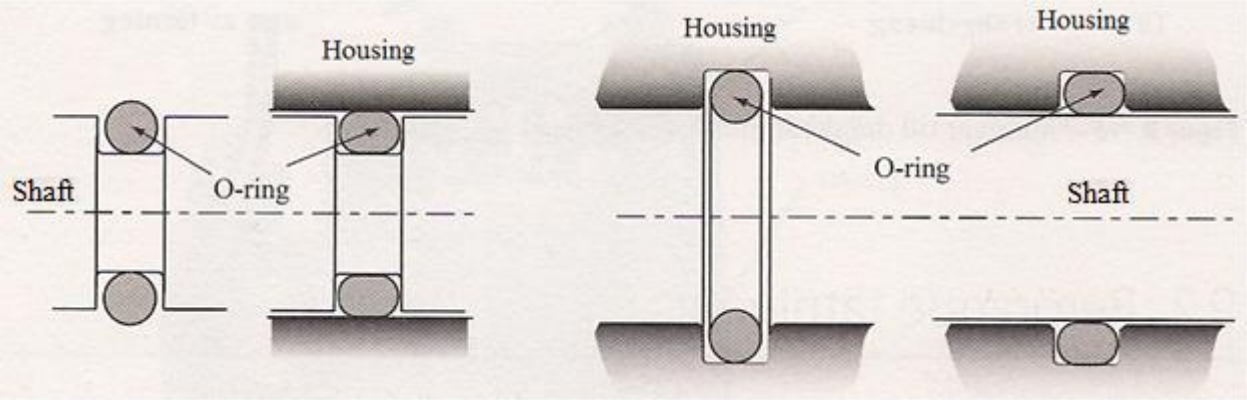

Figure 1.7b: Different positions of the o-ring, both in undeformed and deformed case [9]

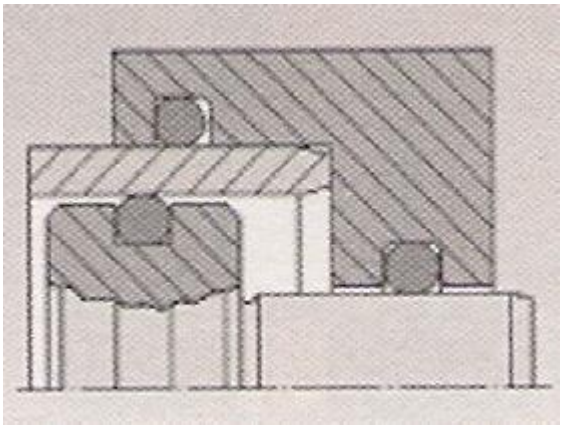

Figure 1.7c: System with multiple o-rings. [9]

It is used for radial as well as for axial sealing, both for rotating and static cases. The QUAD-ring works in the same way as the o-ring except the QUAD-ring have an x shaped cross-section instead of the o-rings circular. This layout promotes usage for forward and backward cycles without torsion. [9]

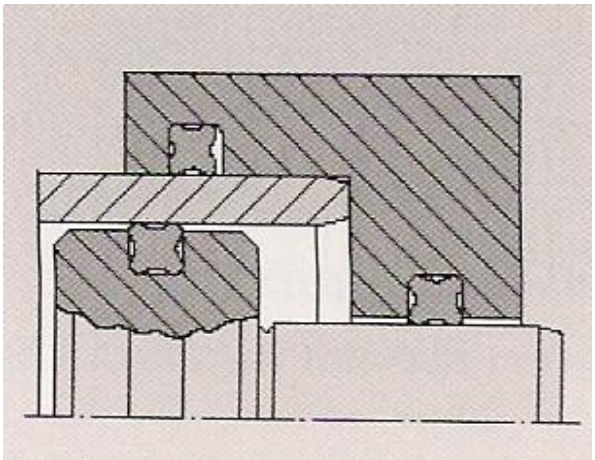

Figure 1.7d: System with multiple QUAD-seals. [9]

Lip seal is another kind of seal that have a soft part (the lip) which will press against the shaft or the housing depending on the positioning. The lip will prevent the media from passing. The higher pressure the lip withstands the better sealing it does, but the friction also increases. This type of seal is often used for rotating shafts, but can almost only manage rotation in one direction. [9]

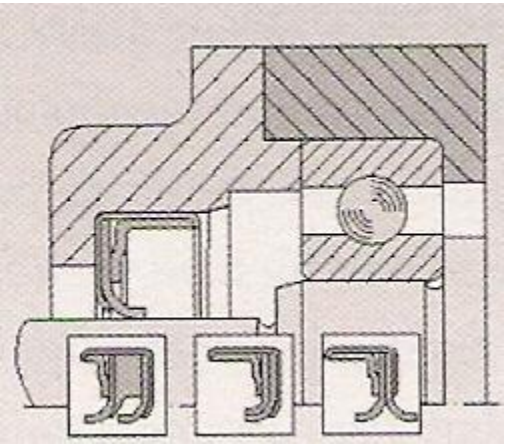

Figure 1.7e: System with lip seals and also shows different layouts of lip seals. [9]

Gaskets are another seal alternative, which consists of impregnated textiles that should enhance the sealing ability and lower the friction. These are often used to seal different applications from water like pump houses etc. To get the gasket to stay in its position and fulfill the sealing a gland is used to press and secure it. The harder the gland press the better the gasket seals, but just as for the other types of seals the friction will increase. [9]

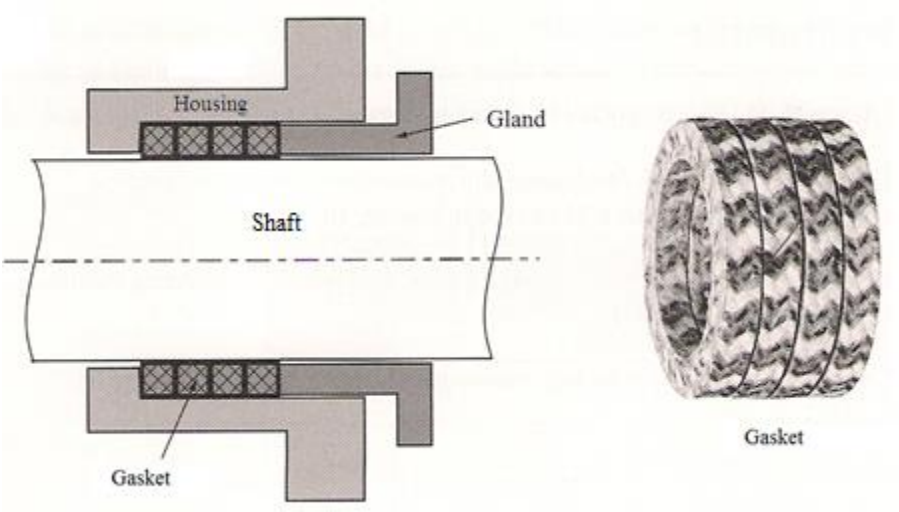

Figure 1.7f: Show the positioning of the packing and gland and also a real packing. [9]

These different groups have a broad range of material selection to be able to meet the specific case requirements like environment demands. They also are made in different shapes and sizes and can be custom made if required.

2. Experimental

2.1 Conditions

2.1.1 Geometric

The parts of the concept were created and are described in the second report regarding this subject, *"Water jet steering concept – evaluation of an environmental design, Part 2"*. Locked 3D models of a 125-model were received by Rolls-Royce which was re-created in Pro Engineer to enable getting measurements and angle evaluation. A 125-model insinuates that the pump housing have a diameter of 1250mm. The geometric conditions are illustrated in this report only for an understanding purpose to the rest of the work in this report.

The movements needed to be controlled were:

1. Opening and closing the reversal bucket, causing a deflection angle of 45° in fully opened mode.
2. Controlling the steering unit and making it turn 30˚ in each direction.

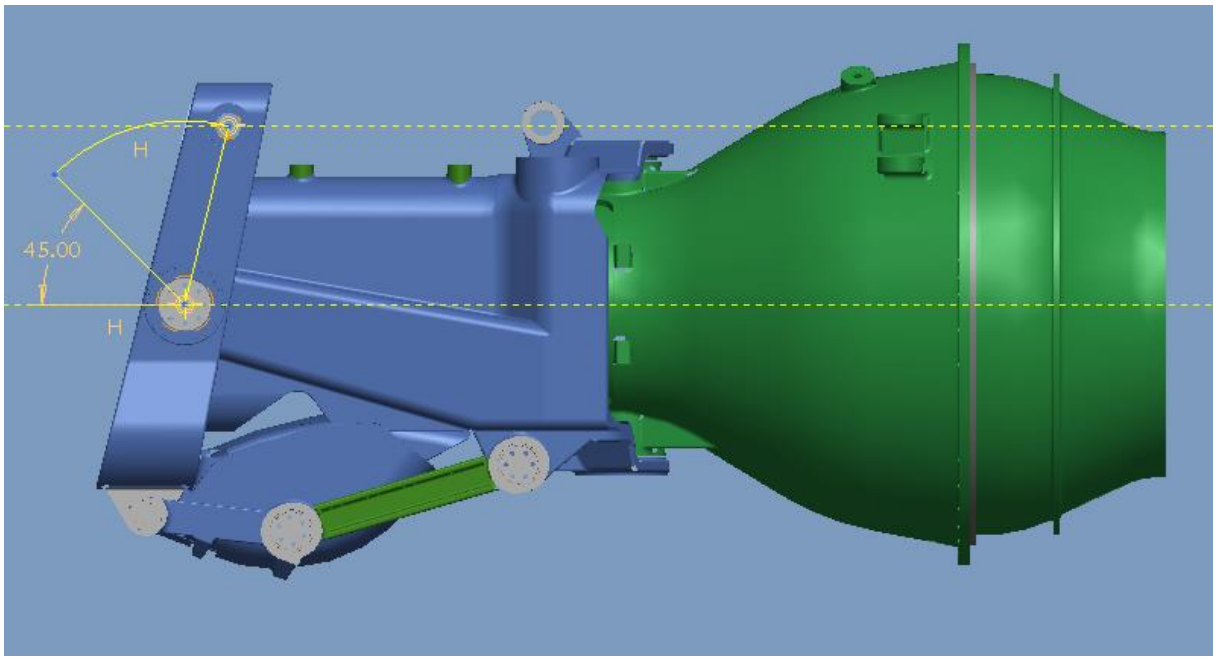

Figure 2.1a: Side view of the Kamewa water jet. Illustration of the motion when opening and closing the reversal bucket according to description 1 above. In the figure the bucket is closed. [10]

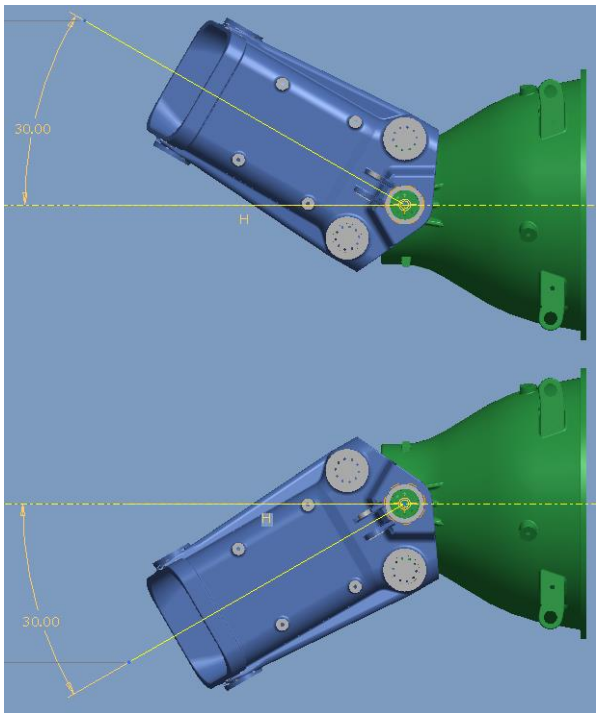

Figure 2.1b: Top view of the water jet. Illustration of the second main function described in 2. [10]

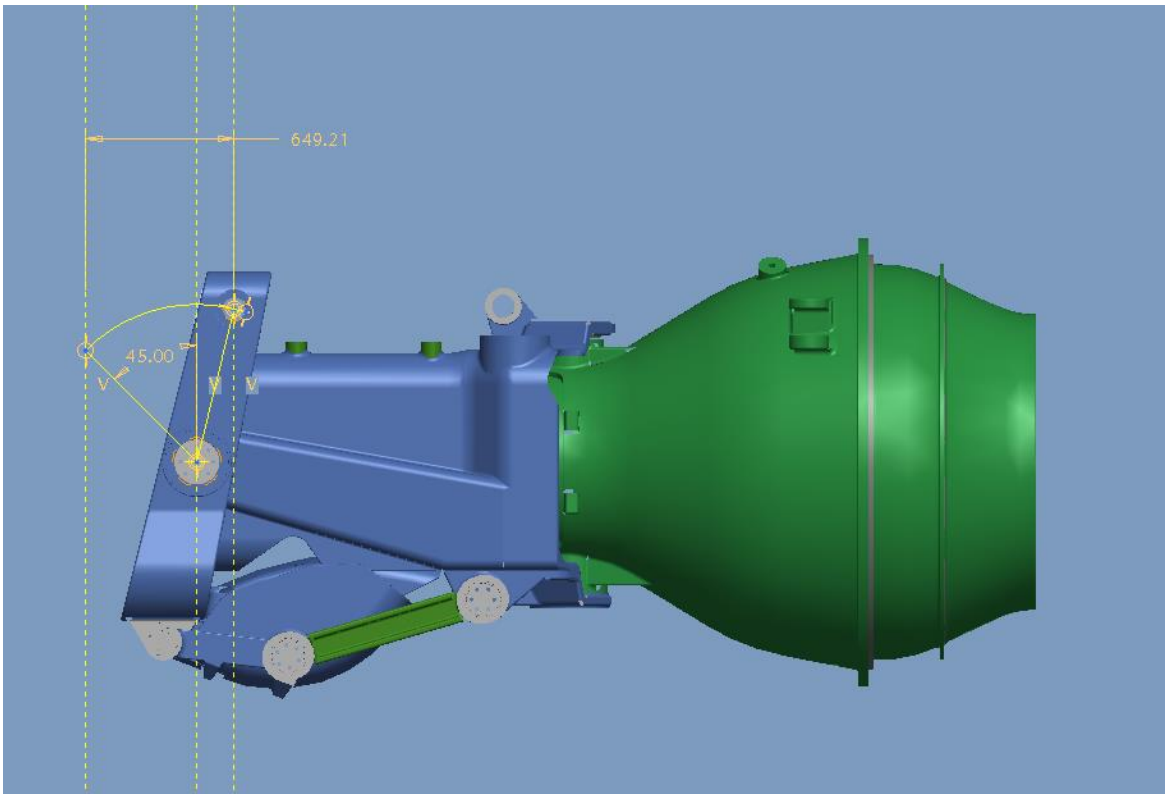

Figure 2.1c: The distance from the closed position to the open position of the reversal bucket. It measures approximately 650mm. [10]

2.1.2 Material

The material selection process would have great impact on the end result. The following material limiters where identified in the attached project specification [1] and from the diagrams in diagram 3.2a under 3.2 *Simulation* provided by Rolls-Royce.

- Mechanical properties; the application cannot weigh too much. Even on those components that the forces remain unaffected the bulk material needs to withstand the load and also pass the demands on fatigue life and so on.

- Environment; since the application is used to maneuver a water jet on boats that operate in seawater environment, issues like corrosion and temperature are key parameters. For example the corrosion issue limits the usage of non-metallic components that might electrically isolate one part from another resulting in a more rapid corrosion process. And if a metallic material is used it has to have good corrosion properties so the lifespan will be of acceptable length. Since the temperature range, some materials can experience embrittlement in the lower regions of the temperature span. This is off course a much undesired feature of the material chosen due to the fact that embrittlement will result in sudden fracture of the component.

- Price; There is a balance between superior performance and a higher price compared to a product with inferior performance and lower price and what the market is prepared to pay for the higher performance. The natural goal of the material selection is achieving a high performance-cost ratio that meets the other material requirements.

2.1.3 Demands

Other demands written in the project specification from Rolls-Royce [1].

Environmental:

- *Ambient water temperature.* Operating in ambient seawater with temperatures ranging between -4°C to +35°C.

- *Cooling water temperature.* Maximum temperature of +60°C.

- *Air temperature inboard.* In the machinery space between 0°C to 55°C.

- *Air temperature outboard.* Ambient air temperature between -25°C to 45°C.

- *Humidity inboard.* Up to 100%.

- *Humidity outboard.* Fully submerged in fresh or salt water at given temperature ranges.

Design:

- *Design oil temperature.* From -20°C to 70°C
- *Fire.* Piping system material should be compatible with the conveyed fluid with regard to the risk of fire.
- *Accidents.* The machinery should be designed and installed so if fire, explosions, accidental pollution, leakage or other accidents occur the damage will be acceptably low.

Number of loading cycles in all types of seas:

- *Corrective steering (5°),* $N_{corrective\ steering}$*.* Assuming a corrective steering cycle of 20 seconds, 12 hours/day for 25 years gives $N_{corrective\ steering} = 1.97x10^7$ cycles.
- *Full steering (30°),* $N_{full\ steering}$*.* Assuming full steering 40 hours/year for 25 years gives $N_{full\ steering} = 1.73x10^5$ cycles.
- *Reversing,* $N_{reversing}$*.* Assuming a maximum reversing load for 20 times/day for 25 years gives $N_{reversing} = 1.83x10^5$ cycles.

Others:

- *Safety factor.* $K_{safety} = 1.2$
- *Fatigue limit for stainless steel currently used in salt water.* $\sigma_{fatigue} = 150MPa$
- *Maximum force of the reversal cylinder for a size 125 with jet stream speed of 25m/s.* $F_{reversal\ cylinder} \approx 125kN$
- *Maximum steering moment for a size 125 with jet stream speed of 40m/s.* $F_{stering\ moment} \approx 125kNm$

2.2 Concepts

The main focus laid on simplicity concerning geometry due to complicity can lead to higher cost and maintenance difficulties. The lever concept is the concept which will be investigated and analyzed thru the rest of the report. This concept was also the conceptual design illustrated in the aims. Other concepts can be seen in the other report but they were thought up by the other author and are not of importance for the rest of this report, and are therefore not illustrated here.

2.2.1 The lever

The point on the middle rod, the lever, is an attachment point and does not move. The systems movement principles are shown in figure 2.2a. The lever rotates around the attachment point to move in position of the wanted mode. The upper rod will be the hydraulic cylinder which operates the system.

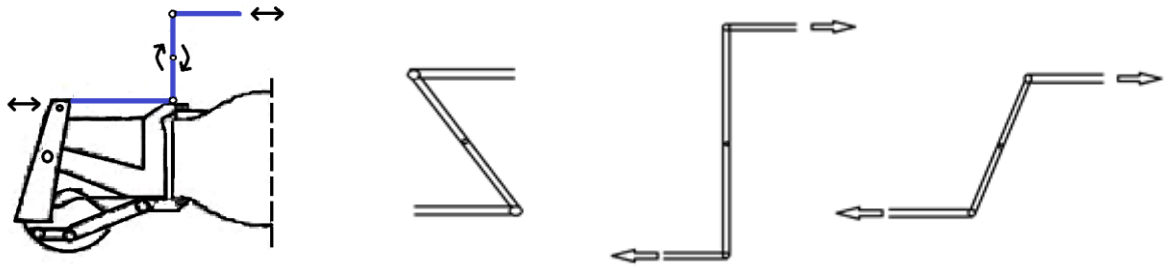

Figure 2.2a: To the left is a lever concept illustration and to the right is the lever concept in forward, neutral respectively reverse mode.

In table 2.2a a comparison of first impression advantages and disadvantages of the concept are summarized.

Table 2.2a. Advantages and disadvantages for the lever concepts.

Concept	Advantage	Disadvantage
The lever	Transfers force with simple components that are easily dimensioned to withstand the loads. Does not need to be immersed in a lubricant.	The height of the concept will differ depending on position.
		Difficult transition from the levers movement in a downward semicircle to the pushrods movement in an upward semicircle. Sealing issues also due to the circular motion of the bottom part.

2.3 Free-body diagram

Understanding what forces affect the system can be reveled with a free-body diagram.

At the attachment point the lever should be free to move which implies that there is no torque present. By analyzing only three specific positions of the reversing mechanism makes it possible to assume a static problem. A static problem implies that there is no movement in the system and the sum of all the acting forces should be equal to zero. The three chosen positions are the forward mode, the neutral mode and the reversal mode. Figure 2.3a show a simplified illustration of the lever as a single line. The main acting forces are taken from the diagram 3.2a given by Rolls-Royce, which illustrates the force needed from the hydraulic cylinder to compensate for the water jet stream. [11]

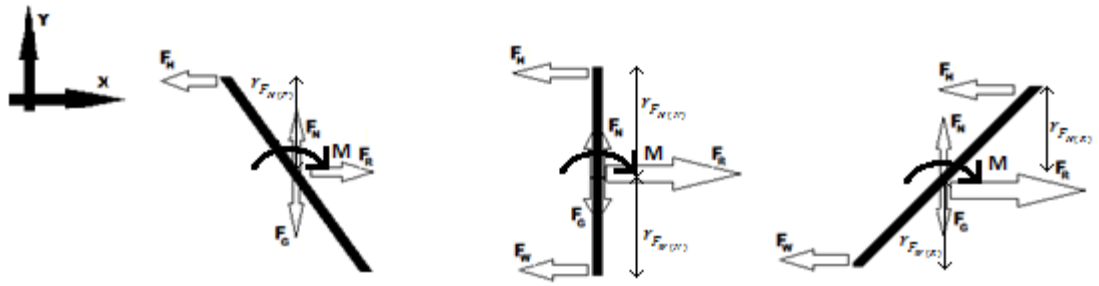

Figure 2.3a: Free-body diagram of the lever concept in forward, neutral and reverse mode.

All three free-body diagrams relations are coherent:

Forward mode:

$$\begin{cases} \rightarrow x: F_R - F_H = 0 \\ \uparrow \quad y: F_N - F_G = 0 \end{cases} \qquad \begin{matrix} \text{Eq. (2.3a)} \\ \text{Eq. (2.3b)} \end{matrix}$$

$$M = -F_H \times r_{F_{H(F)}} = 0$$

Neutral mode:

$$\begin{cases} \rightarrow x: F_R - F_H - F_W = 0 \\ \uparrow \; y: F_N - F_G = 0 \end{cases} \qquad \begin{matrix} \text{Eq. (2.3c)} \\ \text{Eq. (2.3d)} \end{matrix}$$

$$M = F_W \times r_{F_{W(N)}} - F_H \times r_{F_{H(N)}} = 0$$

Reverse mode:

$$\begin{cases} \rightarrow x: F_R - F_H - F_W = 0 \\ \uparrow \; y: F_N - F_G = 0 \end{cases} \qquad \begin{matrix} \text{Eq. (2.3e)} \\ \text{Eq. (2.3f)} \end{matrix}$$

$$M = F_W \times r_{F_{W(R)}} - F_H \times r_{F_{H(R)}} = 0$$

, where F_H = Force needed from the hydraulic cylinder

F_W = Force from the water jet

F_R = Reaction force

F_N = Normal force

F_G = Gravitational force

M = Torque

$r_{F_{H(F)}}$, $r_{F_{H(N)}}$, $r_{F_{H(R)}}$ = The lever for F_H in forward, neutral respectively reverse mode.

$r_{F_{W(N)}}$, $r_{F_{W(R)}}$ = The lever for F_H in neutral respectively reverse mode.

From the above relations it was seen that $F_H + F_W = F_R$ and $F_N = F_G$ because the system is at rest. Also known is that F_H and F_W is applied on an equal distance from the attachment point and therefor F_H is equal to F_W otherwise the system would rotate. The gravitational force was then approximately calculated with the force definition $F_G = m \cdot a$ (where m is mass and a is acceleration) according to Newton's second law. Thus when F_G was known so was F_N.

The relation focused on in the simulation part is the reverse mode and further relations are explored in parts *2.4 Calculations to support the simulation* and *2.5 Parameter variations* to be able to vary the difference forces needed when changing the input data. In the reverse mode the system is under the highest load and is therefore most critical to make functional first.

The first model of the lever had the simple shape of a rectangular beam with measurements 0.08x1.204x0.08m and the volume is then about 0.0077 m^3. The magnitude of the gravitational force acting on the beam can then be calculated if knowing the density for the wanted material. For the simulation part, material properties are first set to 210GPa as the Young's modulus and 0.3 as Poisson's ratio due to these are the general properties for steel. According to the material database CES EduPack, common steel values give a density of around 8000kg/m^3.

Table 2.3a. Material properties summarized from CES EduPack.

Material	Young's modulus (E) [GPa]	Poisson's ratio (ν)	Density [kg/ m^3]
Stainless steel	189-210	0.265-0.275	7.6e3-8.1e3
High carbon steel	200-215	0.285-2.95	7.8e3-7.9e3
Cast iron (grey /ductile)	80-138/165-180	0.26-0.28/0.26-0.28	7.05e3-7.25e3/ 7.05e3-7.25e3
Aluminum[1] (age-hardened & wrought)	68-80	0.32-0.36	2.5 e3-2.9 e3
Titanium[1] (pure/alloy)	100-105/110-120	0.35-0.37/0.35-0.37	4.5 e3-4.52 e3/ 4.4 e3-4.8 e3

[1] Does not apply to these materials general properties due to they are not counted as steel. It is a basic element or an alloy where iron and carbon are not the main element as it is for steel.

To form an idea of the gravitational force acting on the system a rough calculation shows that it would be around 605N when the volume (V) times the density (ρ) gives the mass (m) and then multiplying that with the gravitational acceleration constant (g,) equal to 9.82m/s^2. That is;

$$V \cdot \rho = m \rightarrow 0.0077 \cdot 8000 = 61.6kg$$

$$F_N = m \cdot g \rightarrow F_N = 61.6 \cdot 9.82 \approx 605N$$

By comparison of the magnitude of the forces, that is between the hydraulic cylinder (or water jet) force and the gravitational (or normal) force there is a major magnitude difference except for the forward mode. The magnitude of the force in the three free-body diagram positions is 0N, 75kN respectively 125kN based on the data in diagram 3.2a. The gravitational force is not insignificant in the forward mode otherwise the force is considered neglected. The maximum force mode is used during simulation to evaluate maximum loading case, which is the reverse mode and therefor is the gravitational force disregarded.

When the lever got its final shape, the diamond shape (see figure 3.2d), the loading condition in the reverse mode was calculated. In the point of attachment there is a pin going thru the lever which is suspended in the housing surrounding the lever. An equation used in construction mechanics which concerns pressure on an edge of a hole was used to perform the calculations. [12].

$$P = \frac{F}{d \cdot t}$$ Eq. (2.3c)

Where P = pressure acting on the edge

F = force acting on the edge, in this case the gravitational force

d = diameter of the hole

t = thickness of the hole

The pressure acting in the attachment points is 3.69Pa, which is supported by the calculations below, by table2.3b and the approximate density of 8000kg/m^3 used above.

Table 2.3b. Approximate data concerning the diamond shaped lever.

Part	Volume [m^3]	Diameter [m]	Thickness [m]
Diamond shaped lever pin	≈ 0.0047	0.10	0.05

In the same way as the beams gravitational force where calculated the diamond shaped levers gravitational force is achieved.

$$F = m \cdot g = (V \cdot \rho) \cdot g = (0.0047 \cdot 8000) \cdot 9.82 \approx 369N$$

$$P = \frac{369}{(10 \cdot 5) \cdot 2} = 3.69Pa$$

The denominator is multiplied by two due to there is two ends which suspends the lever.

Translating this pressure into a force requires a contact area, which is set to be in this case half the circumference times the thickness. The calculated contact area is for one end.

$$A_{contact} = \left(\frac{\left(2 \cdot \pi \cdot \left(d/2\right)\right)}{2} \right) \cdot t = \left(\frac{\left(2 \cdot \pi \cdot \left(0.10/2\right)\right)}{2} \right) \cdot 5 = \left(\frac{\pi \cdot 0.10}{2} \right) \cdot 5 \approx 0.79m^2$$

Then to calculate the force, the pressure is multiplied with the contact area.

$$F = P \cdot 2A_{contact} = 3.69 \cdot (2 \cdot 79) \approx 5{,}83N$$

This is the total force acting on the two ends supporting the lever. The force per end is 2.92 N. This force is also disregarded due to its magnitude compared with the hydraulic/water jet force.

2.4 Calculations to support the simulation part

2.4.1 Acting forces from the steering hydraulics

The steering hydraulics will push the upper part (see figure 3.2g) of the lever concept in a way which will contribute to two forces, one at each end, see figure 2.4a where H_1 and H_2 each represent a hydraulic cylinder. They are dependent of each other. The steering torque (M) is known from the diagrams in 3.2a and is also the point of attachment for the upper part. The triangle in figure 2.4a represents the bottom plate of the upper part, where the hydraulic cylinders are attached. The tip of the bottom plate is fixed in its position due to it is the attachment point and can only rotate around its own axis, which is z-direction from this angle. The torque can be translated into two equal magnitude forces the hydraulic cylinders H_1 and H_2 need to achieve to replace the torque. They will have a circular movement due to the attachment point.

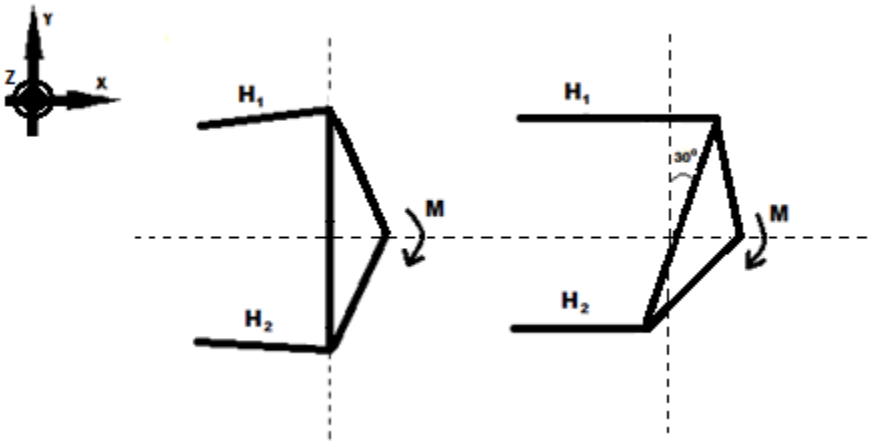

Figure 2.4a: Illustration of the movement of the upper part when turning the steering unit with maximum deflection of 30 degrees. H_1 and H_2 each represent a hydraulic cylinder.

Below relation gives the magnitude of the forces translated from the torque.

$$M = F \times r \qquad \text{Eq. (2.4a)}$$

Where, M = Torque

F = force

r = lever

Modifying the relation to this specific case gives eq. 2.4b knowing that

$F = F_{H1}+F_{H2}$ and F_{H1} should be equal to F_{H2}

M_{max}=125MPa (from diagram 3.2a)

Only r is left to be decided. Measurements are taken from the 3D model of the affected part which is called the upper part (see 3.2.2.2). Below is a simple sketch of the actual bottom plate, to show the measurements needed for calculation.

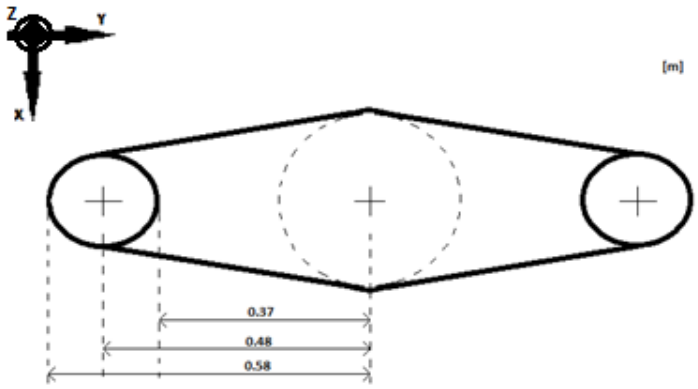

Figure 2.4b: Illustration of upper part with measurement indications.

The lever, r, is defined after the coordinate system in figure 2.4a. The maximum steering angel (30°) is needed to determine r. The hydraulic cylinder will be attached around the cylinder at the end of the bottom plate. An assumption of the location for the acting force will in average be at the center (0.48m).

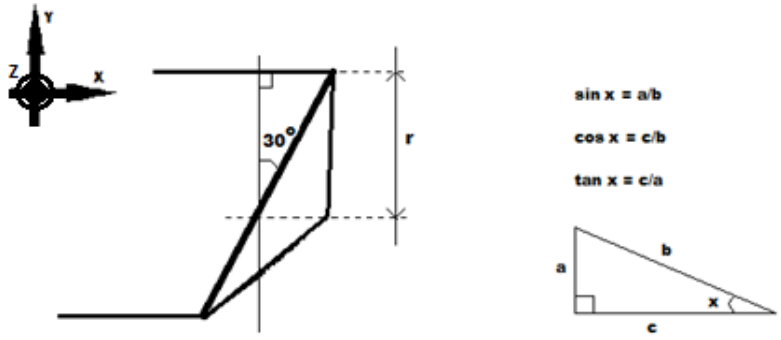

Figure 2.4c: Trigonometrical support for the calculations.

$r = \cos(30°) \times 0.48m$

$\rightarrow M = F_{H1} \times r + F_{H2} \times r$ Eq. (2.4b)

$M = (F_{H1} + F_{H2}) \times r$

$F_{H1} + F_{H2} = M/\mathrm{r}$

$F = {}^{(M/r)}/_{2} \approx 150kN$

This force is coherent with the forces acting on the hydraulic holder (see 3.2.2.4) as well.

2.5 Parameter variations

The current lever concept has its attachment point in the middle of the lever and its starting point is tilted. This layout was chosen due to simplicity. That is if the attachment point is in the middle then the forces acting on the ends of the lever is equal and a smaller swing motion is needed when the lever is tilted to start with.

Exploration of what happens if moving of the attachment point either higher or lower on the lever (which makes the lever length change on each side of the attachment point) was executed. Also exploration on how this affected the force needed from the hydraulic cylinder and the height of the concept.

To calculate this, the lever concept was divided in different sections as seen to the right in figure 2.5a. The lengths to the left in figure 2.5a used for the calculations are from the 125-model of the Kamewa water jet series. These values were used based on measurements done on the CAD part provided from Rolls- Royce shown in figure 1.1a under aims.

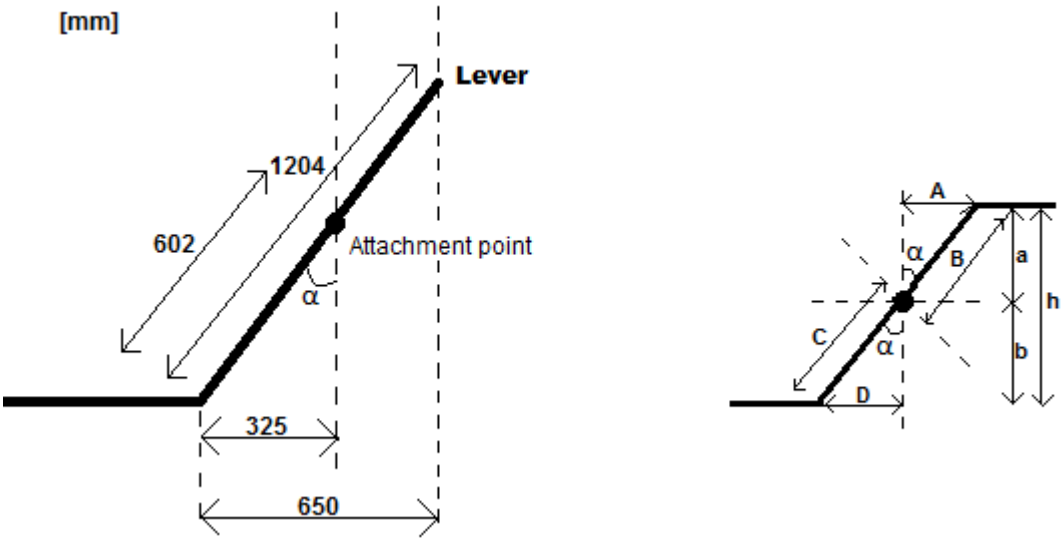

Figure 2.5a: Mathematical illustration of the lever concepts maximum angle at maximum reversing condition of a 125-model, and the lever concept length sections.

The angle the lever would have to rotate to move the pushrod 650mm to extend the reversing bucket to its maximum on a 125-model were calculated. With the statements that the lever should rotate equal distance at both sides of the attachment point and also that the attachment point is in the middle of the lever gives an angle of about 31.6° based on trigonometry.

From trigonometry of the right angle;

$$\sin\alpha = {}^{b}\!/_{c} \Leftrightarrow \alpha = \sin^{-1}\left({}^{b}\!/_{c}\right) = (\,from \quad figure \quad 2.5a) = \sin^{-1}\left({}^{D}\!/_{C}\right) = \sin^{-1}\left({}^{0.325}\!/_{0.62}\right) \approx 31.6^{\circ}$$

Different trigonometric relations for the lever concept;

For α:

$$\tan\alpha = {D}/{b} \qquad \sin\alpha = {A}/{B} \qquad \cos\alpha = {a}/{B}$$
$$\tan\alpha = {A}/{a} \qquad \sin\alpha = {D}/{C} \qquad \cos\alpha = {b}/{C}$$
$$\cos\alpha = {h}/{(B+C)}$$

For h:

$$h = a + b$$
$$h = (B+C)\cos\alpha$$
$$h_{\max} = B + C$$

For A:

$$A = a \cdot \tan\alpha$$
$$A = B \cdot \sin\alpha$$

For B:

$$B = {a}/{\cos\alpha}$$
$$B = {A}/{\sin\alpha}$$

For C:

$$C = {b}/{\cos\alpha}$$
$$C = {D}/{\sin\alpha}$$

For D:

$$D = b \cdot \tan\alpha$$
$$D = C \cdot \sin\alpha$$

For a:

$$a = {A}/{\tan\alpha}$$
$$a = B \cdot \cos\alpha$$
$$a = h - b$$

For b:

$$b = {D}/{\tan\alpha}$$
$$b = C \cdot \cos\alpha$$
$$b = h - a$$

To see how these relations can be connected to the forces a free body diagram was made, similar to the ones in *2.3 Free body diagram.* The length of the lever on the upper side of the attachment point, B, was varied to see the force needed from the hydraulic cylinder.

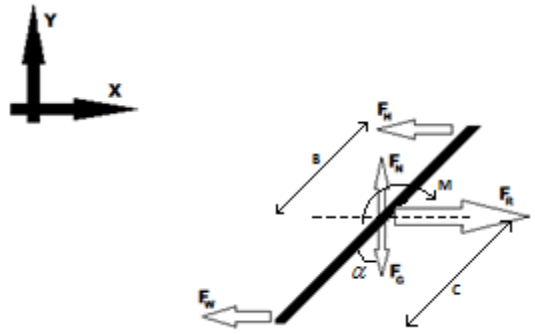

Figure 2.5b: Free-body diagram of the lever concept in reverse mode.

Relations:

$$\begin{cases} \rightarrow: F_R - F_H - F_W = 0 & \text{Eq. (2.5a)} \\ \uparrow: F_N - F_G = 0 & \text{Eq. (2.5b)} \end{cases}$$

$$M = F_W \times C \cdot \cos\alpha - F_H \times B \cdot \cos\alpha = 0 \qquad \text{Eq. (2.5c)}$$

Rearranging eq. 2.5a to get F_H expressed in F_R and F_W, and then using it in equation 2.5c gives below expression.

$$F_W \times C \cdot cos\alpha - (F_R - F_w) \cdot B \cdot cos\alpha = 0$$

With this expression you can compose an equation for F_R and then both F_H and F_R can be decided in below equations due to that in the current model of the lever concept the magnitude of F_W is 125kN which is implied by diagram 3.2a.

$$F_H = F_R - F_W \qquad \text{Eq. (2.5d)}$$

$$F_R = \left(F_W(C \cdot cos\alpha + B \cdot cos\alpha)\right) \Big/ B \cdot cos\alpha \qquad \text{Eq. (2.5e)}$$

When all relations needed for the exploration were establish, MATLAB were used to calculate wanted values. Note that these results are valid for a 125-model only due to the measurements are taken from that specific model and as the size of models changes so does the measurements of them.

What MATLAB calculated was a F_H at angle α=31.6°, when the length of B is varied from 0.05m to 1.0m in 20 equal steps. Then the values of the lever concept's maximum height were calculated. To be able to solve these equations constants had to be set. The length D was equal to 0.325m at all times, representing half the swing motion of the lever on a 125-model. The angle, α, was constant 31.6° representing the maximum tilt on the lever in maximum reversing mode. C was also constant (0.602m) due to be able to meet the demands of the constant swinging distance and angle. F_W was equal to

125kN as stated above because the force from the water would be the same whether the variables were changed or not.

The code written in MATLAB is found in appendix 2 and the results from the calculations are found in table 2.5a, the force needed from the hydraulic cylinder, the length of B and the total height of the lever concept. Figure 2.5c show a diagram of how the force needed from the cylinder, F_H, changes as B's length changes.

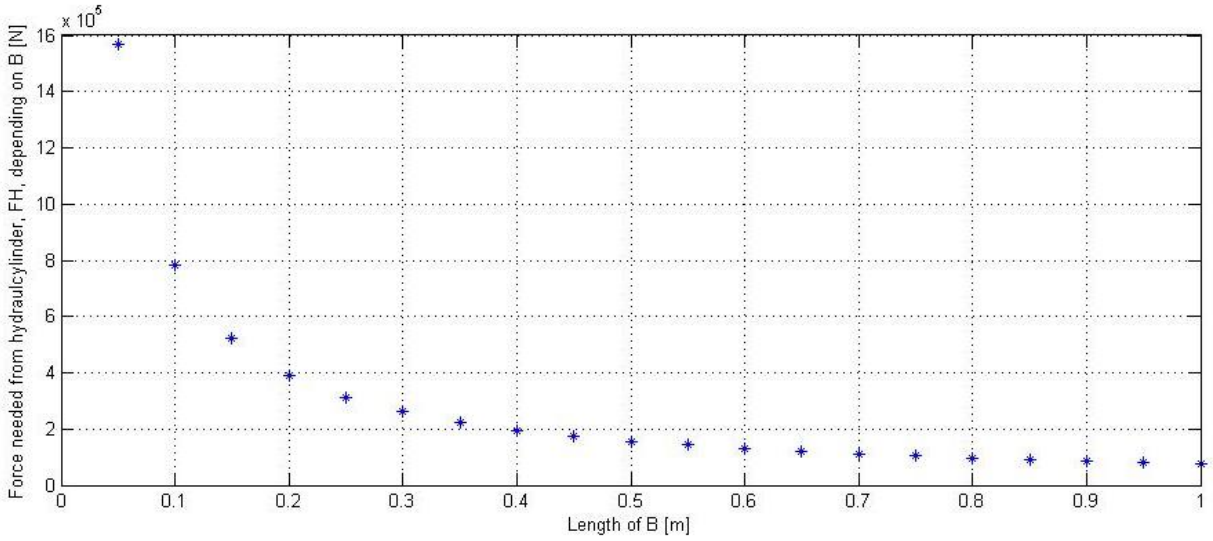

Figure 2.5c: Show the force, FH, needed from the hydraulic cylinder verses the length of B in reverse mode.

Table 2.5a. Values corresponding to the diagram in figure 2.5c as well as the corresponding total height of the concept.

B [m]	F_H [kN]	h [m]
0.10	FH =784	h= 0.7274
0.20	FH =392	h= 0.8274
0.30	FH =261	h= 0.9274
0.40	FH =196	h= 1.0274
0.50	FH =157	h= 1.1274
0.60	FH =131	h= 1.2274
0.70	FH =112	h= 1.3274
0.80	FH =98	h= 1.4274
0.90	FH =87	h= 1.5274
1.00	FH =78	h= 1.6274

The current lever concept fits in where B is equal to 0.60m in table 2.5a. These dependencies of the different values can be of guidance for example when evaluating the lever concept for different boat types when the hull differs or if a smaller hydraulic cylinder is wanted.

The MATLAB code is a base for varying the different parameters. It can be rewritten so another parameter could be varied as well, so the most interesting parameter for each model can be evaluated.

2.6 Lifecycle calculations

The difficulty of these calculations is to determine the safety factor restricting the allowed stress level. The safety factor can be found as a standard at companies otherwise it will have to be determined in another way for example from books with tabulated data. In this report a standard from Rolls-Royce was used, $F_{safe} = 1.2$. To calculate the maximum allowed stress level for the different components the fatigue strength from the current material is divided with the safety factor. The components have to withstand a lifetime of 1.97×10^7 cycles for corrective steering, 1.73×10^5 cycles for full steering and 1.83×10^5 cycles for full reversing. Data taken from CES EduPack concerning the fatigue strength is specified that the value applies for 10^7 cycles which means that the values achieved with this data can be used for comparison for the simulation part. Table 2.6a below shows the fatigue strength for the materials in table 2.3a.

Table 2.6a. Data for different metals taken from CES EduPack.

Material	Fatigue strength (σ_{fat}), [MPa]
Stainless steel (ss)	175-753
High carbon steel (hcs)	281-606
Cast iron (grey /ductile) [cig/cid]	40-170/180-330
Aluminum (age-hardened & wrought) [aahw]	57-210
Titanium (pure/alloy) [tip/tia]	200-300/589-617

Data from table 2.6a gives the allowed maximum stress level for these material groups to;

$$\sigma_{ss} = {\sigma_{fat,ss}}/{K_{safe}} = {753}/{1.2} = 627.5MPa \qquad \sigma_{aahw} = {\sigma_{fat,aahw}}/{K_{safe}} = {210}/{1.2} = 175.0MPa$$

$$\sigma_{hcs} = {\sigma_{fat,hcs}}/{K_{safe}} = {606}/{1.2} = 505.0MPa \qquad \sigma_{tip} = {\sigma_{fat,tip}}/{K_{safe}} = {300}/{1.2} = 250.0MPa$$

$$\sigma_{cig} = {\sigma_{fat,cig}}/{K_{safe}} = {170}/{1.2} = 141.7MPa \qquad \sigma_{tia} = {\sigma_{fat,tia}}/{K_{safe}} = {617}/{1.2} = 514.2MPa$$

$$\sigma_{cid} = {\sigma_{fat,cid}}/{K_{safe}} = {330}/{1.2} = 275.0MPa$$

These values are compared to the ones from the simulations. If the values exceed this maximum stress level they will not be able to last the requested amount of lifecycles. As stated in *2.1.3 Demands* Rolls-Royce maximum fatigue strength of the material currently use is 150MPa.

3. Result and discussion

3.1 Modeling

All 3D models have been constructed in ProEngineer Wildfire. The same models were imported to Abaqus CAE and used for the simulation work done on each component. The ProE models originate from the concept drawings and the first step in constructing the assembly was to identify each individual component. Then the model was built, component by component, tested and simulated via Abaqus. Small changes were made after each run in Abaqus to optimize the geometry of each component.

The individual parts are shown under the simulation part and the actual models are documented in the other report. The complete assembly is shown here four understanding purpose only. [10]

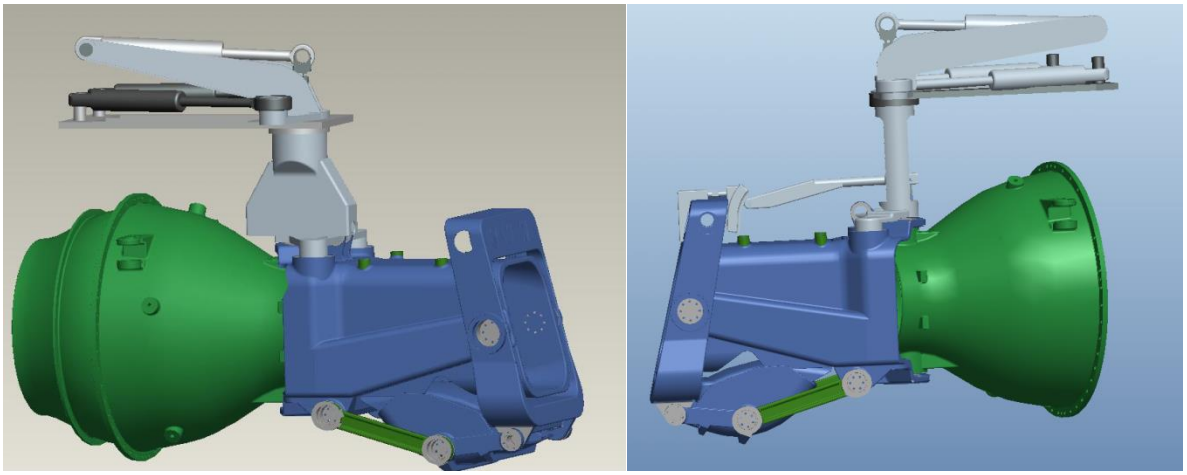

Fig 3.1a: left, steering device with the protection cover mounted (but with missing push rod). Right, steering device with the cover removed. [10]

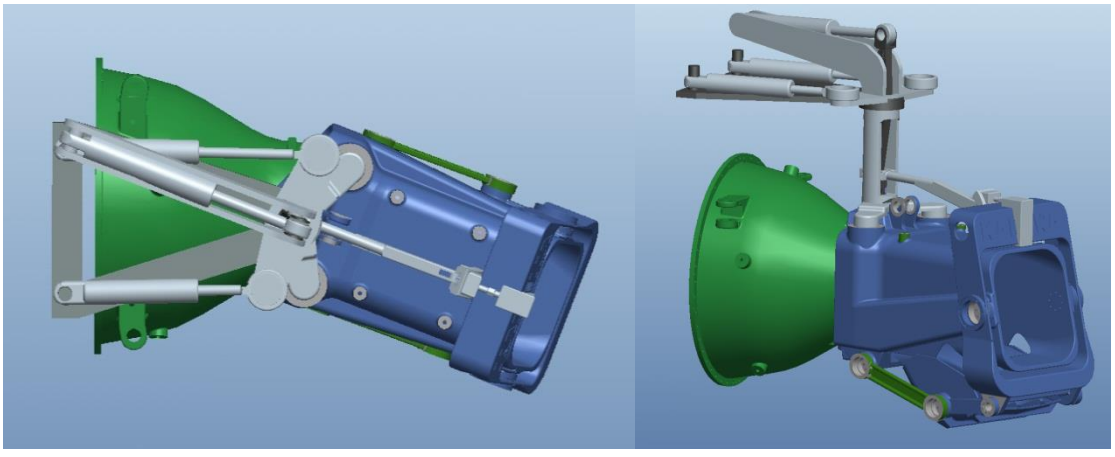

Fig 3.1b: Top view and side view of the steering device. [10]

3.2 Simulation

To determine the stresses and strains in the components are crucial to be able to evolve the final dimensions. It is also important concerning material selection, that the mechanical properties withstand eventual problem areas. Simulation is necessary to get an idea of the strains and stresses that form in the different parts when they undergo different loading cases.

The forces affecting the components were given in diagram 3.2a. The upper illustrate the steering moment verses the steering angle. The torque arises when turning. The lower illustrate the force needed to extend the reversal mechanism versus the angle of the reversal mechanism. The forces in these diagrams correspond to the force generated of the water jet stream causing the hydraulics to overcome/match the force depending on the action of the boat.

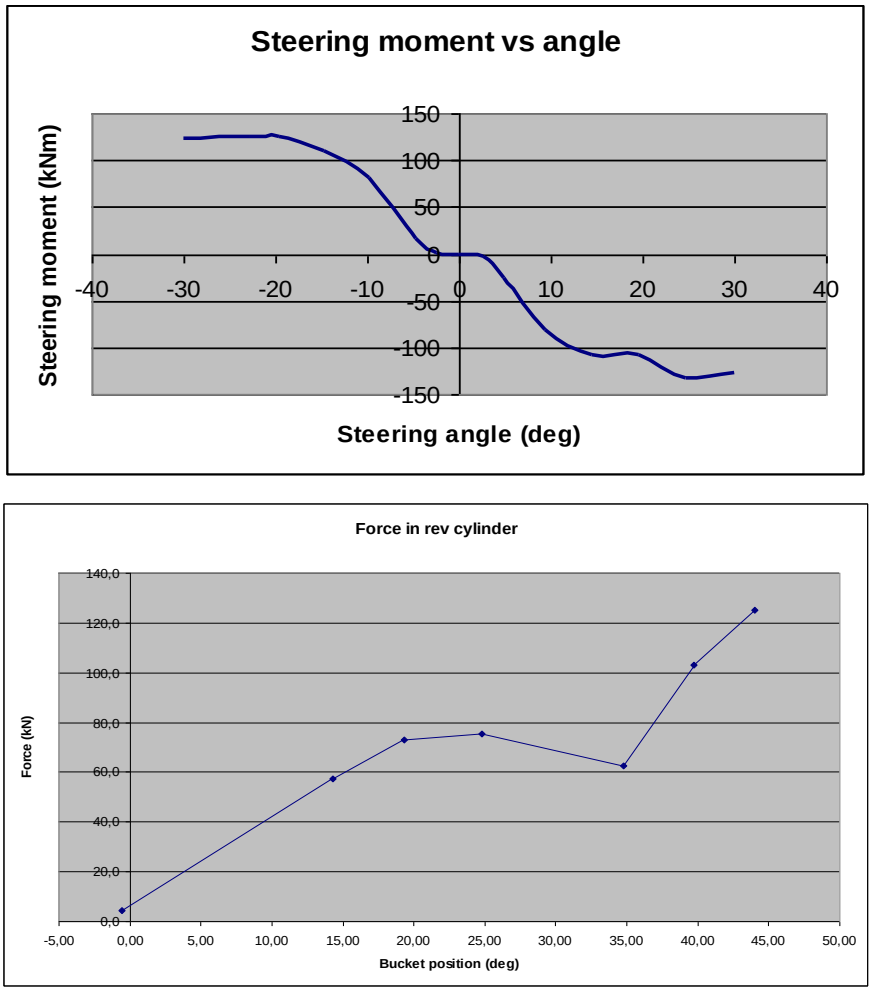

Diagram 3.2a: Upper; the steering moment vs. steering angle diagram for a water jet of model 125 and water jet velocity of 40m/s. Lower; the diagram for reversal cylinder force vs. reversing mechanism angle for a water jet of model 125 and water jet velocity of 25m/s.

3.2.1 Test beam

From the basic concept of the lever a simple geometry was first simulated. A beam which would represent the lever was tested to see how the approximate dimensioning based on the received CAD model of a 125 sized model manages the affecting forces from the reversal hydraulic cylinders.

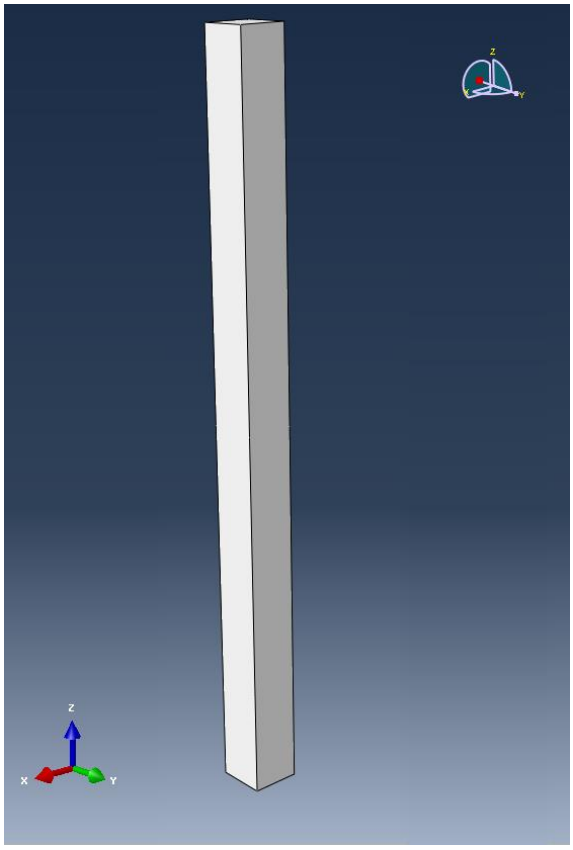

Figure 3.2a: Illustration of the beam.

The acting forces on the lever were taken directly out of diagram 3.2a due to the relationships are already known from earlier calculations (see 2.3 *Free-body diagram*) which implied that the normal force and gravitational force could be disregarded.

The test beam is only simulated in the neutral mode due to this test simulation was made in an early stage for investigation regarding how realistic this assumption were. The force is higher in the full reverse mode but the bending forces were assumed to be higher in the neutral mode due to the levers positioning therefor this was the chosen first mode to investigate regarding high force and high elongation.

Material properties, component properties and boundary conditions also need to be specified. For the test beam the conditions can be seen in table 3.2a. The material properties represent those of regular steel.

Table 3.2a. Abaqus data of the beam needed to make a simulation.

Property	**Description of what has been set**
Component	3D, deformable 0.08x1.204x0.08m
Material	Elastic Young's modulus (E) = 210GPa Poisson's ratio (v) = 0.3
Load/Force/Torque	Concentrated force Top: 4 points, 18750N/point Middle: 2 points, 75000N/point Bottom: 4 points, 18750N/point
Boundary condition	Rigid in the middle representing the attachment point. It cannot move in x, y or z direction.
Mesh	Structured hexagonal elements Seed; 0.020 Number of elements; 960

Figure 3.2b shows how the load and boundary conditions are applied. The yellow arrows at the ends and at the middle of the beam represent the forces and in which direction they are working. This is consistent throughout the rest of the simulations too. Concentrated forces were chosen for simplicity and it would not affect the stress results in the beam. They will on the other hand give a misleading result of the stresses and strains at the positions they are placed, so if gathering information concerning those positions that will have to be redone. In figure 3.2b the midpoint have orange/blue triangles which indicate that a boundary condition is present, which is also consistent throughout the rest of the simulations.

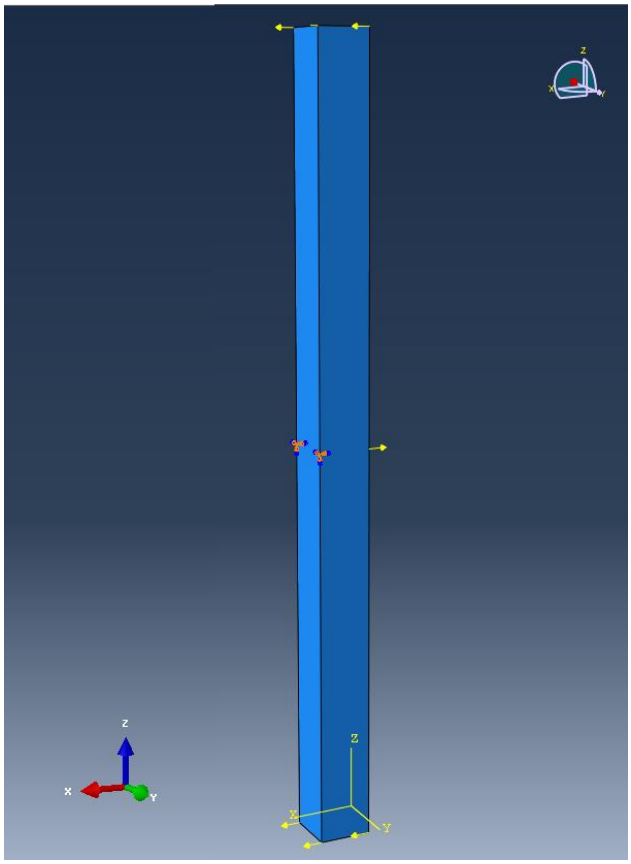

Figure 3.2b: Illustrative image of the beam with forces and boundary conditions. See table 3.2a for details.

Results from the simulation are shown in figure 3.2c, both stresses and strains. The stresses in the box are compared to the fatigue limits of the current material which will determine if the result is reasonable or not. The strain is monitored to see if it will affect the system in a destructive way.

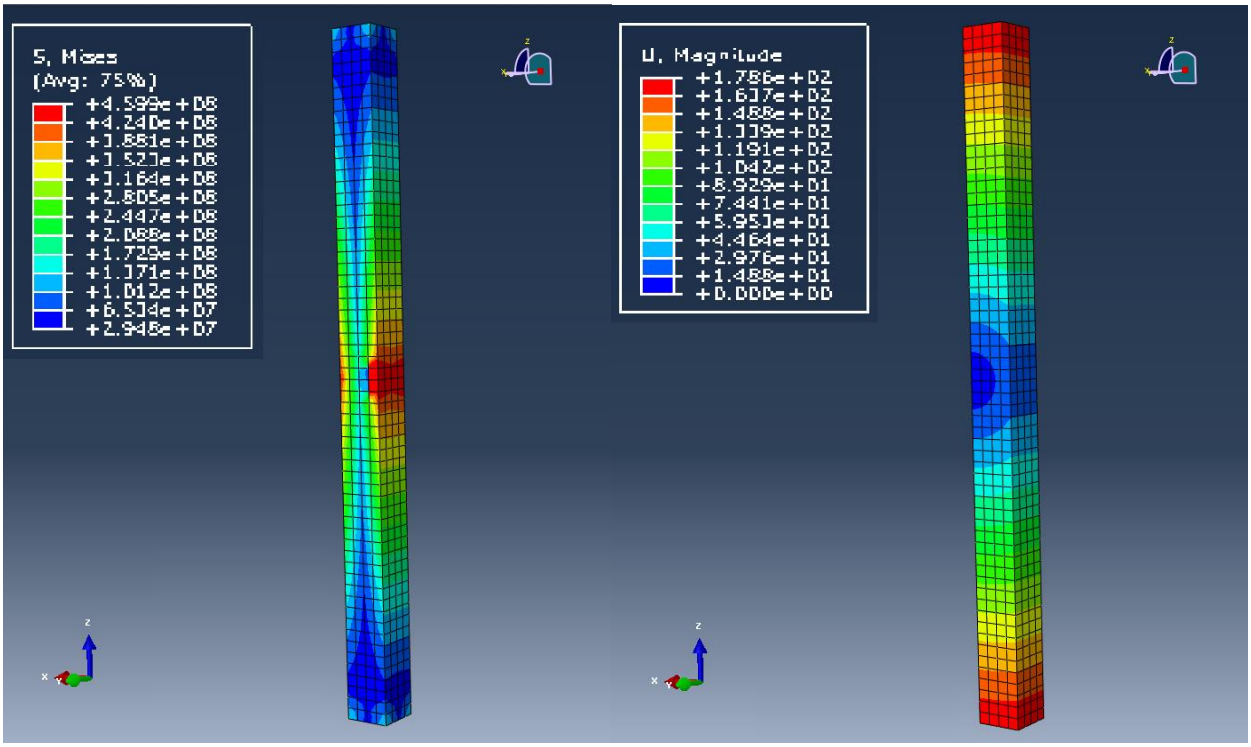

Figure 3.2c: Results from the simulation of the beam, the stress magnitude in Pascal and areas with different stresses. The same principle for the strain where the results are given in meters.

The result of the stresses lay in the upper of the fatigue strength interval for the materials in table 2.6a under *2.6 lifecycle calculations*. As mentioned they have similar values of Young's modulus and Poisson's ration as regular steel which were used during the first round of simulations, that is Young's modulus of 210GPa and Poisson's ratio of 0.3. These results are reasonable enough for enable continuation with dimensioning.

The following simulations are investigated in the reverse mode to make sure that full force mode is able to execute. The lever is therefore tilted and that is because the reversing mechanism reached its maximum at 45 degrees. This tilt is 31.6 degrees which has been calculated under *2.5 parameter variations*.

The full revers mode is now the primary property and the elongation the secondary and will not in this report be further investigated. Instead it is suggested as continuation work under section *4. Suggestions on continuation*.

3.2.2 The lever concept

The simulation process is similar from component to component the difference lies in how and where the forces should be applied. The entire concept put together are illustrated in of *3.1 Modeling*.

3.2.2.1 The lever

Figure 3.2d show that the geometry has changed from the simple test beam to a more complex diamond shape. The specific shape was evolved during multiple simulations where the results have shown where reinforcement is needed in regards to how light it can be. This repeating simulation process has also formed the final design of all the other parts in this section.

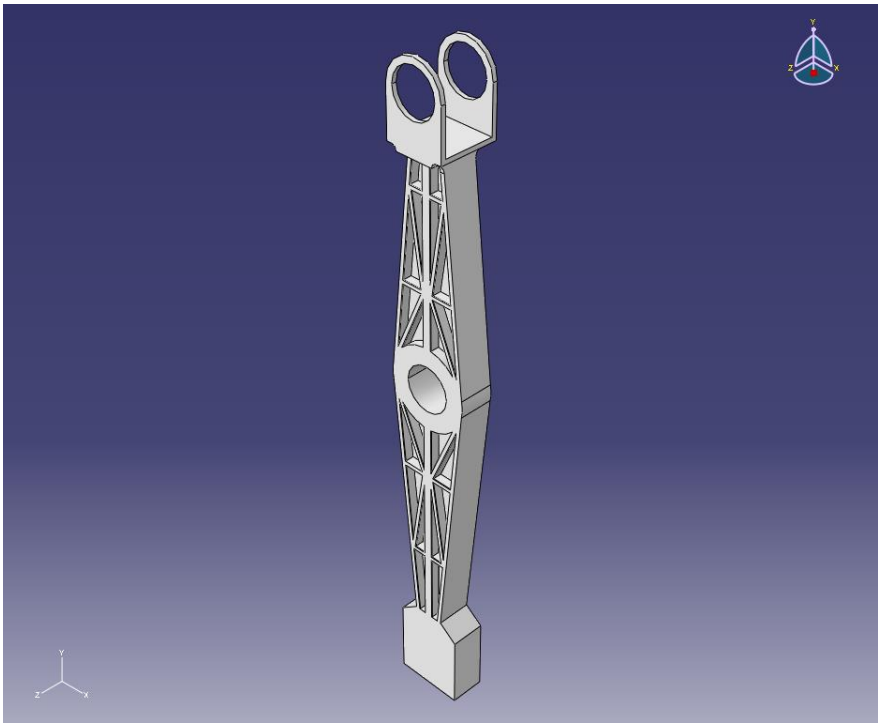

Figure 3.2d: Illustration of the diamond shape lever.

The boundary condition and forces are applied at a different location as for the test beam due to the different shape although in the same area, which is shown in figure 3.2e. In table 3.2b the properties can be found concerning the diamond shaped lever.

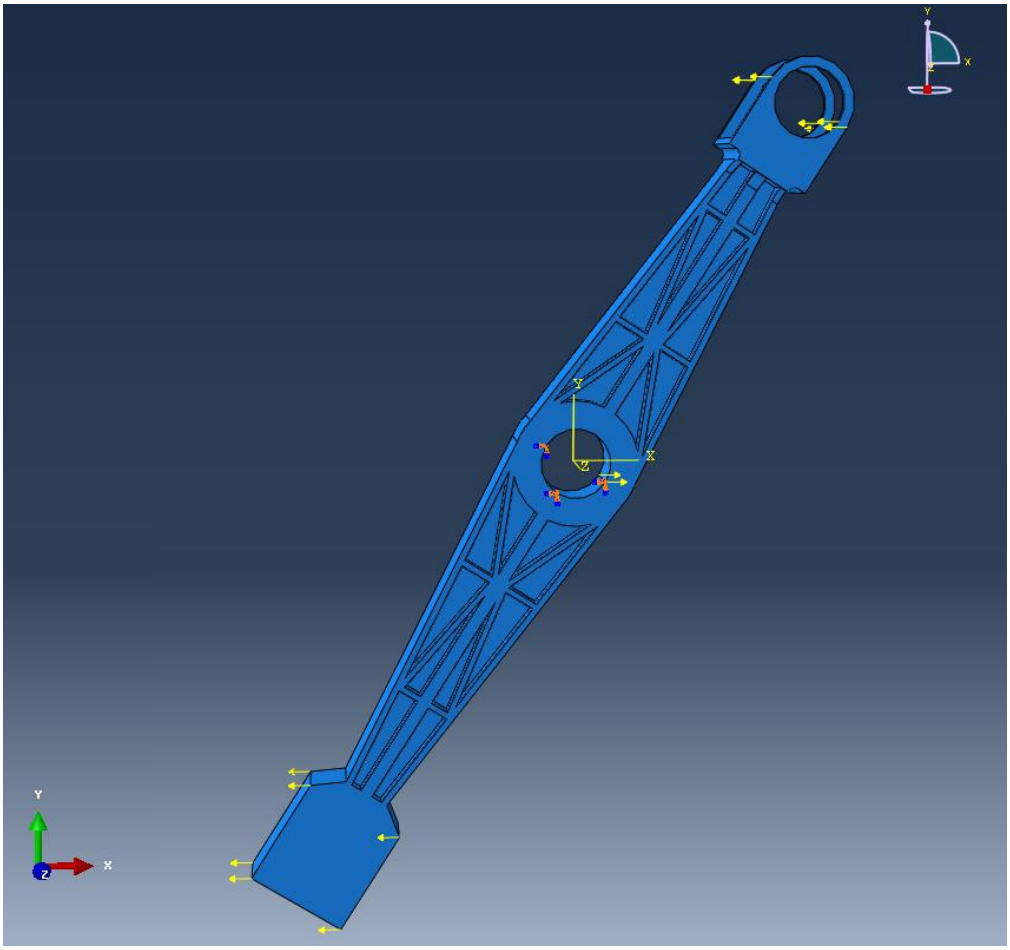

Figure 3.2e: Illustration of the diamond shaped lever with forces and boundary conditions. See table 3.2b for details.

Table 3.2b. Abaqus data of the diamond shaped lever needed to make a simulation.

Property	**Description of what has been set**
Component	3D, deformable
Material	Elastic Young's modulus (E) = 210GPa Poisson's ratio (ν) = 0.3
Load/Force/ Torque	Concentrated force Top: 16 points, 7812.5N/point Middle: 2 points, 125000N/point Bottom: 8 points, 15625N/point
Boundary condition	Rigid at the hole in the middle representing the point of attachment. It cannot move in x, y or z direction.
Mesh	Free tetragonal elements Seed; 0.02 Number of elements; 34623

The result from this simulation is shown in figure 3.2f. It displays the part with stress respectively strain distribution. As stated before at the point where the forces are applied give misleading results and are disregarded in the simulations.

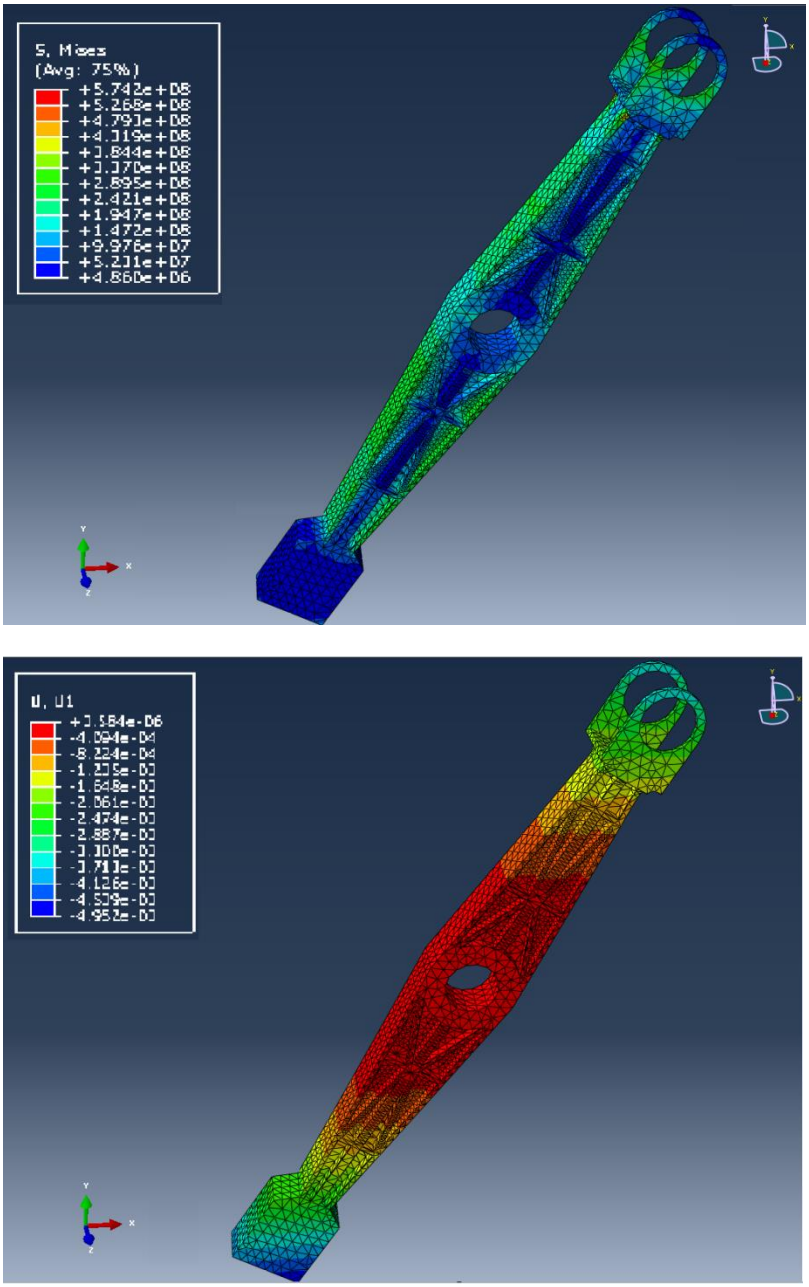

Figure 3.2f: Result from the simulation of the diamond shaped lever, showing the stress magnitude in Pascal and areas with different stresses. The same principle for strain where the result is given in meters.

3.2.2.2 The upper part

This is the top part of the lever concept. It is attached at the top of the cylinder in which the lever is moving. The lever is placed in the hole on the plate where the top half of the lever is showing and is attached to the hydraulic cylinder that provides the force to move the reversing mechanism. The other end of the hydraulic cylinder is attached in the upper parts extension. Also at the plate two cylindrical elevations serve as the attachment point for the steering hydraulics.

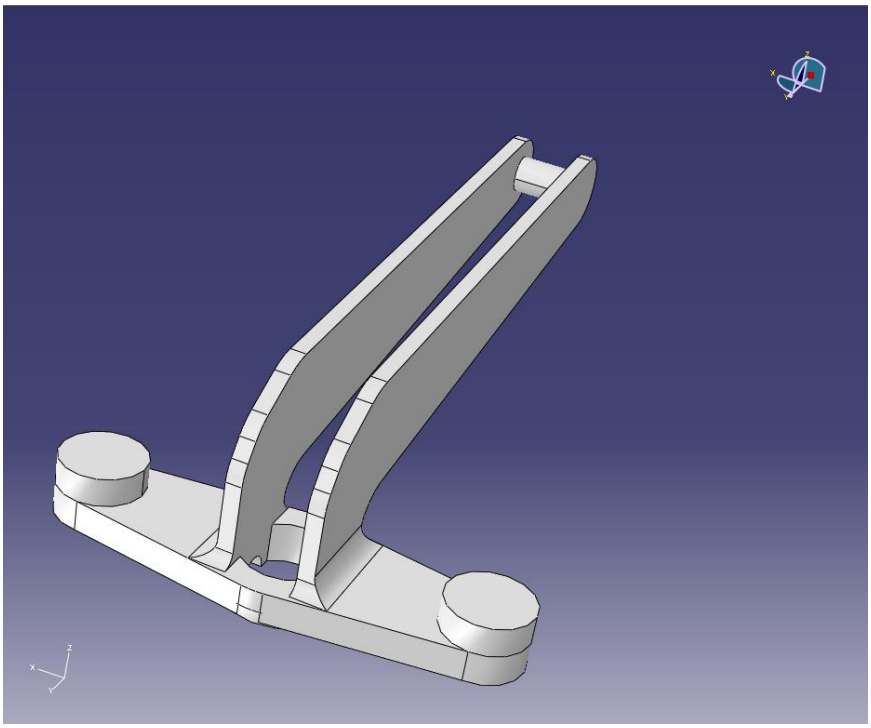

Figure3.2g: Illustration of the upper part which holds the lever and hydraulics in place.

This layout represents the maximum steering case (30 degrees) combined with the maximum loading case at maximum angle (45 degrees) of the reversing mechanism. The forces at the bottom attachments are calculated with help from the steering diagrams in diagram 3.2a where the torque is translated into two equal forces in opposite direction. These calculations are seen under 2.4 *Calculations to support the simulation part*. See table 3.2c for properties.

Also the force acting from the hydraulic cylinder connected to the lever is simulated at the top. The boundary conditions are set at the area of where the upper part is attached in the cylinder.

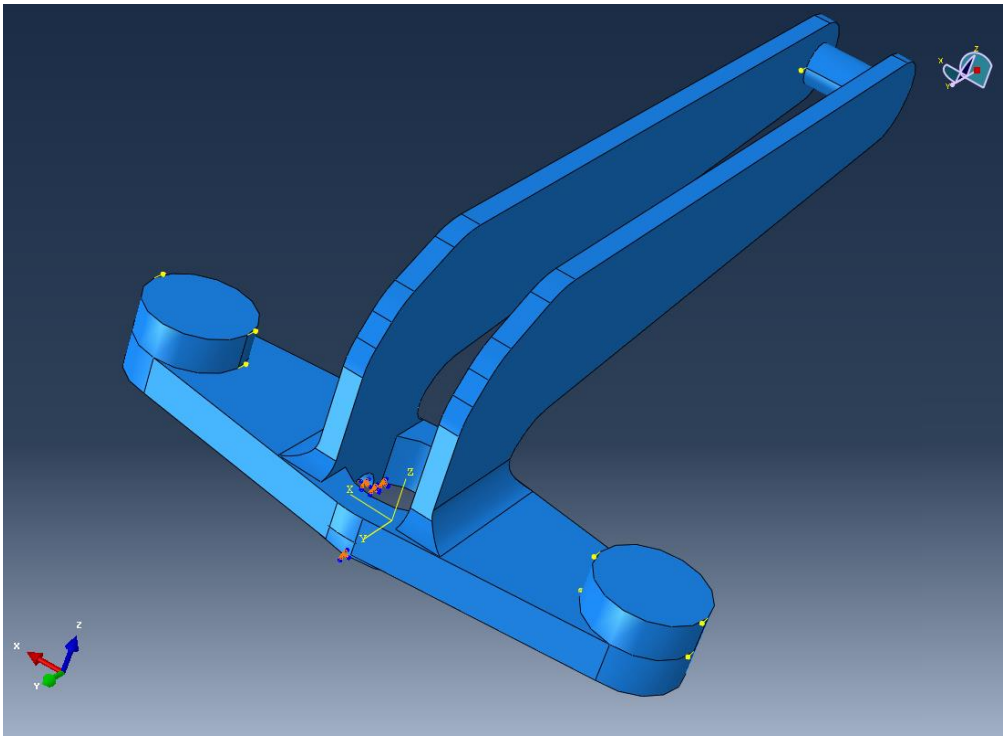

Figure 3.2h: Illustration of the upper part with forces and boundary conditions. See table 3.2c for details.

Table 3.2c. Abaqus data of the upper part needed to make a simulation.

Property	**Description of what has been set**
Component	3D, deformable
Material	Elastic Young's modulus (E) = 210GPa Poisson's ratio (ν) = 0.3
Load/Force/ Torque	Concentrated force; At the top: 4 points, 31250N/point At the bottom; 4 points on each side, 37500N/point
Boundary condition	Rigid at the bottom face. It cannot move in x, y or z direction.
Mesh	Free tetragonal elements Seed; 0.03 Number of elements; 21686

The result from the simulation is presented in figure 3.2i.

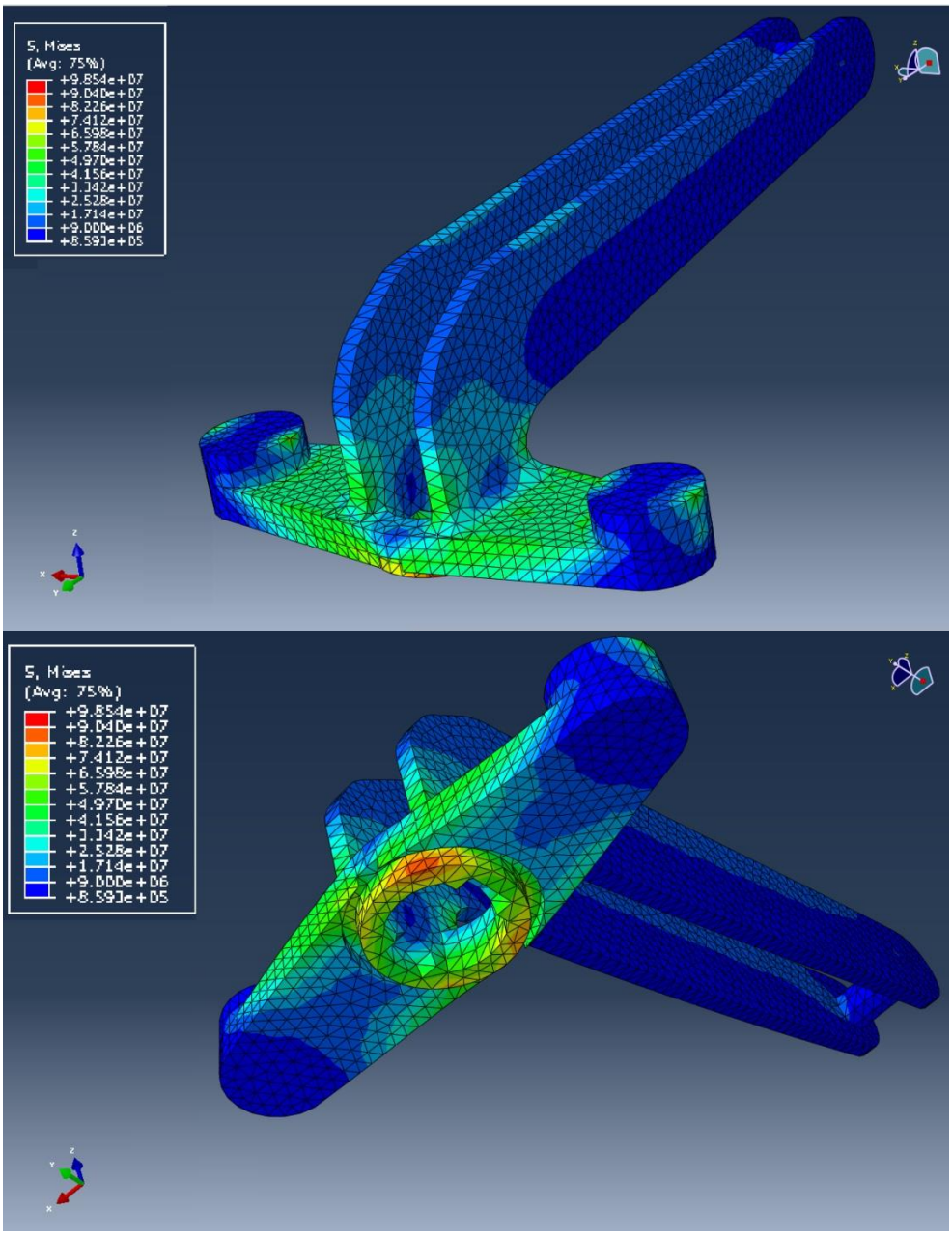

Figure 3.2i: Result from the simulation of the upper part, showing the stress magnitude in Pascal and areas with different stresses. The same principle for the strain, where the result is given in meters.

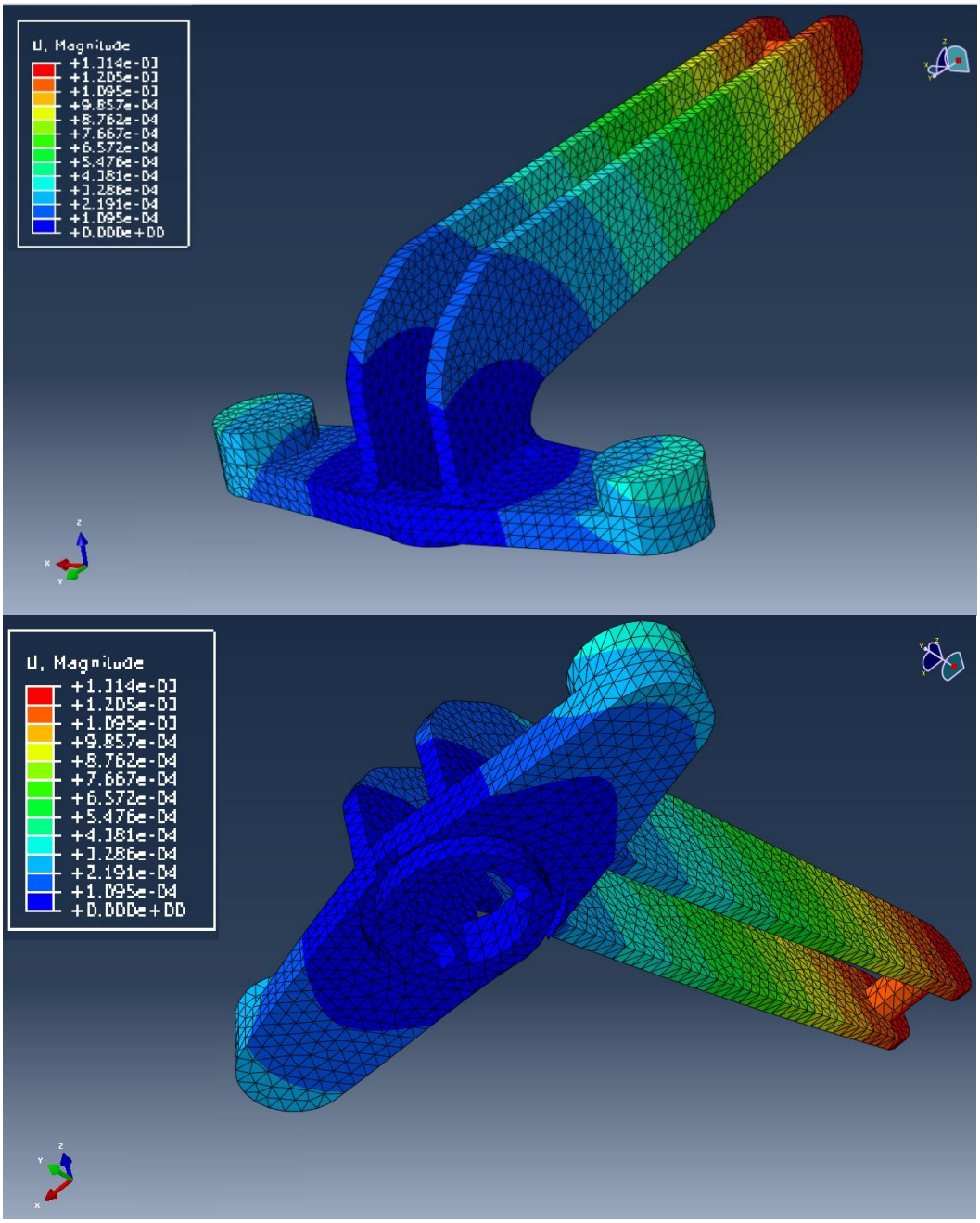

Figure 3.2i: Continued.

3.2.2.3 The lower part

This is the lower part of the lever concept which hold the lower half of the lever. The extending parts at the bottom are attached in the steering unit and the top is attached with the upper part. When the steering hydraulics turn the upper part, the lower part will also turn causing the steering unit to turn. The lever moves back and forth in the void in the cylinder pushing the rod attached to the reversing mechanism.

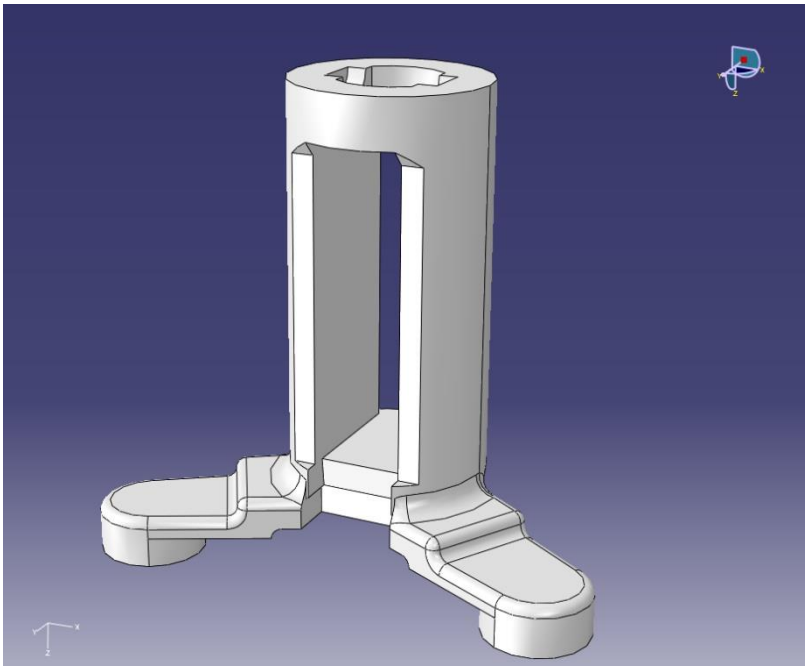

Figure 3.2j: illustration of the lower part.

The rotation causes a torque in this construction rather than forces acting in different directions. This torque is the one given in diagram 3.2a and illustrated with a purple arrow in the top center in figure 3.2k. The torque is constrained to apply for the whole top surface of the lower part. The results of this simulation are shown in figure 3.2l. The boundary condition is placed in the attachment point positioned at the steering unit.

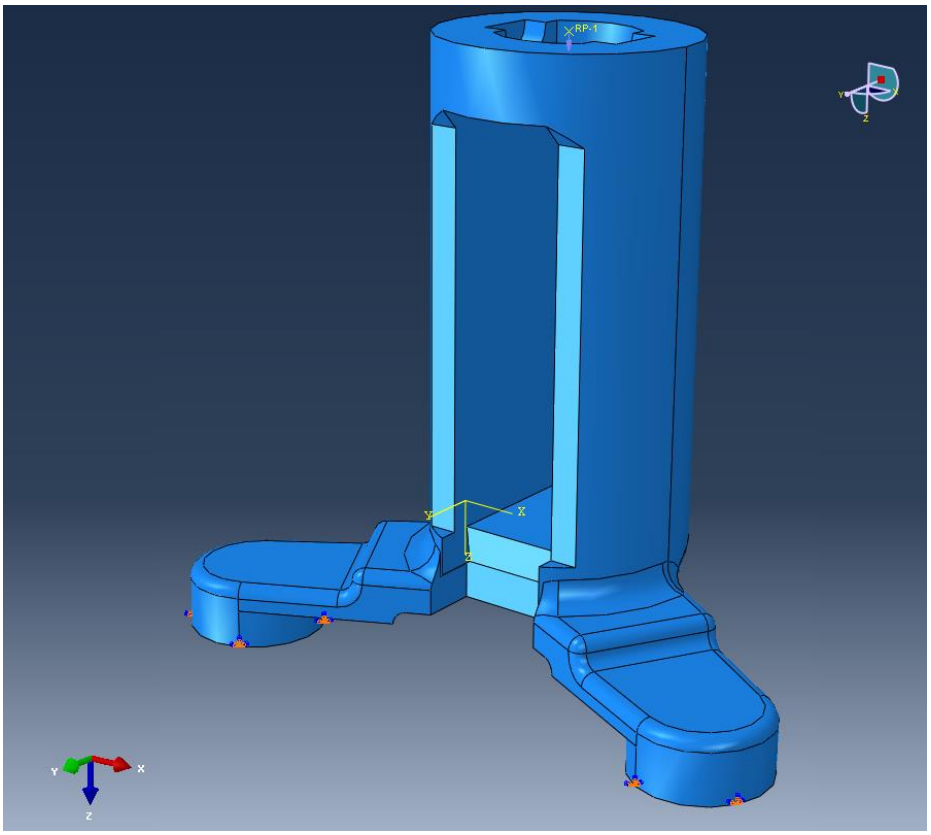

Figure 3.2k: Illustration of the lower part with torque and boundary conditions. See table 3.2d for details.

Table 3.2d. Abaqus data of the lower part needed to make a simulation.

Property	**Description of what has been set**
Component	3D, deformable
Material	Elastic Young's modulus (E) = 210GPa Poisson's ratio (v) = 0.3
Load/Force/ Torque	Torque At RP1 on the top surface, magnitude of 125000N.
Boundary condition	Rigid at the bottom surface of the attachments. It cannot move in x, y or z direction.
Mesh	Free tetragonal elements Seed; 0.03 Number of elements; 22281

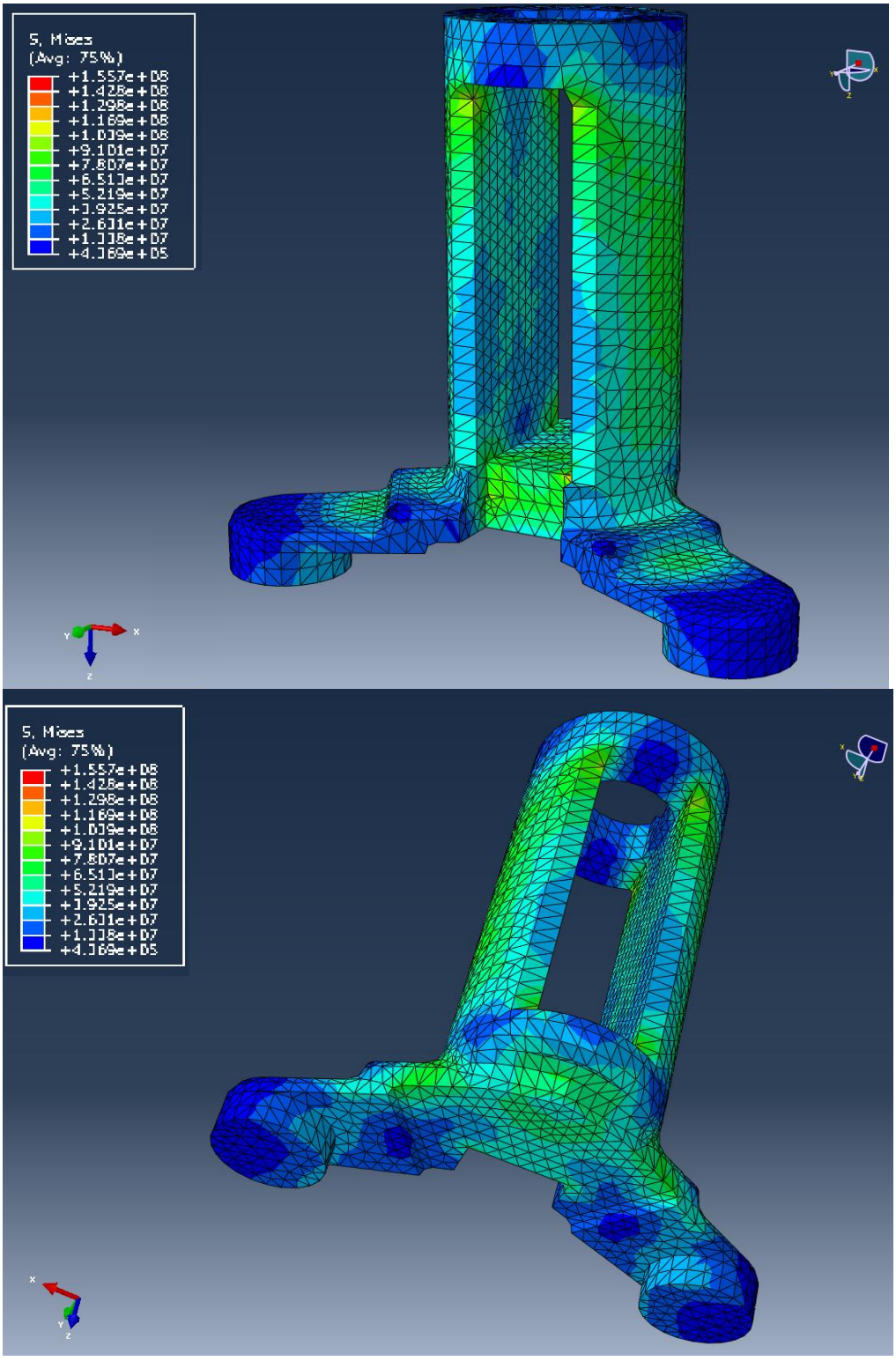

Figure 3.2l: Result from the simulation of the lower part, showing the stress magnitude in Pascal and areas with different stresses. The same principle for the strain where the result is given in meters.

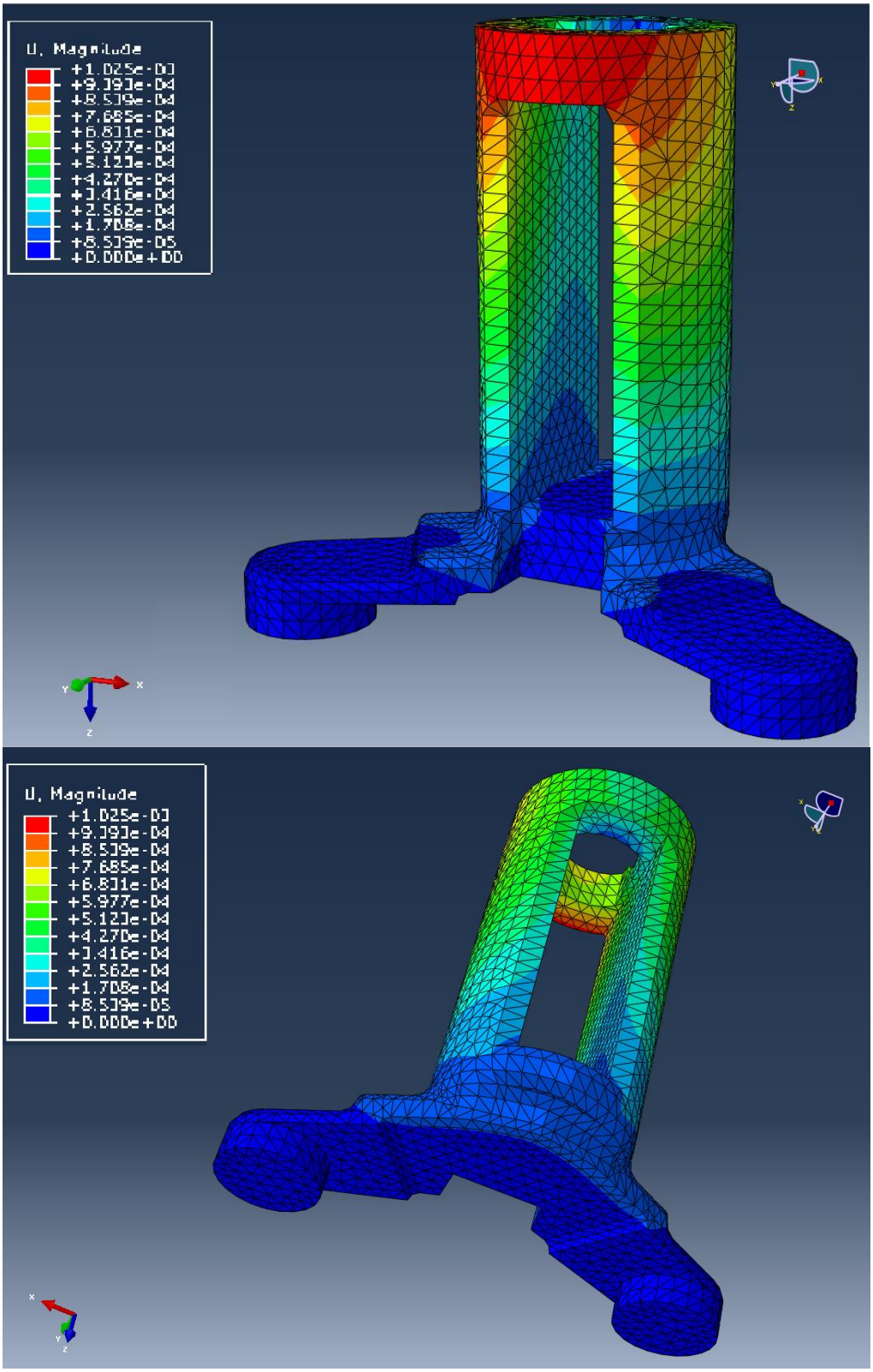

Figure 3.2l: Continued.

3.2.2.4 The steering hydraulic holder

Depending on how the lever concept is attached, directly in the boat or not, there may be need for a support for the steering hydraulics attached to the upper part. This is shown in figure 3.2m. The circular hole in the front will coincide with the attachment point of the upper part. One end of the hydraulic cylinder is attached in the cylindrical elevations on the upper part, the other end will be attached to the cylindrical attachments on this part.

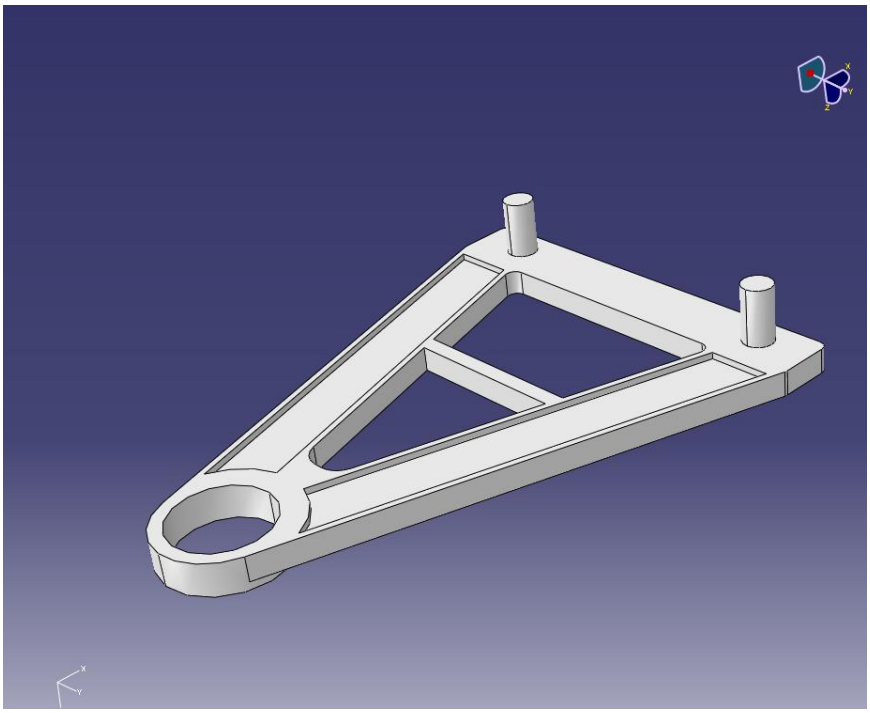

Figure 3.2m: Illustration of the holder for the steering hydraulics.

Table 3.2e shows the properties for the supporting holder and figure 3.2n show how the boundary condition and forces are applied. The direction of the forces and positioning of the boundary conditions is in agreement with the same arguments as for the upper part of the concept.

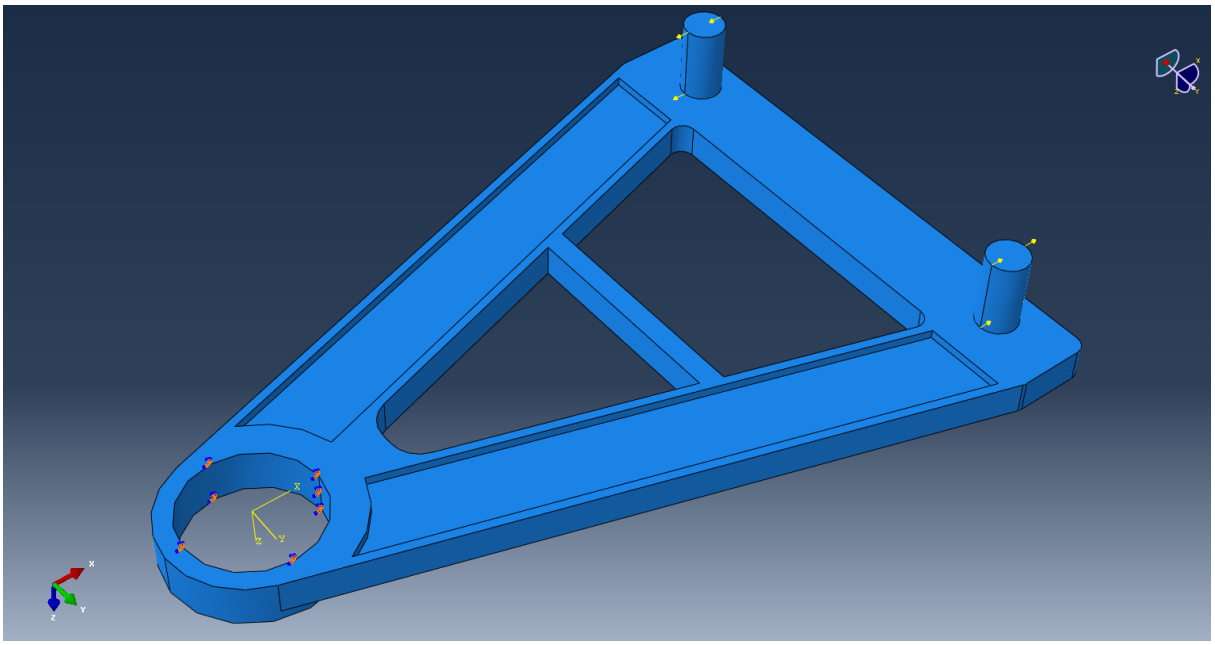

Figure 3.2n: Illustration of the support holder with forces and boundary conditions. See table 3.2e for details.

Table 3.2e. Abaqus data of the steering hydraulic holder needed to make a simulation.

Property	**Description of what has been set**
Component	3D, deformable
Material	Elastic Young's modulus (E) = 210GPa Poisson's ratio (ν) = 0.3
Load/Force/ Torque	Concentrated force 4 points/end, 37500N/point
Boundary condition	Rigid at the round hole. It cannot move in x, y or z direction.
Mesh	Free tetragonal elements Seed; 0.03 Number of elements; 18566

The result for the support holder is shown in figure 3.2o.

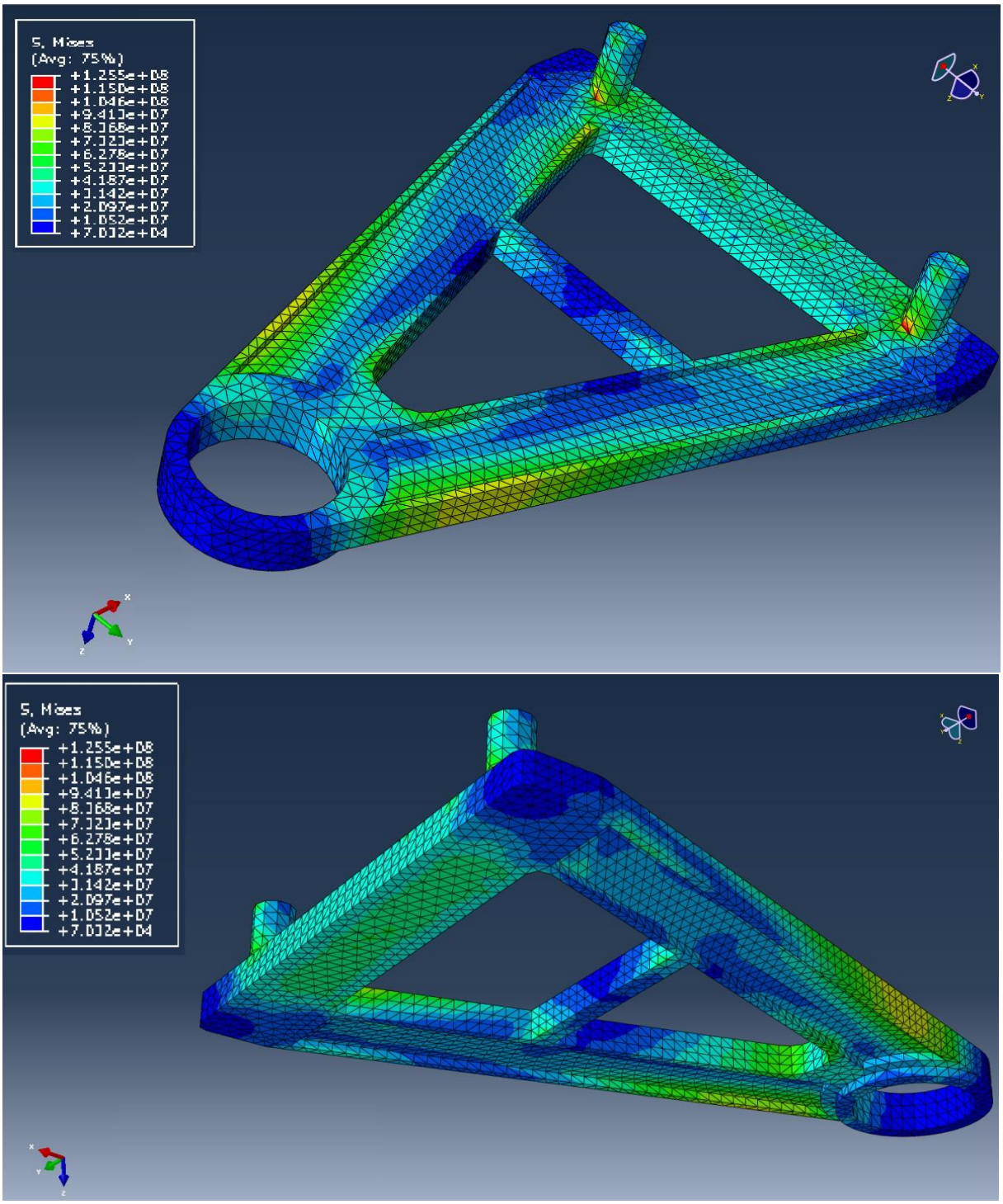

Figure 3.2o: Result from the simulation of the hydraulic holder, showing the stress magnitude in Pascal and areas with different stresses. The same principle for the strain where the result is given in meters.

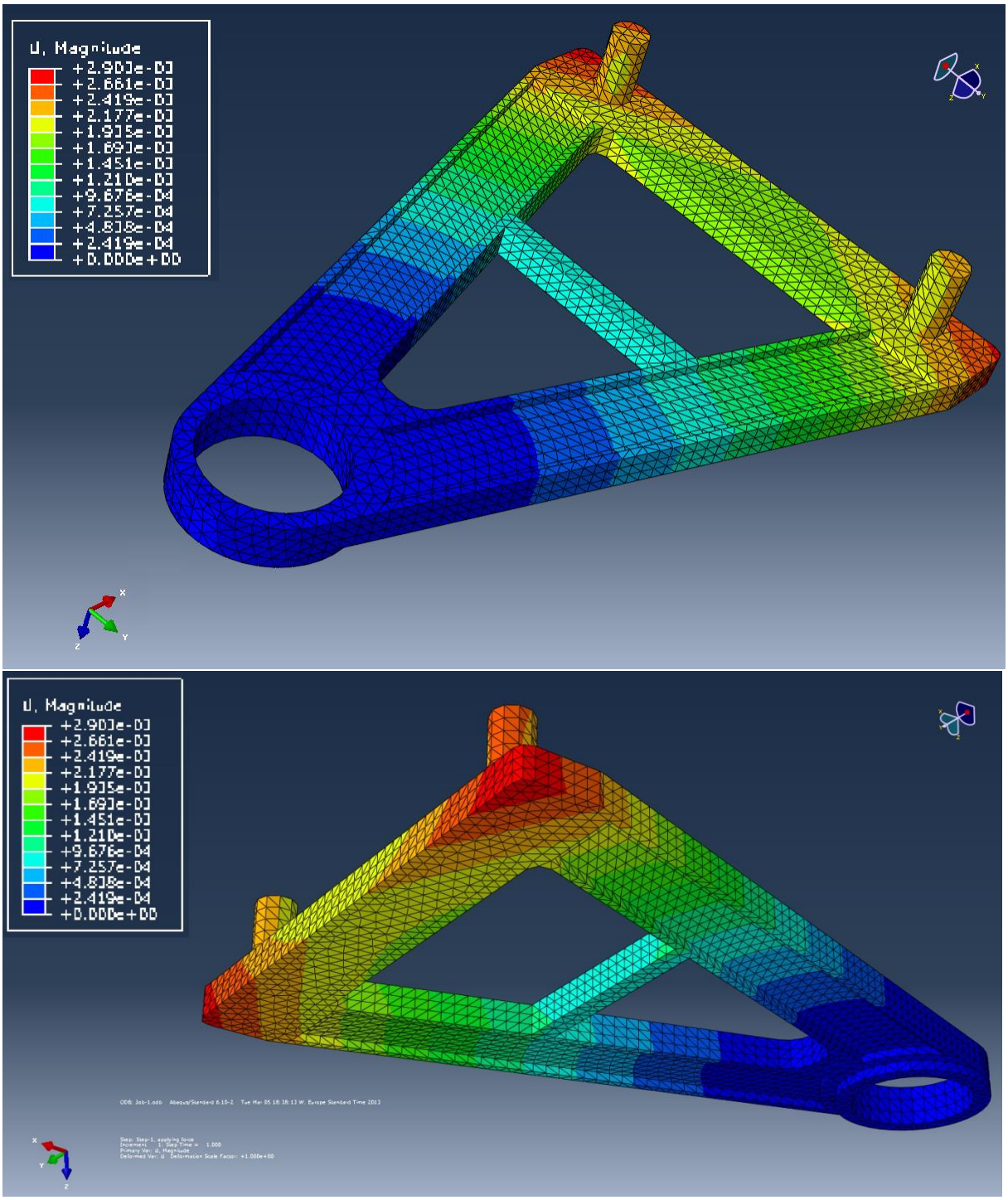

Figure 3.2o: Continued.

3.2.2.5 The pushrod

This part will transfer the force from the lever to the reversing mechanism. The fork end of this part is attached to the lever. The other end is attached to the reversing mechanism.

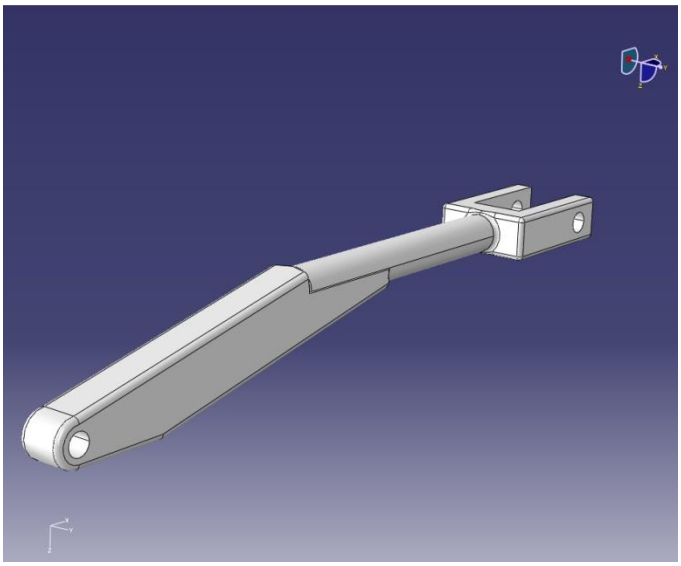

Figure 3.2p: Illustration of the pushrod.

The forced applied in the fork end is the forces acting from the lever when it is in full reverse mode. The boundary conditions represent the attachment in the reversing mechanism.

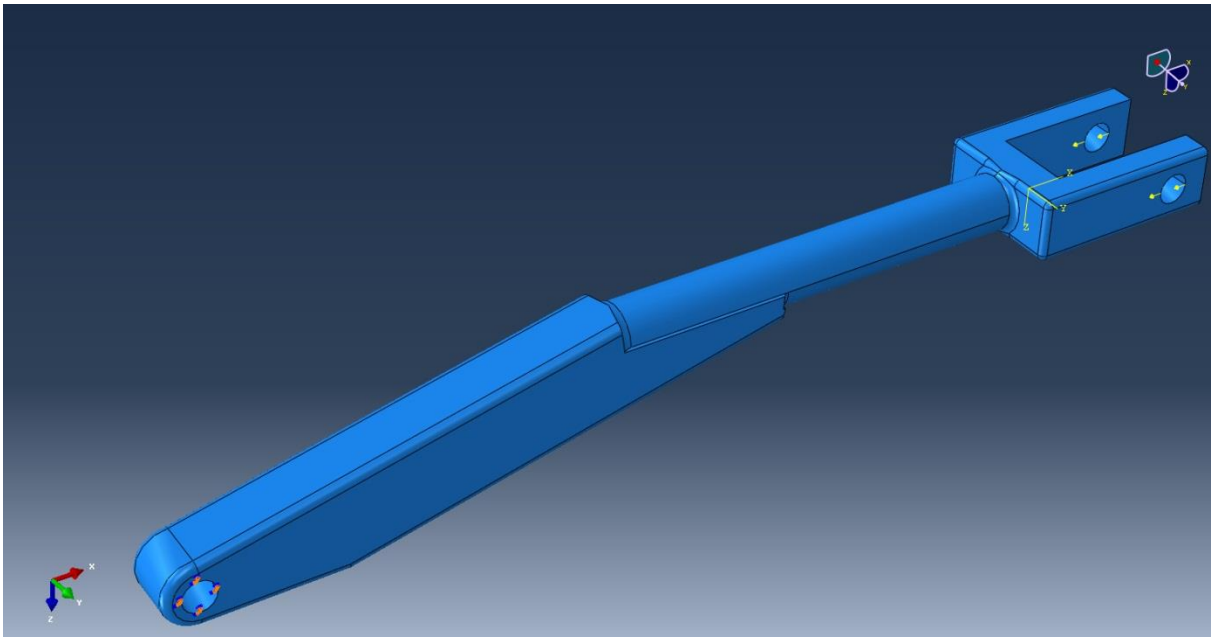

Figure 3.2q: Illustration of the pushrod with forces and boundary conditions. See table 3.2f for details.

Table 3.2f. Abaqus data of the pushrod needed to make a simulation.

Property	**Description of what has been set**
Component	3D, deformable
Material	Elastic Young's modulus (E) = 210GPa Poisson's ratio (ν) = 0.3
Load/Force/ Torque	Concentrated force 8 points, 15625N/point
Boundary condition	Rigid at the hole where it should be attached to the reversing bucket. It cannot move in x, y or z direction.
Mesh	Free tetragonal elements Seed; 0.015 Number of elements; 24813

The result from the simulations are shown in figure 3.2r.

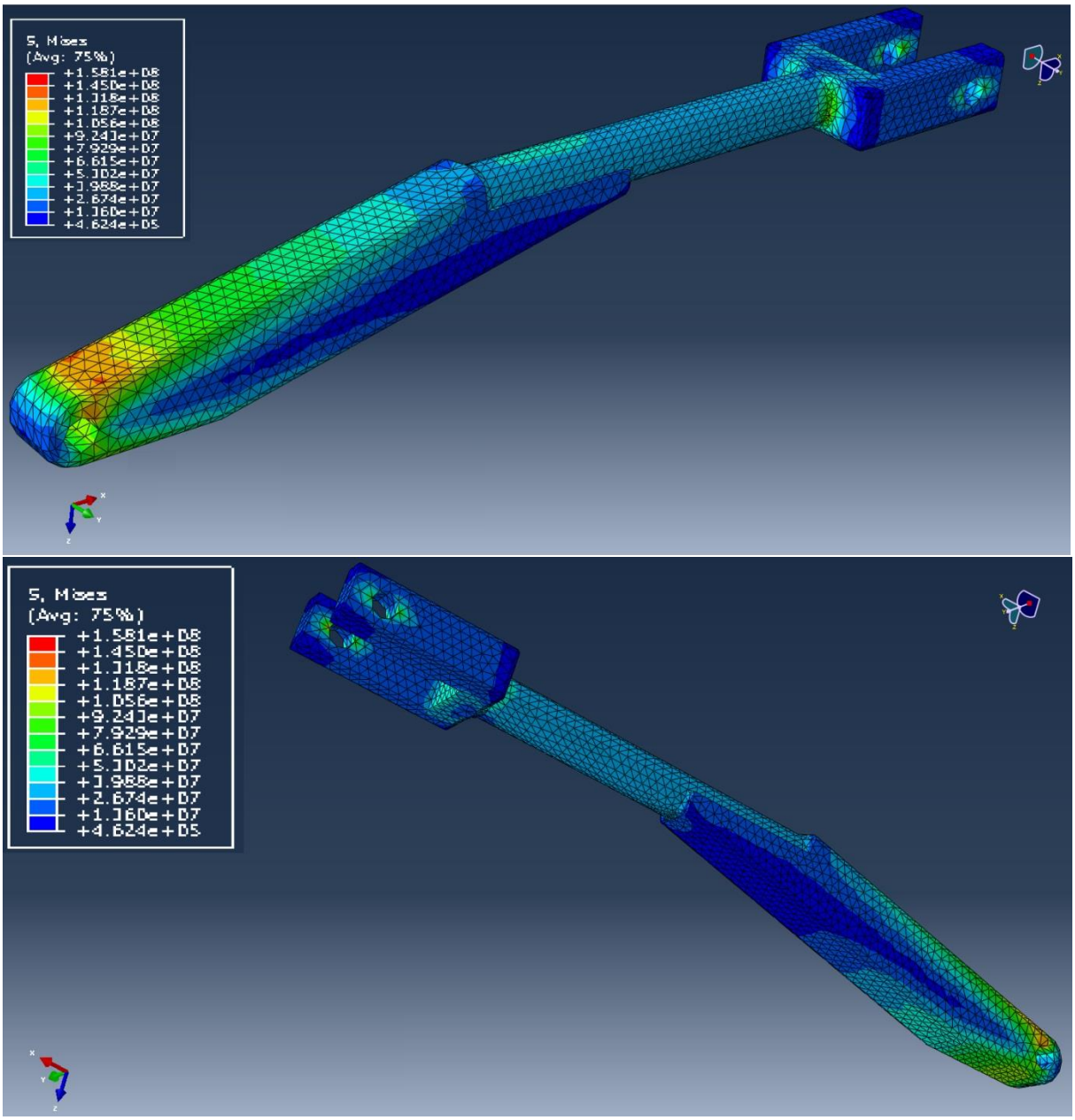

Figure 3.2r: Result from the simulation of the pushrod, showing the stress magnitude in Pascal and areas with different stresses. The same principle for the strain where the result is given in meters.

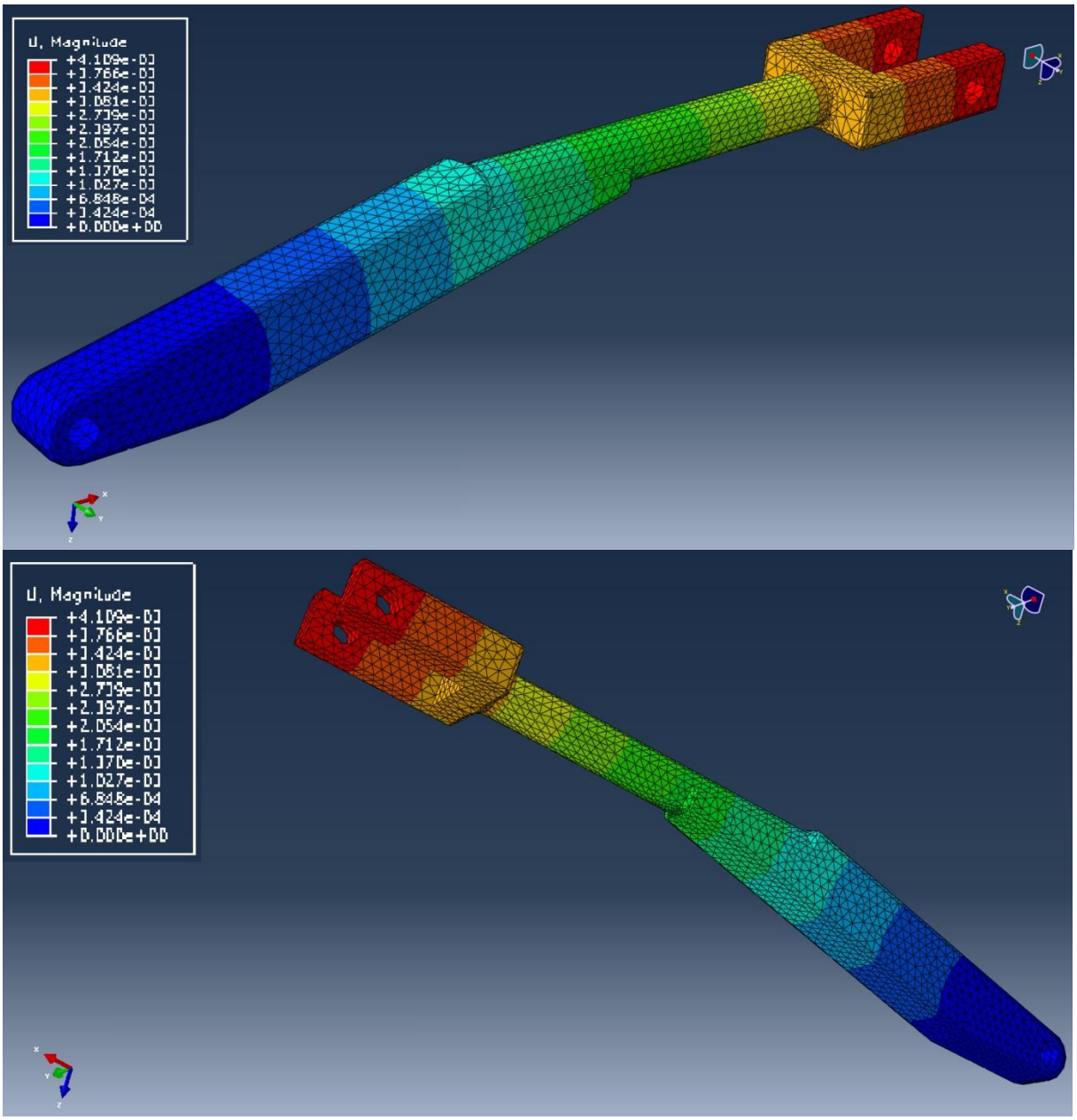

Figure 3.2r: Continued.

3.2.2.8 Overview

To get an overview of the lever concept the simulation results are summarized in table 3.2g.

Table 3.2g. Simulation result of the lever concept with general steel properties.

Part	Young's modulus [GPa]	Poisson's ratio	Maximum stress [MPa]	Maximum elongation/deflection [mm]
The lever	210	0.3	527	5.0
The upper part	210	0.3	58	1.3
The lower part	210	0.3	117	1.0
The hydraulic holder	210	0.3	94	2.9
The pushrod	210	0.3	145	4.1

The simulations have given a good understanding on the major problem areas, thou further development is necessary. Areas which experience rotation or bending is the most important to develop because of the highest loads arise there.

The ridged boundary condition suppresses the otherwise natural movement of the cooperating parts which will lower the stress needed to make the system move. These relationships will have to be studied in assemblies to receive a greater understanding.

Also the force positioning as mentioned before needs to be more homogeneous to avoid the elevated stresses in the points where they are placed even though it will give an understanding of the acting forces in the component.

3.2.2.8.1 Results for materials with other Young's modulus and Poisson's ratio

The lever concept have been tested with general values for steel, but in this section certain steel types have been used during simulation and the values are found in section *1.6 Material properties.* The simulation is carried out on the parts in the same condition as in above respective table, table 3.2b-3.2f, except that the Young's modulus and Poisson's ratio differs.

The new values are summarized in below tables, table 3.2h – 3.2j. Carbon steel and stainless steel results are similar to which is shown in table 3.2g due to their Young's modulus and Poisson's ratio fall under general steel values and are therefore not shown below.

Table 3.2h. Simulation result of the lever concept with general cast iron properties.

Part	Young's modulus [GPa] Gray/Ductile	Poisson's ratio	Maximum stress [MPa] Gray/Ductile	Maximum elongation/deflection [mm] Gray/Ductile
The lever	110/170	0.27	528/528	9.5/6.1
The upper part	110/170	0.27	51/51	1.6/2.5
The lower part	110/170	0.27	132/132	1.9/1.3
The hydraulic holder	110/170	0.27	96/96	5.5/3.6
The pushrod	110/170	0.27	147/147	7.8/5.1

Table 3.2i. Simulation result of the lever concept with general aluminum properties.

Part	Young's modulus [GPa]	Poisson's ratio	Maximum stress [MPa]	Maximum elongation/deflection [mm]
The lever	75	0.34	524	13.8
The upper part	75	0.34	48	3.7
The lower part	75	0.34	127	2.9
The hydraulic holder	75	0.34	100	8.2
The pushrod	75	0.34	143	11.5

Table 3.2j. Simulation result of the lever concept with general titanium properties.

Part	Young's modulus [GPa] Pure/Alloy	Poisson's ratio	Maximum stress [MPa] Pure/Alloy	Maximum elongation/deflection [mm] Pure/Alloy
The lever	103/115	0.36	521/521	10.0/9.0
The upper part	103/115	0.36	64/64	2.7/2.4
The lower part	103/115	0.36	75/75	2.1/1.9
The hydraulic holder	103/115	0.36	98/98	6.0/5.4
The pushrod	103/115	0.36	142/142	8.4/7.5

The results show that changing the material does mostly affect the strain while the stresses remain almost the same. This implies that different materials are suited for different components because they experience different kind of loading conditions.
This behavior can be connected to the article *"A unified fatigue life prediction method for marine structures"* where the present issues related to fatigue resistance for different types of steel.

3.2.2.9 Convergence study

3.2.2.9.1 The lever

Table 3.2k. Data from the simulation to obtain a convergence diagram for general steel properties.

Seed	Number of elements	Maximum stress [MPa]
0.023	25206	380
0.022	26784	432
0.021	30630	487
0.020	34623	527
0.019	37359	512
0.018	41856	543
0.017	46670	463
0.016	54257	511
0.015	61093	520
0.014	68160	525
0.013	78559	541

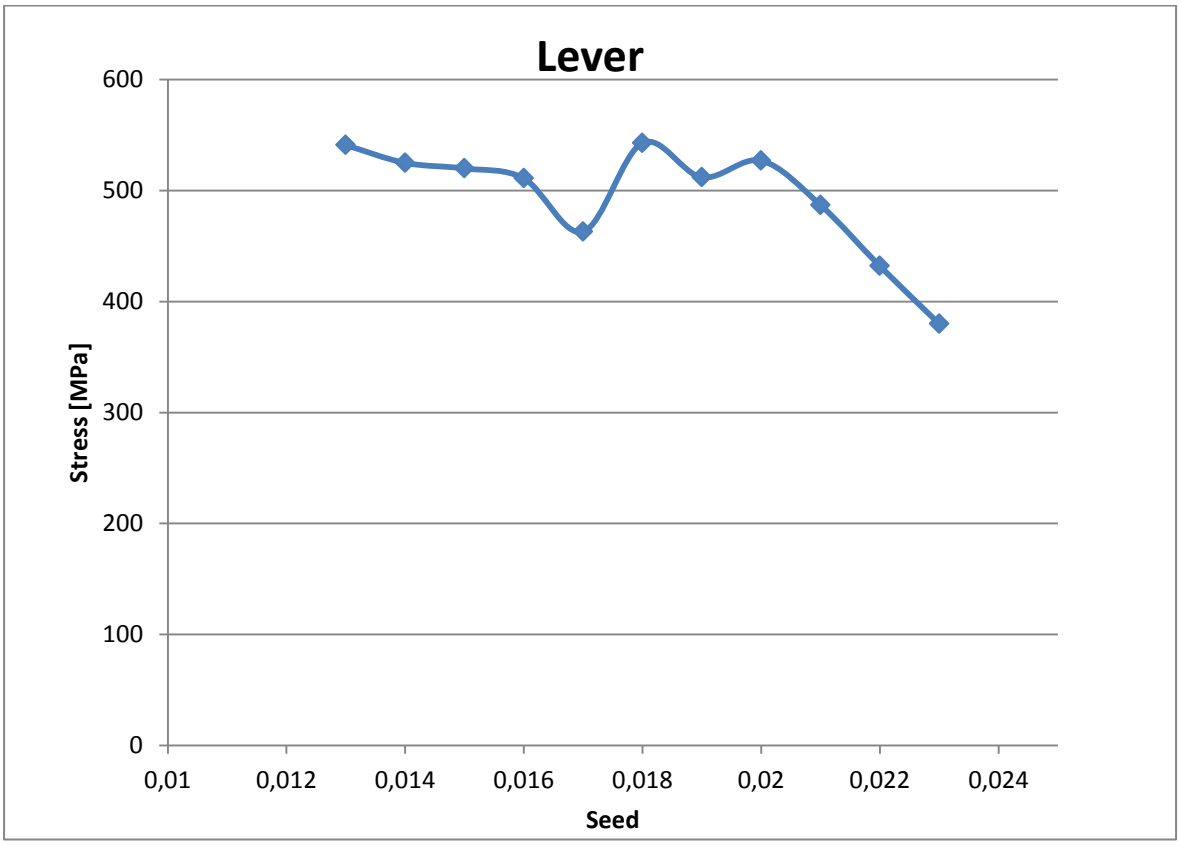

Diagram 3.2b: The curve of seed vs. stress for the lever.

3.2.2.9.2 The upper part

Table 3.2l. Data from the simulation to obtain a convergence diagram for general steel properties.

Seed	Number of elements	Maximum stress [MPa]
0.030	21686	58
0.029	23081	58
0.028	26304	60
0.027	27653	61
0.026	31334	67
0.025	33632	63
0.024	37349	73
0.023	41326	74
0.022	47954	71
0.021	54450	75
0.020	63650	83

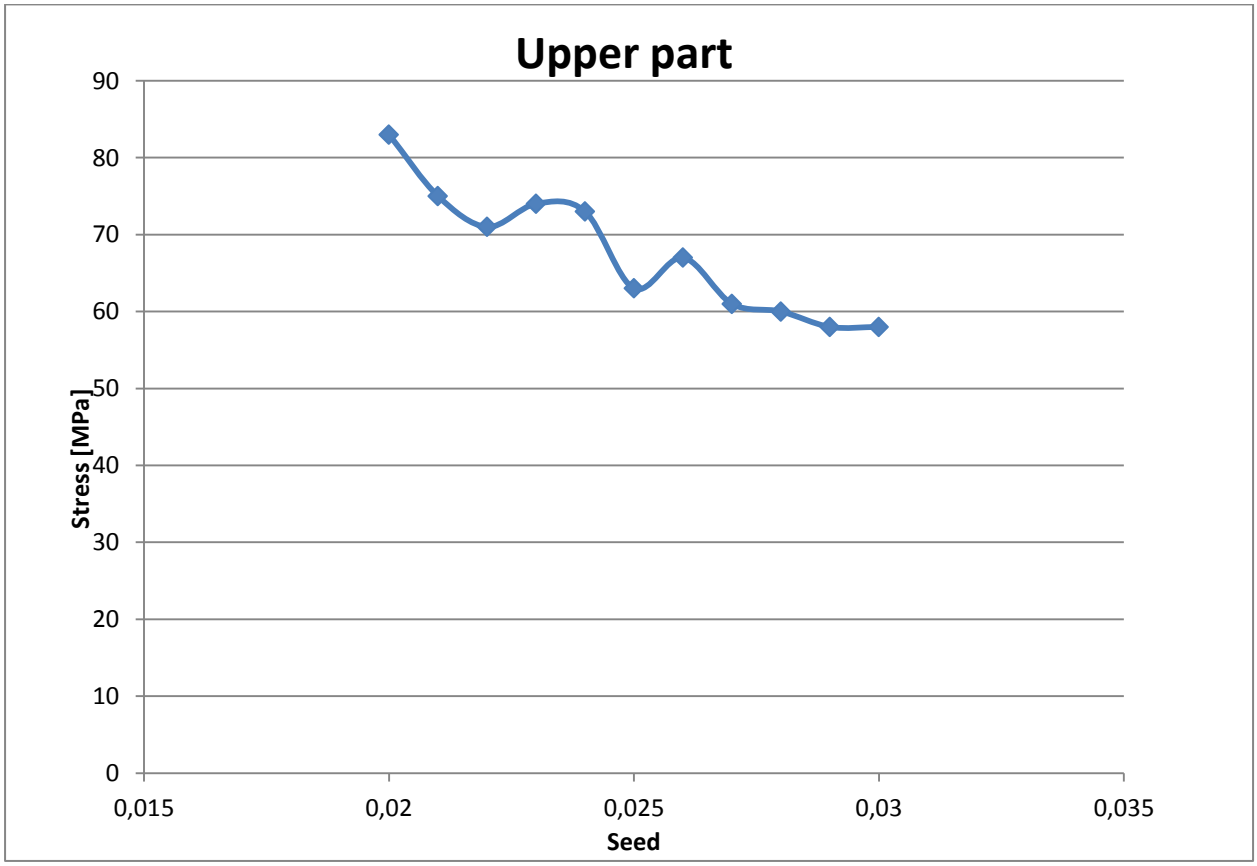

Diagram 3.2c The curve of seed vs. stress for the upper part.

3.2.2.9.3 The lower part

Table 3.2m. Data from the simulation to obtain a convergence diagram for general steel properties.

Seed	Number of elements	Maximum stress [MPa]
0.030	22281	116.9
0.029	23747	122.5
0.028	27014	128.8
0.027	29588	128.7
0.026	31964	123.1
0.025	37489	123.9
0.024	40200	127.0
0.023	45397	133.5
0.022	49537	127.7
0.021	56466	129.2
0.020	63352	143.4

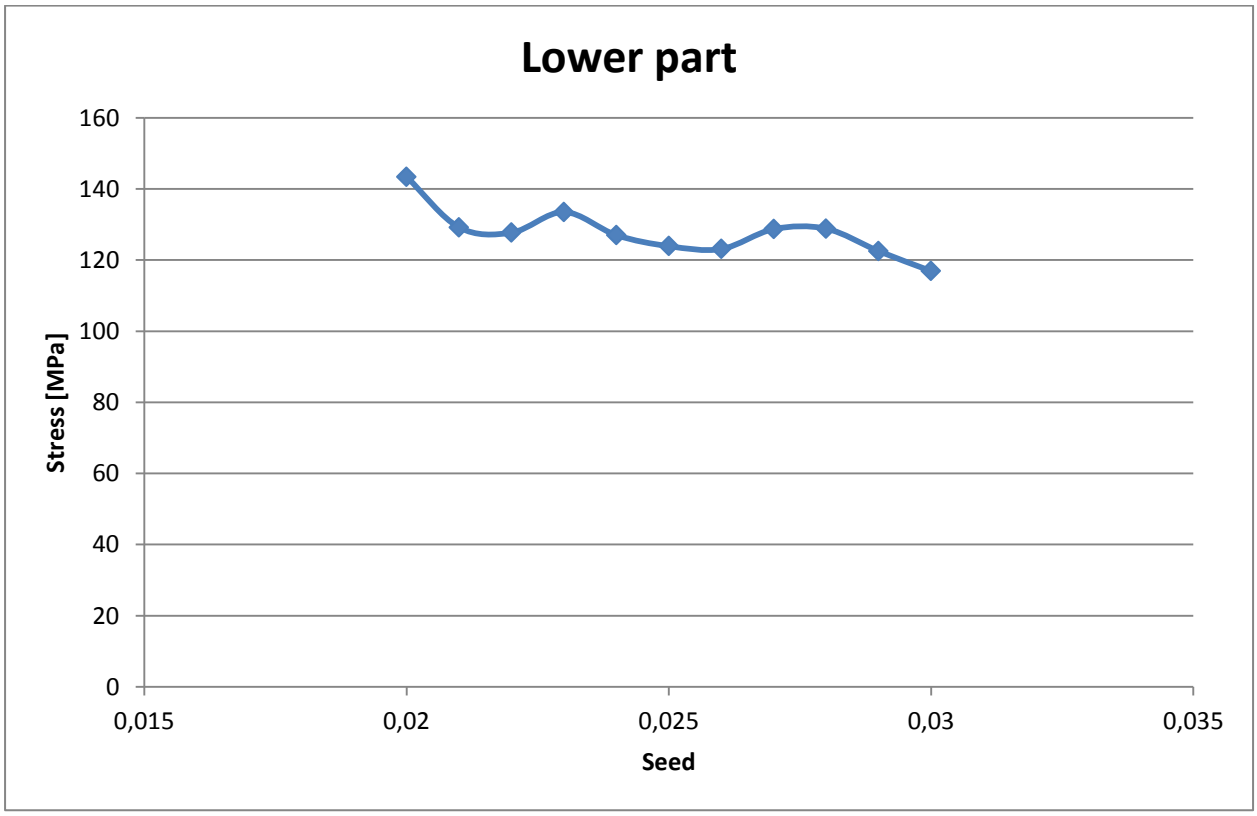

Diagram 3.2d The curve of seed vs. stress for the lower part.

3.2.2.9.4 The steering hydraulic holder

Table 3.2n. Data from the simulation to obtain a convergence diagram for general steel properties.

Seed	Number of elements	Maximum stress [MPa]
0.030	18866	94.1
0.029	20823	103.8
0.028	22201	96.1
0.027	24108	104.0
0.026	25797	104.0
0.025	28892	107.6
0.024	30847	104.5
0.023	34891	102.6
0.022	39675	103.9
0.021	46516	114.1
0.020	50110	112.6

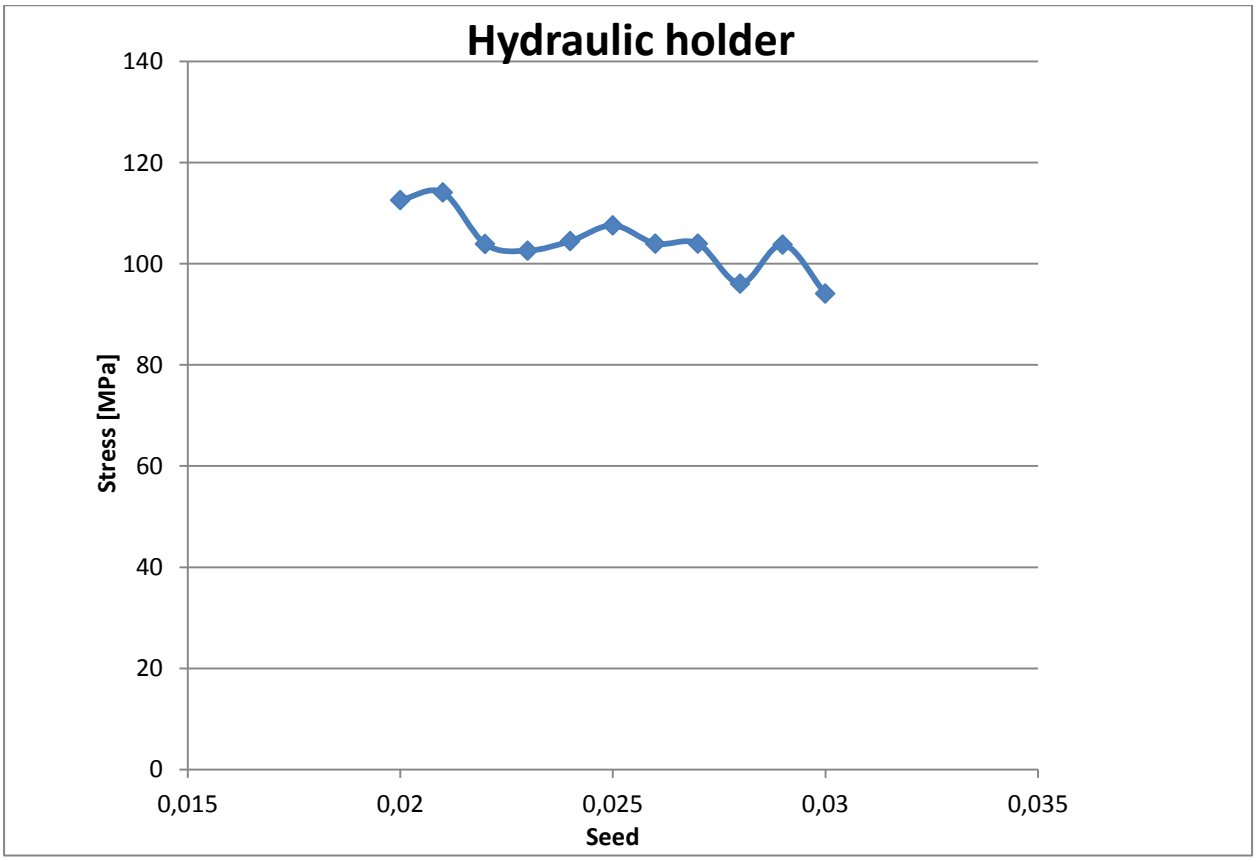

Diagram 3.2e The curve of seed vs. stress for the hydraulic holder.

3.2.2.9.5 The pushrod

Table 3.2o. Data from the simulation to obtain a convergence diagram for general steel properties.

Seed	Number of elements	Maximum stress [MPa]
0.019	15978	134.6
0.018	17060	132.5
0.017	19130	133.0
0.016	22612	134.7
0.015	24813	145.0
0.014	31169	150.0
0.013	36850	144.0
0.012	44166	153.2
0.011	55946	148.5
0.010	68971	147.6
0.009	92259	152.5

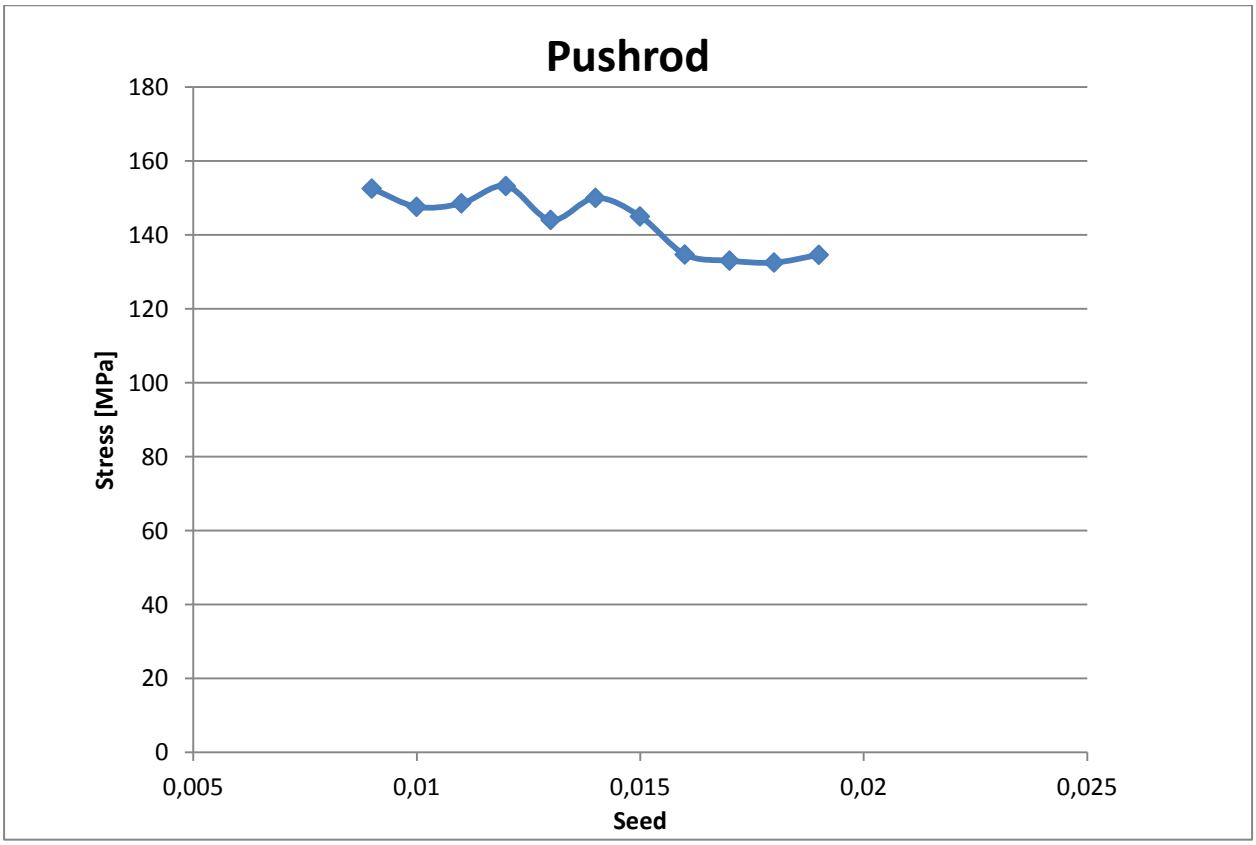

Diagram 3.2f The curve of seed vs. stress for the pushrod.

The above diagrams should converge to a specific value which represents the maximum load. In most of the diagrams the maximum load is going towards infinity which is not acceptable. Possible reasons for this error can be caused by wrong interpreted results or the mesh used should be heterogeneous and not the same size all over.

Other reasons can be that the values are manually read after studying the different color areas from the simulation and due to that the forces are not uniformly applied these values may not be able to converge until new more specific simulations are made.

4. Suggestion of continuation

4.1 Deeper material investigation

A more thorough material investigation must be done as mentioned. One needs to know the exact properties the surrounding environment and the forces acting on the material demands. There are a lot more variables which influence these demands than corrosion and fatigue strength, where only fatigue is mentioned in this report. How well the material will coincide with other steels grades for example, which probably will be the case for this concept due to the different loading cases and different environmental aspects depending on which part is treated. Also the physical size of the concept will limit the material properties. There is a maximum size which will demand a minimum stress level which must be achieved, but the dimensioning will not be able to compensate. That maximum size will help precise the life time and fatigue calculations of the different parts which will narrow the material properties interval. Also the budget for developing projects will force a balance between material properties and cost.

4.2 More detailed simulation

When the material study is complete the result can be implemented in the simulations. To make the simulation more thorough the different part should be simulated as dynamic, that is the boundary conditions should be further developed to represent the concurrency with the other parts. As mentioned before the forces should be applied homogenously to be able to get stress and strain results from the entire part.

Also a complete assembly must be simulated to see the effect the different parts have on each other and what is reasonable regarding the elongation so it does not influence the rest of the concept.

4.3 Parameterization

For this concept to be economical it must be able to be applicable for all the different sizes of the Kamewa water jet. That means that a new parameterization must be performed once the concept is optimized. The size increase is almost linear between the different models and should hopefully not be a problem but further investigation is needed. The *2.5 Parameter variations* in the report is to help with this matter so each model of the water jet will be optimized in terms of efficiency and size.

4.4 More specific calculation for all the parts

The calculations that are done generally include a lot of assumptions and simplifications. The calculations make out a good starting point in taking the next step towards deeper analysis. To investigate if the concept could be realized more work has to be done in this area. As of today this report proves that the concept could work if certain assumptions are made. There are also different issues that are not yet addressed like analysis of the interfaces between moving parts. The interfaces between the different parts are the weak links in the system and these needs to be secured that they can withstand the stresses that will arise during operation.

Also not treated in this report is to calculate when possible cracking phenomena will occur, in this report an assumption was made that if the stresses stay below the fatigue stress the specific part will withstand the specified cycle life written in CES EduPack. As mentioned in the article *"A unified fatigue life prediction method for marine structures"* it is an accumulative damage made to the material and especially if there is a crack present in the material. So the life cycle needs to be evaluated after hand because the conditions changed depending on how many cycles the material have withstand.

5. Conclusion

The initial task of relocating the hydraulic steering cylinders from outboard to inboard proved to be a complex mechanical problem. Due to the given conditions this could only be done by elevating the hydraulic cylinders from the plane of where the power output is needed. The two main functions of the steering bucket are very complicated when trying to incorporate them with each other. In an early stage it was also noticed that other variables would dominate the concepts problematic. Good basic analyses of the problems were needed to get an understanding of which parts needed what continuation to be able to evolve this to a functional concept.

6. Acknowledgment

The author would like to thank Christer Häger for giving them the main task of this report and Robin Holmgren for providing data from Rolls-Royce to support the simulations and for giving feedback along the way.

Special thanks to Nils Hallbäck, Jens Bergström, Marianne Johansson and Anders Gåård at the Faculty of Health, Science and Technology at Karlstad University for supervision and guidance throughout the process.

Also a final thanks to Nichlas Westerlund, the author of *"Water jet steering concept - evaluation of an environmental design, Part 2"*, for cooperation with this master thesis even though we could not finish it together.

7. References

[1]: [Project specification]

[2]: Cornell, G.C, (1999). Should a Jet Drive Be Considered For Your Next Boat? Marine Jet Drives -- The Wave of the Future, http://www.ultradynamics.com/sections/educational/why.asp, 2010-11-13.

[3] Weicheng Cui a,Fang Wang , Xiaoping Huang, *"A unified fatigue life prediction method for marine structures"*, Marine Structures 24 (2011) 153–181.

[4]: Hertzberg, Richard W, *"Deformation and fracture mechanics of engineering materials"*, forth edition, 1996 John Wiley & sons, Inc.

[5]: Askeland Donald R, Phulé Pradeep P, *"The science and engineering of materials",* fifth edition, 2006 Nelson a division of Thomson Canada Limited.

[6]: Jakubowski M., "*Fatigue crack propagation in austenitic stainless steel under low frequency loading and saltwater conditions*", 21:937-946, 1998, Fatigue & Fracture of engineering materials & Structures

[7]: Budinski Kenneth G, Budinski MichaelK., *"Engineering materials – properties and selection"*, eighth edition, 2005 Pearson Education Inc., Upper saddle River, New Jersey 07458.

[8]: www.skf.com , Svenska Kullagerfabriken, *"SKF industrial seals product structure"*, http://www.skf.com/skf/content/popupimage.jsp?popupimage=/cmimages/241717.gif&lang=en&imgCaption=SKF+Industrial+seals+product+structure , 2010-11-22.

[9]: Olsson Karl-Olof, *"maskinelement"*, first edition, 2006 Karl-Olof Olsson and Liber AB.

[10] Westerlund Nichlas, "Water Jet Steering Concept - evaluation of an environmental design, Part 2", Master Thesis 30hp, Karlstad University, Ongoing.

[11]: Meriam J.L, Kraige L.G, *"Engineering Mechanics Statics"*, fifth edition, 2003 John Wiley & sons, Inc.

[12]: Björk Karl, *"Former och tabeller för mekanisk konstruktion",* sixth edition, Karl Björks förlag HB

Appendix 1 – Project specification and Maneuvering profiles S3

Rolls-Royce

RR AB's Info. class: Limited

M.Sc. thesis project at Rolls-Royce AB – Inboard hydraulics for S3 range of waterjets

The purpose of this document is to act as a reference for a design study by Karlstad University Students and should not be distributed nor copied outside this group.

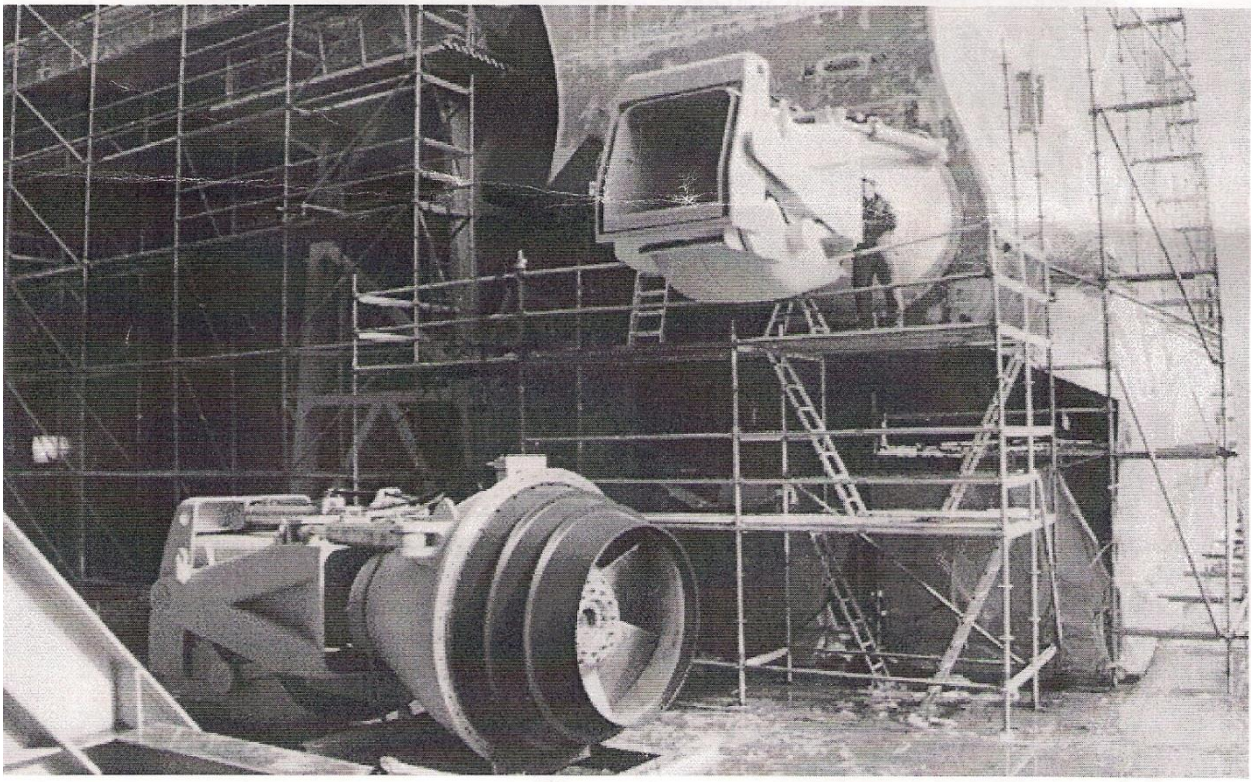

General description

The Kamewa water jet system consists of an inlet duct, a pump with an outlet nozzle shaping the jet stream, and a steering and reversing gear. A steering nozzle accomplishes steering by deflecting the jet stream. A reversing bucket in the steering nozzle achieves astern thrust. An outboard positioned bearing arrangement carries the axial and radial load.

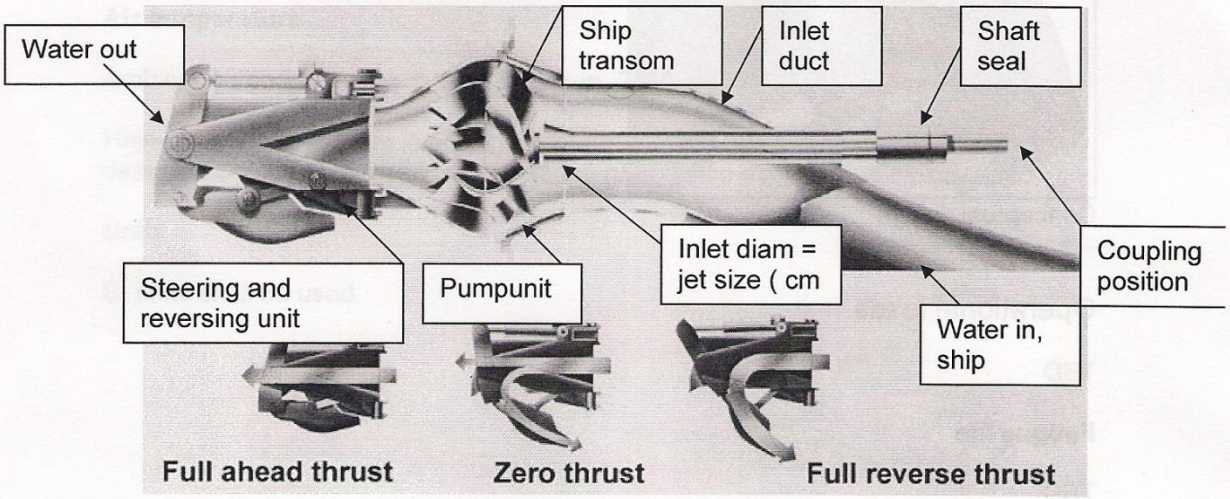

Problem description

Steering and reversing actuation is performed by using outboard hydraulic cylinders. This position presents always a risk of oil spill because of the existence of flexible hoses outside the transom. If any problem occur regarding the function of the cylinders the position also requires outboard and in-water service procedures which can be very time consuming depending of the actual environmental conditions. Moving the cylinders inboard will reduce all the above disadvantages.

Design task

Design an inboard cylinder mechanism capable of handling both the outboard steering and reversing mechanism. The design work should follow the principles outlined in the following concept and focus on dimensioning and selection of materials and detail solutions through CAD and FEM work

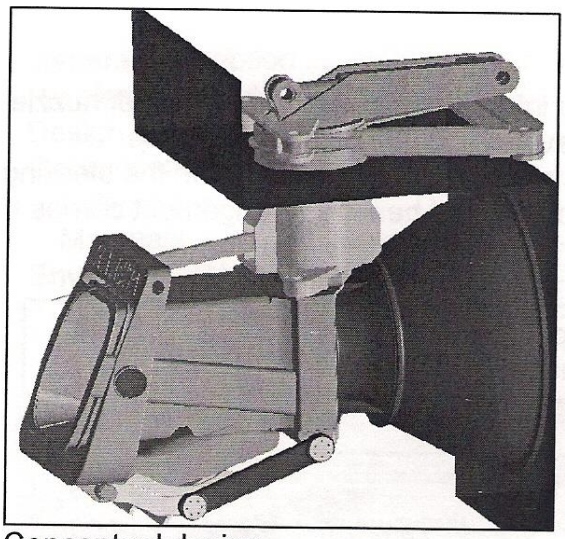

Conceptual design

Operational loads

TBD

Fatigue life

TBD

Materials

If the design work shows that materials other than duplex stainless steel can be used, the influence on system corrosion properties must be evaluated.

The design shall consider the use of environmental friendly materials and components to minimize the impact on the environment during the product life cycle.

Environmental conditions

TBD.

Water temperature

Ambient seawater temperature of between -4°C and +32°C (DNV Pt.5 Ch.10 Sec.3 A 302).

Air temperature

Ambient outboard temperature of between -20°C and +40°C.

High reliability is of great importance, therefore the actuating mechanism should be designed so risk of damage due to marine growth, ice-accretion, etc. is avoided.

Units

SI units shall be used.

Maintainability

The system should be designed for an overhaul of minimum 5 years at the anticipated operational profile described. All components shall be designed for easy normal service and maintenance.

Classification

The product must be produced in such way that the classification societies such as Det Norske Veritas, Lloyds Register, and ABS etc will accept the product for worldwide use in marine applications. The subcontractor must carry out the application for approval.

A classification society or other relevant authority can request material certificates, calculations and detail drawings for approval.

Handling

Suitable lifting points should be well described.

List of Appendix

Record of changes

Rev No	Date of Revision	Relevant paragraph	Brief description / By
A B C D			

Rolls-Royce

Manoeuvring profiles S3

Kamewa waterjets will be designed according to DNV Class Notes 30.8. The equipment shall have a service life of at least 25 years in operation (DNV Class Notes 30.8 calculate with 20 years).

Steering
The steering load varies with the angle ranging from corrective steering 5° and full steering 30°. Assuming corrective steering cycle of 20 seconds, 12 hours per day for all sea-states. Assuming full steering 40 hours per year.

Total number of steering cycles for 25 years is estimated to;

- $N_{\text{corrective steering}}=1{,}97 \times 10^{7}$
- $N_{\text{full steering}}=1{,}73 \times 10^{5}$

Reversing

Assuming maximum reversing load 20 times per day at all sea-states.

Total number of reversing cycles for 25 years is estimated to:

- $N_{\text{reversing}}=1{,}83 \times 10^{5}$

Remaining time is standstill in water.

Appendix 2 – The MATLAB code

```
clear all

D=0.325; % half swinging distance for the lever at a 125-model.[m]

alfa=31.2; %maximum angle in reverse mode. [degrees]

FW=125000; %Force generated by the water jet in reverse mode. [N]

C=D/(sin(alfa*pi/180));%the length of C, constant. [m]

B=linspace(0.05,1.0,20);%values of B from 0.05 till 1 in 20 equal sized
steps. [m]

k=length(B);%The length of the loop, here as long as B = 20 steps.

for i=1:1:k % loop starts from 1 and goes to k in steps of 1.

FR(i)=(FW*((C*cos(alfa*pi/180))+(B(i)*cos(alfa*pi/180))))/(B(i)*cos(alfa*pi/1
80)); %calculates the values of FR (reaction force)for each 20 steps of B.[N]

    FH(i)=FR(i)-FW; %Calculates the force needed from the hydraul cylinder
when B varies from 0.05m to 1.0m in 20 equal sized steps. [N]

    h(i)=B(i)+C; %calculates the different hights at revers mode for when B
varies from 0.05m to 1.0m in 20 equal sized steps.

end % end of loop.

plot(B,FH,'*');% plots the force in relation to B
```